IMPLEMENTING THE WRF-CHEM MODELING SYSTEM TO INVESTIGATE THE INTERACTIONS BETWEEN AIR QUALITY AND METEOROLOGY

ALESSANDRA BALZARINI

UNIVERSITY OF MILANO-BICOCCA
Doctoral school in Environmental Science
XXVI cycle

IMPLEMENTING THE WRF-CHEM MODELING SYSTEM TO INVESTIGATE THE INTERACTIONS BETWEEN AIR QUALITY AND METEOROLOGY

Ph.D. thesis by

ALESSANDRA BALZARINI

Tutor
PROF. EZIO BOLZACCHINI
Co-tutor
ENG. GUIDO PIROVANO

External reviser
DR. PHILIPPE THUNIS

Academic year 2012/2013

The work presented in this thesis was financed by the Research Fund for the Italian Electrical System under the Contract Agreement between RSE (Ricerca sul Sistema Energetico - RSE S.p.A.) and the Ministry of Economic Development - General Directorate for Nuclear Energy, Renewable Energy and Energy Efficiency, stipulated on July 29th, 2009, in compliance with the Decree of March 19th, 2009.

The Ph.D. research was carried out at the Sustainable Development and Energy Sources Department (SFE) of Ricerca sul Sistema Energetico (RSE S.p.A.) in collaboration with the department of Environmental and Landscape Science of the University of Milano-Bicocca. The activities were also partially developed at the Assimilation and Modeling Branch of the NOAA/ESRL Global Systems Division at Boulder (CO).

Cover image: Hurricane Isabel seen from the International Space Station (NASA; www.nasa.gov).

Acknowledgments: Author is grateful to Prof. Ezio Bolzacchini, Guido Pirovano, Maurizio Riva and Anna Toppetti for their support in all these years. Thanks!

TABLE OF CONTENTS

1 GENERAL INTRODUCTION

The knowledge and study of air quality are important because atmospheric pollutants can induce adverse effects on human health as well as natural ecosystems (e.g., Utell, 2006 and Krupa et al., 2006).

Air quality managers seek to protect public health through control policies and more stringent air quality standards for both short and long term situations (Jacob and Winner, 2009). As a result megacities has been shown a significant decrease in concentrations of primary pollutants (e.g. nitrogen oxides, sulphur dioxide, carbon monoxide, volatile organic compounds and heavy metal) over the last decades and they will certainly continue to decrease in the future as a result of energy choices and social and economic concerns.

On the contrary, secondary pollutants, such as ozone and particulate matter, have revealed a fewer reduction in air concentrations despite a striking decrease in the emission trend of their precursors. Ozone and aerosols are known to generate health problems especially inside or in the surroundings of large cities (Schwartz et al., 1996). The effects on human health connected to fine particle exposure are well documented in literature (Pope and Dockery, 1999; Schwartz et al., 1996; Biggeri, 2004). Particles have been associated with some different health effects, such as mortality, asthma, and pulmonary disease (Schwartz et al., 1996), due to their ability to penetrate into the cardiovascular system and into the lung (Biggeri, 2004). Moreover, recent studies have identified a connection between fine particle exposure and lung cancer (WMO, 2013).

Since most of the population is foreseen to live in megacities within the next decades, health problems due to poor air quality are

expected to increase, despite the efforts in developing new technologies for cleaner combustion processes and new emission control strategies (Monks et al., 2009).
Moreover, as we enter an era of rapid climate changes, potential reductions in anthropogenic emission due to control strategies may be also modulated by changes in meteorological variables (Jacob and Winner, 2009).
Aerosols and gas species are strongly influenced by meteorological variables. Dispersion and dilution of chemical effluent is a result of wind advection, thermal diffusion, and dry and wet depositions. At the same time, aerosols are known to affect both weather and climate. Depending on their composition aerosols can absorb or scatter the incoming solar radiation, cooling the surface and warming the atmosphere (Brasseur and Roeckner, 2005; Menon et al., 2004). These effects, together with the role played by aerosols as cloud condensation nuclei, impact the hydrogeological cycle by altering cloud cover and precipitations (Brasseur and Roeckner, 2005; Koren, 2004, Menon et al., 2004).
Although the existence of the interactions between air quality and meteorology (feedback effects) is well known, only few studies tried to assess their regional effect (Forkel et al. 2012, 200; Zhang et al., 2010). In order to do this a modeling approach is needed.
Chemistry and transport models (CTMs) are fundamentals tools to understand the complex and dynamic interactions between meteorology and chemistry at multiple temporal and spatial scales (Kindap et al., 2006; Kallos et al., 2007). Even European legislation supports modeling techniques to increase knowledge on air quality processes and in developing air quality plans and programs (Directive 2008/50/EC).
Chemistry and transport models, such as CAMx (Comprehensive Air quality Model with eXtension; ENVIRON, 2011), are generally implemented with an "*off-line"* approach, meaning that turbulence characteristics are provided by an independent meteorological run. Moreover, atmospheric chemical and physical processes are decoupled in this method ("*un-coupled*"), avoiding the reconstruction

and the estimation of the coupled interactions between meteorology and air quality, and, hence, their effects on policies.
In past years, CTMs were extensively evaluated and analyzed in many modeling inter-comparison projects either at continental (Cuvelier et la., 2007; van Loon et al, 2007) or regional scale (Pernigotti et al., 2013), achieving a comprehensive evaluation of the main gaps and phenomena driving the regional-scale numerical estimations.
More recently, the AQMEII initiative (Air Quality Modeling International Initiative; http://aqmeii.jrc.ec.europa.eu/; Rao et al., 2011) proposed a further modeling inter-comparison exercise to systematically and objectively evaluate Chemistry and Transport models in order to improve understanding about atmospheric relevant processes and increasing confidence in model performance evaluation for better support of policy development.
However, the atmospheric modeling community is moving toward an "*on-line"* integrated approach that aims at incorporating chemistry and meteorology in the same regional model and including the effect of aerosols on incoming solar radiation, cloud and precipitations ("*coupled*"), thus, allowing a more complete and realistic representation of the lower atmosphere and its driving phenomena.
The Weather Research and Forecasting model coupled with chemistry (WRF-Chem; Grell et al., 2005) is a state-of-the-art on-line coupled model, in which chemistry transformations are completely embedded into the meteorological model WRF (Skamarock et al., 2008). The model simulates emissions, transport, mixing, and chemical transformation of gases and aerosols species simultaneously with meteorology. In this way, meteorological and chemical processes have same vertical and horizontal coordinates, same physics parameterization and same time step (Grell et al., 2005). WRF-Chem is, thus, an essential tool in both understanding the atmospheric processes related to pollution events and determining the interactions with meteorology.
Even though this on-line coupled model is becoming more and more popular in the atmospheric modeling community, only few works explored WRF-Chem performances over complex terrains (Saide et

al., 2011; Tie et al, 2007; Žabkar et al., 2011) such as the Italian one (Schurmann et al., 2009). Therefore, its skills need to be better explored and examined.
In this contest, the comparison to well-known and extensively-evaluated systems, such as CTMs (e.g. CAMx), and to other application of the same model are important steps in order to improve the knowledge on its processes as well as to investigate the effect of on-line and coupled approaches on air quality simulations.
Nevertheless, accurately reproduce the ground-based concentrations requires a good reconstruction of the main meteorological process that aid the dispersion and the chemical reaction of atmospheric pollutants e.g. temperature, precipitation, wind speed and wind direction. Among others, the Planetary Boundary Layer height (PBL) plays a key role in air quality simulations; since it determines the air volume in which emissions and the main atmospheric pollutants are trapped near the earth's surface (Stull et al., 1989), influencing the ground-level concentrations of atmospheric particulate matter.
PBL thickness is highly variable in time and space (Stull et al., 1989), so it needs to be evaluated from case to case on a regionally specific basis.
Italy often suffers high ozone and PM concentrations, due to the interaction of both anthropogenic and biogenic emissions, enhanced by rather complex circulation conditions. Particularly, the Po valley is a highly industrialized and densely populated area where wind speed is generally low and the atmospheric circulation is often stagnant especially during winter times, when frequent thermal inversion, low PBL heights and prolonged foggy or hazy periods occur (Vecchi, 2004). This situation can lead to accumulation processes and frequently exceedances of air quality standards, making the Italian Peninsula an interesting case study for modeling applications that aims to evaluate emission control strategies and, then, interactions between meteorological fields and aerosols. Indeed, the answers to both phenomena tend to be more pronounced when high aerosol loads are available.

The goal of this study is to build a comprehensive modeling environment in order to analyze the interaction between air quality and meteorology, especially in high-emissive areas (e.g. Italy and the Po valley), through the state-of-the-art air quality and meteorological model WRF-Chem.
Moreover, the work aims at exploring the main problems related to the representation of air pollution events, thus reducing the uncertainties in air quality simulations by improving the model reconstruction of meteorological processes. This study focuses on WRF-Chem, but it explores and investigates problems that are easily spanned over other chemistry and transport models.

In the following Chapter (Chapter 2) the sensitivity of meteorological algorithms (WRF model) to several PBL schemes will be presented. This work aimed at defining the best meteorological configuration adopted in air quality simulations. In Chapter 3 is discussed a comprehensive evaluation of the well-known Chemistry and Transport model CAMx in the framework of the AQMEII phase 1 exercise in order to analyze the validation techniques that will be used in the following Chapters. CAMx is also used as a benchmark for the WRF-Chem outcomes in Chapter 4 that considers the first application of WRF-Chem over Italy. Chapter 5 is dedicated to the analysis of direct and indirect feedback effects over Italy either in a past case (2010) or in a future case (2030) where emission control strategies are employed based on the application of the current European Directives. Finally Chapter 6 discusses the main finding and general conclusions of this work.

1.1 REFERENCES

Biggeri A., Pierantonio B., Benedetto T., 2004. Meta-analysis of the Italian studies on short-term effects of air pollution 1996-2002. Epidemiologia & Prevenzione, Year 28 (4-5), July-October 2004.

Brasseur, G. P., and E. Roeckner, 2005. Impact of improved air quality on the future evolution of climate. Geophys. Res. Lett., 32, L23704, doi:10.1029/2005GL023902.

Cuvelier, C., Thunis, P., Vautard, R., Amann, M., Bessagnet, B., Bedogni, M., Berkowicz, R., Brandt, J., Brocheton, F., Builtjes, P., Carnevale, C., Copalle, A., Denby, B., Douros, J., Graf, A., Hellmuth, O., Honoré, C., Hodzic, A., Jonson, J., Kerschbaumer, A., de Leeuw, F., Minguzzi, E., Moussiopoulos, N., Pertot, C., Peuch, V.H., Pirovano, G., Rouil, L., Sauter, F., Schaap, M., Stern, R., Tarrason, L., Vignati, E., Volta, M., White, L., Wind, P., Zuber, A., 2007. CityDelta: A model intercomparison study to explore the impact of emission reductions in European cities in 2010. Atmospheric Environment 41, issue 1, 189-207.

ENVIRON, 2011. User's Guide to the Comprehensive Air Quality Model with Extensions (CAMx). Version 5.4. Report prepared by ENVIRON International Corporation Novato, CA.

EU, 2008. Directive 2008/50/EC of the European Parliament and of the Council of 21 May 2008 on ambient air quality and cleaner air for Europe. Official Journal L 152, 11.6.2008, p. 1–44 http://eur-lex.europa.eu/LexUriServ/LexUriServ.do?uri=OJ:L:2008:152:0001:0044:EN:PDF

Forkel R., Werhahn J., Hansen A.B., McKeen S., Peckham S., Grell G., Suppan P., 2012. Effect of aerosol-radiation feedback on regional air quality - A case study with WRF/Chem. Atmospheric Environment, 53, 202-211.

Grell, Peckham, Schmitz, McKeen, Frost, Skamarock and Eder, 2005. Fully coupled "online" chemistry within the WRF model. Atmospheric Environment, 39(37), 6957-6975.

Jacob D.J. and Winner D.A., 2009. Effect of climate change on air quality. Atmospheric Environment, 43, 51-63, doi:10.1016/j.atmosenv.2008.09.051.

Kallos, G., Astitha,, M., Katsafados, P., and Spyrou, Ch., 2007. Longrange transport of anthropogenically and naturally produced particulate matter in the Mediterranean and North Atlantic: Current state of knowledge. J. Appl. Meteorol. Climatol., 46, 1230–1251.

Kindap, T., Unal, A., Chen, S. H., Hu, Y., Odman, M. T., and Karaca, M., 2006. Long-range aerosol transport from Europe to Istanbul, Turkey. Atmos. Environ., 40, 3536–3547.

Koren I., Kaufman Y.J., Remer L.A., Martins J.V., 2004. Measurments of the effect of amazon smoke on inhibition of cloud formation. Science, 303, 1342-1345.

Krupa, S.V., Grunhage, L., Jager, H.J., Nosal, M., Manning, W.J., Legge, A.H., Hanewald, K., 2006. Ambient ozone (O3) and adverse crop response: a unified view of cause and effect. Environmental Pollution 87, 119–126.

Menon Surabi, 2004. Current uncertanties in assessing aerosol effects on climate. Annu. Rev. Environ. Resour 29:1–30, doi: 10.1146/annurev.energy.29.063003.132549.

Monks, P.S., Granier C., Fuzzi S., Stohl A., Williams M.L., Akimoto H., Amann M., Baklanov A., Baltensperger U., Bey I., Blake N., Blake R.S., Carslaw K., Cooper O.R., Dentener F., Fowler D., Fragkou E., Frost G.J., Generoso S., Ginoux P., Grewe V., Guenther A., Hansson H.C., Henne S., Hjorth J., Hofzumahaus A., Huntrieser H., Isaksen I.S.A., Jenkin M.E., Kaiser J., Kanakidou M., Klimont Z., Kulmala M., Laj P., Lawrence M.G., Lee J.D., Liousse C., Maione M., McFiggans G., Metzger A., Mieville A., Moussiopoulos N., Orlando J.J., O'Dowd C.D., Palmer P.I., Parrish D.D., Petzold A., Platt U., Poschl U., Pre'vot A.S.H., Reeves C.E., Reimann S., Rudich Y., Sellegri K., Steinbrecher R., Simpson D., ten Brink H., Theloke J., van der Werf G.R., Vautard R., Vestreng V., Vlachokostas Ch., von Glasow R., 2009. Atmospheric composition change–global and regional air quality. Atmospheric Environment 43, 5268–5350.

Pernigotti D., Thunis P., Cuvelier C., Georgieva E., Gsella A., De Meij A., Pirovano G., Balzarini A., Riva G.M., Carnevale C., Pisoni E., Volta M.,Bessagnet B., Kerschbaumer A., Viaene P., De Ridder K., Nyiri A., Wind P., 2013. POMI: a model inter-comparison exercise over the Po Valley. Air Qual Atmos Health 6(4), 701-715. doi: 10.1007/s11869-013-0211-1.

Pope, C., & Dockery, D., 1999. Chapter 31. Epidemiology of particle effects. In S. T. Holgate, H. S. Koren, J. M. Samet, & R. L. Maynard (Eds.), Air pollution and health (pp. 673–705). San Diego: Academic Press.

Rao, S. T., Galmarini, S., Puckett, K., 2011. Air Quality Model Evaluation International Initiative (AQMEII): Advancing the State of the Science in Regional Photochemical Modeling and Its Applications. BAMS, Volume 92, Issue 1, 23-30.

Saide, P.E, Carmichael, G.R., Spak, S.N., Gallardo, L., Osses, A.E., Mena-Carrasco, M.A., Pagowski, M., 2011. Forecasting urban PM10 and PM2.5 pollution episodes in very stable nocturnal conditions and complex terrain using WRF–Chem CO tracer model Original. Atmospheric Environment, 45 (16), 2769-2780.

Schwartz, J., Dockery, D., Neas, L., 1996. Is daily mortality associated specifically with fine particles?. Journal of the Air & Waste Management Association, 46(10), 927–939.

Skamarock W.C., Joseph B. Klemp, Jimy Dudhia, David O. Gill, Dale M. Barker, Michael G. Duda, Xiang-Yu Huang, Wei Wang , Jordan G. Powers, 2008. A Description of the Advanced Research WRF Version 3. NCAR Technical Note NCAR/TN-475+STR, Boulder, Colorado.

Stull Roland B., 1989. An introduction to Boundary Layer Meteorology. Kluwer Academic Publishers, ISBN: 90-277-2769-4.

Schürmann, G.J. , Algieri, A., Hedgecock, I.M, Manna, G, Pirrone, N., Sprovieri, F., 2009. Modelling local and synoptic scale influences on ozone concentrations in a topographically complex region of Southern Italy. Atmospheric Environment 43 (29), 4424-4434.

Tie, X., Madronich, S., Li, G., Ying, Z., Zhang, R., Garcia, A.R., Lee-Taylor, J., Liu, Y., 2007. Characterizations of chemical oxidants in Mexico City: A regional chemical dynamical model (WRF-Chem) study. Atmospheric Environment 41 (9), 1989-2008.

Utell, M.J., 2006. Inhalation of ultrafine particles alters blood leukocyte expression of adhesion molecules in humans. Environmental Health Perspectives 114, 51–58.

Van Loon, M., Vautard, R., Schaap, M., Bergstrom, R., Bessagnet, B., Brandt, J., Builtjes, P., Christensen, J.H., Cuvelier, K., Graf, A., Jonson, J., Krol, M., Langner, J., Roberts, P., Rouil, L., Stern, R., Tarrason, L., Thunis, P., Vignati, E., White, L., Wind, P., 2007. Evaluation of long-term ozone simulations from seven regional air quality models and their ensemble average. Atmos. Environ. 41, 2083–2097.

Vecchi R., Marcazzan G., Valli G., Cerini M., Antoniazzi C., 2004. The role of atmospheric dispersion in the seasonal variation of PM1 and PM2.5 concentration and composition in the urban area of Milan (Italy). Atmopheric Environment, 38, 4437-4446.

World Health Organization (WMO), 2013. Review of evidence on health aspects of air pollution – REVIHAAP Project. Technical Report. http://www.euro.who.int/__data/assets/pdf_file/0004/193108/REVIHAAP-Final-technical-report-final-version.pdf

Žabkar, R., Rakovec, J., Koračin, D., 2011. The roles of regional accumulation and advection of ozone during high ozone episodes in Slovenia: A WRF/Chem modelling study. Atmospheric Environment, 45 (5), 1192-1202.

Zhang Y., Wen X.-Y., Jang C.J., 2010. Simulating chemistry – aerosol – cloud –radiation – climate feedbacks over the continental U.S. using the online-coupled Weather Research Forecasting Model with Chemistry (WRF/Chem). Atmospheric Environment, 44, 3568-3582, doi: 10.1016/j.atmosenv.2010.05.056.

2 SENSITIVITY ANALYSIS OF PBL SCHEMES BY COMPARING WRF MODEL AND EXPERIMENTAL DATA

A. Balzarini, F. Angelini, L. Ferrero, M. Moscatelli, G. Pirovano, G.M. Riva, A. Toppetti, E. Bolzacchini

Submitted manuscript

Air quality is normally investigated at local or regional scale by the aid of Chemistry and Transport Models (CTMs) that allow reproducing the fate of the main atmospheric pollutants, both primary and secondary, such as ozone, nitrogen oxides and particulate matter. CTMs are generally driven by 3D meteorological fields provided by a previous run of a mesoscale meteorological model. Consequently, the correct representation of air quality is strongly affected by the simulation of meteorological processes and parameters. The main controlling variables are wind, temperature, turbulent fluxes and, among others, the height of the Atmospheric Boundary Layer (ABL), also called Planetary Boundary Layer (PBL).

In recent years, there has been significant progress on the characterization of atmospheric turbulence, but the determination of the PBL remains one of the most uncertain parameters, especially in modeling estimations affecting the reconstruction of dispersion

processes and, then, ground concentrations (Misenis and Zhang, 2010; Yerramilli et al., 2010).

The Weather Research and Forecasting (WRF; Skamarock, 2005) model is a state-of-art in meteorological applications and offers several schemes to reconstruct PBL heights, each adopting different assumptions when describing the turbulence or eddy activities in stable, neutral or convective conditions. Furthermore, new PBL schemes have been recently embedded to WRF version 3.3, such as the University of Washington Moist Turbulence (UW) scheme (Bretherton and Park, 2009).

Several studies have explored the sensitivity of PBL schemes in WRF model (Misenis et al., 2006; Zhong et al., 2007; Borge et al., 2008) showed discrepancies between different simulations and among these and observations. More recently, Ferrero et al. (2011) proposed a sensitivity analysis of four PBL schemes over the Po Valley region comparing results of the Fifth-Generation Penn State/NCAR Mesoscale meteorological model (MM5; Grell et al., 1994) with vertical profiles by balloon soundings. However, all these studies do not investigate the relationship between model performances and differences in PBL parameterizations.

Hu et al. (2010) attempted to evaluate the causes of model biases for three PBL schemes of WRF model in south-central United States. In this work a similar study is presented for the Po Valley area (North of Italy), in order to identify the best PBL scheme that will be employed to simulate air quality over Italy using the chemical extension of the WRF meteorological model, namely the WRF-Chem model (Grell et al., 2005).

If we exclude certain sporadic cases due to Föhn winds (Gandino et al., 1990), in the Po Valley area the ventilation is generally poor and the atmospheric circulation is often stagnant, especially during winter when frequent thermal inversion at low altitude and prolonged foggy periods induce very low PBL depths (Rodriguez et al., 2007). These conditions often limit model performances in estimating the height of Boundary Layer (Ferrero et al. 2011a), making the Italian area an interesting case study for modeling applications.

The present application focuses on analyzing the differences in five model schemes allowing conclusions on the influence of PBL formulations on the modeled results. To this aim WRF, version 3.3.1, has been applied to the critical area of the Po Valley and compared to experimental data in order to evaluate the skill of WRF in reconstructing PBL structure and evolution for air quality applications. Five PBL parameterizations were selected for winter 2008. In particular, three frequently used schemes (YSU, Hong et al., 2006; MYJ, Janjic, 1994; and MRF, Hong and Pan, 1996) as well as the ACM2 scheme (Pleim, 2007) and the new UW (Bretherton and Park, 2009) are considered.
Winter 2008 was chosen because of the availability of measurement data. Indeed, in this study many experimental techniques (ground level measurements, particle vertical profiles by balloon soundings, meteorological balloons and Lidar measurements) were combined together in order to obtain a correct and thorough representation of the PBL structure.
At the same time, this work represents one of the few investigations (Ferrero et al., 2011) of PBL heights over the Po valley throughout a comparison between model results and observations.

2.1 MODEL AND OBSERVATIONS

2.1.1 WRF description and modeling setup

In this study, the Weather Research and Forecasting (WRF) model version 3.3.1 has been applied. WRF is a non-hydrostatic meteorological model designed to simulate mesoscale and regional scale atmospheric circulation. It includes many physical and dynamical options for microphysics, radiation, cumulus processes and Planetary Boundary Layer (www.wrf-model.org).
The main physical parameterizations adopted here are reported in Table 1 and they include the Rapid Radiative Transfer Model (RRTM) longwave radiation scheme (Mlawer et al., 1997) and the Goddard shortwave radiation scheme (Chou et al., 1998), the Noah

land surface model (Chen and Dudhia, 2001), the Morrison double moment microphysics scheme (Morrison et al., 2009) and the Grell 3D ensemble cumulus parameterization (Grell and Devenyi, 2002).
RRTM is based on Mlawer et al. (1997) and is a spectral-band scheme that uses correlated-k method and pre-set tables to accurately represent longwave processes due to water vapor, ozone, CO_2 and trace gases, and it also accounts for the cloud optical depth. The Goddard shortwave scheme has a total of 11 spectral bands and considers diffuse and direct solar radiation components in two-stream approach that accounts for the scattered and reflected components. Ozone is considered with several climatological profiles.
Noah land-surface model is a 4-layer soil temperature and moisture model with canopy moisture and snow cover prediction. The layer thicknesses are 10, 30, 60 and 100 cm from top down. It includes root zone, evapotranspiration, soil drainage and runoff, taking into account for the monthly vegetation categories and soil texture.
Morrison-2mom microphysics scheme is based on the two-moment bulk microphysics scheme of Morrison et al. (2005), and it includes six species of water: vapor, cloud droplets, cloud ice, rain, snow, and groupel/hail. The two-moment approach refers to the ability of the scheme to predict both mass mixing ratio and the number concentrations of five hydrometeor species (e.g. cloud droplets, cloud ice, rain, snow, and groupel/hail). The prognostic calculation of number concentration and mixing ratios allows a robust treatment of the particle size distributions (Morrison et al., 2009). Since the release 3.3, the Morrison 2-moment cloud microphysics scheme has been coupled with aerosol modules and extensively evaluated by Yang et al. (2011).
Finally the Grell 3D ensemble scheme is an evolution of Grell and Devenyi (2002) and is based on an ensemble mean approach in which multiple cumulus schemes are run within each grid box and then results are averaged to give a feedback to the model.

Table 1 - Physical options.

Process	Scheme
Cumulus parameterization	Grell 3D scheme
Shortwave radiation	Goddard scheme
Longwave radiation	RRTM
Microphysics	Morrison 2-mom
Land Surface Model	Noah LSM

Five Planetary Boundary Layer (PBL) schemes have been selected for the sensitivity test: Medium Range Forecast (MRF) scheme (Hong and Pan, 1996), Yonsei University (YSU) scheme (Hong et al., 2006), Mellor Yamada Janjic (MYJ) formulation (Janjic, 1994), University of Washington Moist Turbulence (UW) parameterization (Bretherton and Park, 2009) and the Asymmetrical Convective Model version 2 (ACM2; Pleim, 2007).

The differences among the five PBL schemes are related to the turbulence or eddy diffusivity assumption, the parameterization of the PBL top and the treatment of the entrainment zone in stable, neutral and convective conditions (Table 2).

The MRF scheme adopts a nonlocal-K approach proposed by Troen and Mahrt (1986) to simulate the mixed-layer diffusion with an implicit parameterization of the entrainment processes. The Boundary Layer height is enhanced by comparing the computed bulk Richardson number with a critical value (= 0.5; Hong et al., 2006). The entrainment effects are merely reproduced by additional mixing above the minimum flux level (Hong et al., 2006). The YSU scheme is a modification of the MRF approach. The major changes include the explicit treatment of the entrainment processes at the inversion layer by means of an asymptotic entrainment flux term added to the turbulence diffusion equation and a critical bulk Richardson number sets to zero (Hong et al., 2006). The YSU scheme is further modified in WRF version 3 by increasing the critical bulk Richardson number from zero to 0.25 over land during stable boundary conditions (Hong and Kim, 2008).

Table 2 - PBL schemes.

Scheme	Mixed Layer	Entrainment zone	PBL Top	Surface Layer
YSU	Non-local K profile	explicit term	from *Ri*	MM5 similarity theory
MYJ	K from prognostic TKE	part of PBL mixing	From TKE	Eta similarity theory
ACM2	Non-local and local K profile	part of PBL mixing	from *Ri*	MM5 similarity theory
UW	K from diagnostic TKE	explicit term	From TKE	Eta similarity theory
MRF	Non-local K profile	part of PBL mixing	from *Ri*	MM5 similarity theory

MYJ is an implementation of the Mellor Yamada level 2.5 model (Mellor and Yamada, 1982). It applies a local approach to determine eddy diffusion coefficients from prognostic turbulent kinetic energy (TKE). Since the TKE is largest within the PBL, MYJ defines its top as the height where the TKE becomes negative or drops to a prescribed lower bound (Hu et al., 2010; Janjic, 2001). A similar approach is used in the recently added UW parameterization, but turbulent kinetic energy is diagnosed rather than prognosed for different regimes (stable or convective) and an explicit entrainment closure is used at the edge of the convective layers (Bretherton and Park, 2009).

Finally, the ACM2 combines the nonlocal transport of the ACM1 model (Pleim and Chang, 1992) and the local eddy diffusivity. In this way, vertical fluxes are described as pure eddy diffusion in stable conditions and a combination of local gradient and nonlocal turbulent transport in unstable conditions (Pleim, 2007). In addition, ACM2 can simulate a convective upward transport from the lowest level to all other model layers and an asymmetrical layer-by-layer downward transport (Pleim, 2007). The height of the Boundary

Layer is calculated starting from the bulk Richardson number. This scheme does not include and explicit treatment of the entrainment processes.
Because in WRF exists a particular surface layer scheme to which each PBL formulation is preferentially coupled, the surface layer schemes are also varied. The MRF, YSU and ACM2 are coupled to MM5 scheme, while MYJ and UW are associated to Eta surface layer. Both surface schemes are based on similarity theory (Monin and Obukhov, 1954), but the second one includes a parameterization of a viscous sub-layer following Janjic (1994).
The WRF model has been applied over three domains in a Lambert Conic Conformal projection for February 2008. The master domain covers the whole Europe (3870x3555 km^2) with a horizontal resolution of 45 km. The first nested domain extends over 1350x1530 km^2 covering the Italian Peninsula with a grid step of 15 km and the second one is centered over the Po valley area (600x420 km^2) with a spatial resolution of 5 km. The cumulus scheme is not applied in the highest resolution domain. All model domains have 27 vertical layers extending from the surface up to 50 hPa, with a finer resolution in the PBL. The first model layer height is set to be approximately 30 m AGL.
The main characteristics of the modeling domain are reported in Figure 1 and Table 3.

Figure 1 - Computational domain.

Table 3 - Domain characteristics.

	u.m.	D01	D02	D03
SW X corner	[km]	-2164.5	-634.5	-439.5
SW Y corner	[km]	-1773.5	-1053.5	-108.5
NE X corner	[km]	1705.5	715.5	160.5
NE Y corner	[km]	1781.5	476.5	311.5
Model top	[hPa]	50	50	50
DX-DY	[km]	45	15	5
NX	[n]	86	90	120
NY	[n]	79	102	84
NZ	[n]	27	27	27

A grid nudging on wind speed, temperature and water vapor mixing ratio has been employed within the Boundary Layer in all model configurations. The analysis nudging forces the model simulations towards a series of analyses grid points. The model simulation is nudged towards spatially and temporally interpolated analyses using a point by point relaxation terms. This type of analysis is particularly useful for atmospheric chemistry simulations where the errors in the wind fields can lead to an erroneous transport of chemical species. In this study, the nudging coefficients were set to the default values of 0.0003 sec^{-1}.
Input terrestrial data were derived from the 24-land use category of US Geological Survey database (USGS; http://www.usgs.gov/). The ECMWF (European Centre for Medium-Range Weather Forecast; http://www.ecmwf.int/) analysis of 6 hourly and 0.5° grid resolution were used as initial and boundary conditions.
The model ran with a spin up time of five days.

2.1.2 Experimental techniques

Planetary Boundary Layer measurements can be obtained by direct and indirect techniques such as tethered balloons (direct measurement) and Lidars (indirect estimation). Only direct techniques allow estimating the real effect of atmospheric turbulence

on pollutants dispersion with a high grade of accuracy; but the concept of measure in the atmosphere requires that a measurement system is placed where the measure is taken, with the all practical difficulties of the experimental design. Otherwise an indirect estimation can be carried on with the first advantage linked to the possibility of measuring a parameter related with the quantitative property of interest, normally continuously in time, but with the disadvantage due to the theoretical difficulties linked with the retrieval processes of the quantitative property itself. The way in which the experiment is carried out depends on the purpose of the study itself; in some cases multi-instrumental approaches are needed (Laakso et al., 2007, Wiegner et al. and 2006, McKendry et al., 2004). In this study both experimental techniques are employed in order to evaluate a comprehensive and reliable reconstruction of the PBL height. PBL height was directly measured through a tethered balloon system. However, these kinds of measurements have the lack to be not continuous in time. In order to fill this gap, indirect methods through Lidar measurements are considered too.

2.1.2.1 Vertical profiles

Direct measurements of Planetary Boundary Layer height can be made through vertical aerosol profiles. Measurements were carried out in the Milan metropolitan area (Torre Sarca site, TS: 45°31'19"N, 9°12'46"E) by the University of Milano-Bicocca, in the midst of the most industrialized area in the Po Valley, using a spherical helium-filled tethered balloon (PU balloon, Ø=4 m, volume 33.5 m^3, payload 15 kg).

The balloon carried aloft a sampling platform consisting of an optical particle counter (OPC, 1.108 *"Dustcheck"* GRIMM) that allowed to measure the particle number concentration in 15 classes from 0.3 μm to up to 20 μm, (0.3-0.4 μm, 0.4-0.5 μm, 0.5-0.65 μm, 0.65-0.8 μm, 0.8-1.0 μm, 1.0-1.6 μm, 1.6-2.0 μm, 2.0-3.0 μm, 3.0-4.0 μm, 4.0-5.0 μm, 5.0-7.5 μm, 7.5-10 μm, 10-15 μm, 15-20 μm, >20 μm). In addition, a portable meteorological station (BABUC-ABC, LSI-Lastem) was adopted to measure pressure, temperature and relative humidity; both instruments acquired data at 6 sec of time resolution.

An electric winch controlled ascent and descent rates; a fixed value of 30.0 ± 0.1m/min was used for all profiles, giving 3.0 meters of measuring vertical resolution. The maximum height reached during each launch depended on atmospheric conditions; for the majority of the profiles it was 600 m AGL.

Further details of the experimental approach can be found in Ferrero et al. (2012 and 2010). The same experimental design has also been successfully adopted in other studies (Wiegner et al., 2006; McKendry et al., 2004; Maletto et al., 2003).

Basing on the observation that atmospheric particles act as tracers of atmospheric plumes, and integrate the effects of both thermal and mechanical forces, the Boundary Layer height was derived using a gradient method applied to the aerosol vertical profiles. At the same time the instantaneous thickness of the Entrainment Zone (EZ), which connects the mixed layer with the layer above it was calculated too (Stull, 1989). Particularly, the EZ thickness is the layer around the mixing zone, measured using the gradient method, extending between the regions in which more than 5%, but less than 95%, of the air in the vertical profile possess above PBL characteristics.

A validation of the aforementioned procedure, through a comparison with potential temperature, relative humidity and Black Carbon profiles, as well as Lidar data (Ceilometer Vaisala LD-40) is reported in literature (Ferrero et al., 2010; Ferrero et al., 2011a and 2011b; Angelini et al., 2009).

Vertical aerosol profile measurements were performed along three years from 2006 to 2008.

Aerosol vertical profiles collected during the experimental campaign for February 2008 are reproduced from Figure 2 to Figure 6. In these figures profiles are represented in Local Standard Time (UTC+1).

Sixteen ascent and descent profiles of total particle number concentration were available within five days.

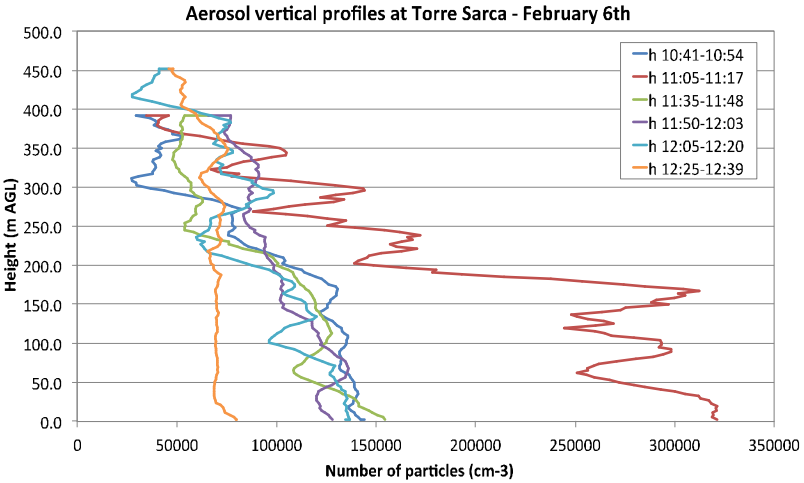

Figure 2 – Aerosol vertical profiles collected at Torre Sarca on February 6th.

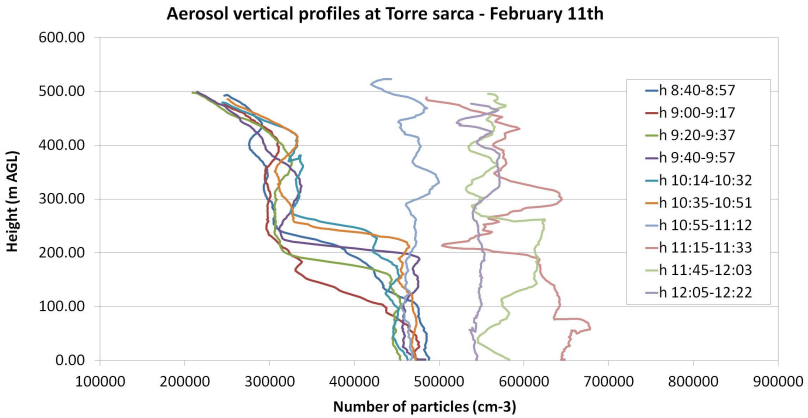

Figure 3 - Aerosol vertical profiles collected at Torre Sarca on February 11th.

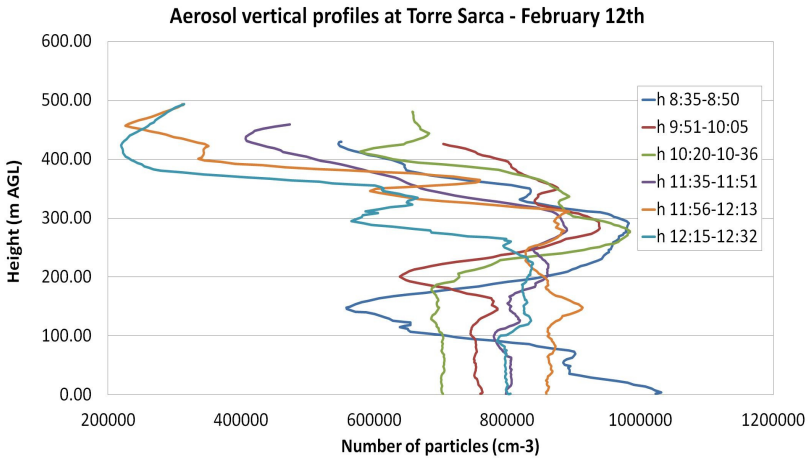

Figure 4 – Aerosol vertical profiles collected at Torre Sarca on February 12th.

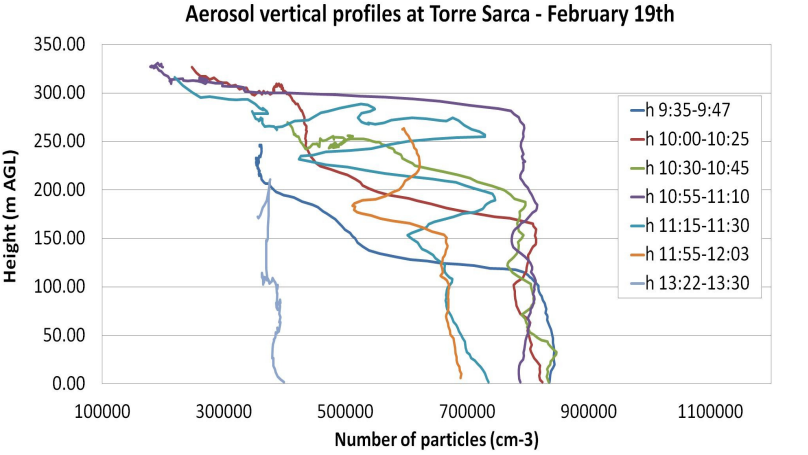

Figure 5 - Aerosol vertical profiles collected at Torre Sarca on February 19th.

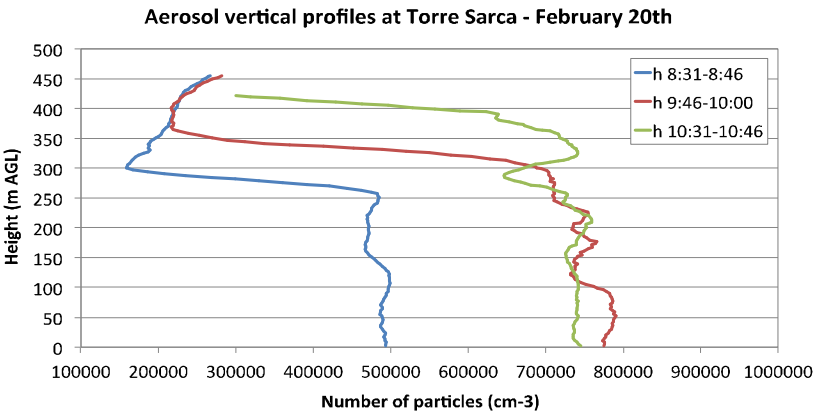

Figure 6 - Aerosol vertical profiles collected at Torre Sarca on February 20th.

It is possible to observe that those profiles were characterized by quite constant particulate matter concentrations going up from the ground level until a layer where a strong negative concentration gradient is present. This strong gradient is very close to the ground; indeed particulate matter is generally accumulated in few hundred meters of atmosphere during winter times. It is also possible to state that profiles become more homogeneous along vertical direction proceeding with the daytime evolution, reaching the maximum mixing during noon due to an increasing in solar forcing and then turbulence.

At ground level aerosol concentrations are generally higher in the early morning (from 8:30 am to 10:00 am), when mixing is lower and surface emissions are more intense (e.g. traffic and heating). Later in the day, ground concentrations slowly decrease for both rising in mixing and losing in ground-based emissions.

However quantitative measurements of the atmospheric dispersion capability are needed; to this aim the strong negative gradient of the atmospheric particulate matter can be related to the height of PBL (Siebert et al., 2000) simply looking at the vertical dispersion of the particulate matter in the atmosphere. PBL heights were directly

calculated from the measured data taking as reference the height at which the strongest negative gradient of particle number concentration is present; in addition the thickness of the transition layer between the mixed layer itself and the free troposphere, can be estimated from the difference among the heights at which respectively the concentration gradient start to become negative and return near zero.
As an example, Figure 7 displays particle number concentration gradient trend of the aerosol particle vertical profile collected on February 20th from 8:31 to 8:46 am.

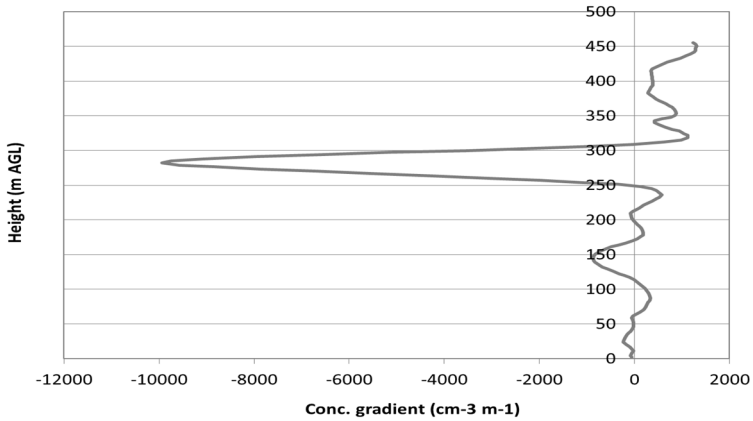

Figure 7 - Particle number concentration gradient for vertical profile of February 2008, 20th at 8:31-8:46 UTC. The strongest negative gradient of particle number concentration corresponds to the PBL height (here 282.4 m agl).

For a complete evaluation of modeled data, radio soundings of Milano Linate airport (about 9 km far from Torre Sarca; 45°26'N, 9°17'E) were considered too. Milano Linate station provides high-resolution vertical profiles of pressure, temperature, relative humidity and dew point temperature every 12 hours.

2.1.2.2 Lidar measurements

Information on PBL can be also obtained through indirect experimental techniques such as Lidar (Kim et al., 2007 and Amiridis et al., 2007), that allows to get useful parameters describing the nature of the PBL, as an example aerosol backscatter. Planetary Boundary Layer height was thus estimated by means of an automated Lidar (ceilometer) Vaisala LD-40 installed at Torre Sarca (University of Milano – Bicocca in collaboration with CNR of Rome) the same days as the balloon launching.

The ceilometer acquired aerosols backscatter profiles at five different heights every 15 seconds at the wavelength of 855 nm from January 2007 to February 2008. Heights are then averaged by the system every 15 minutes in order to increase the signal-to-noise ratio and to correct for the presence of clouds and haze.

Elastic backscatter Lidars can provide information on the aerosol distribution within the PBL, providing the aerosol cross-section profile. Three methods have been proposed so far to infer the PBL height from Lidar data: the threshold method (Melfi et al., 1985), the gradient method (Endlich et al., 1979), and the variance method. At the basis of all these methods there is the assumption that aerosols are produced at ground and mixed in the PBL by effect of turbulence induced by convection. In this work PBL heights were obtained using a gradient method (Angelini et al., 2009), which employs the inflection points in the corrected aerosol backscatter profile to determine the height of the PBL. For a detailed description of the PBL retrieval by elastic Lidar, see, among others, Angelini et al. (2009), Morille et al. (2007), Martucci et al. (2007) and Haeffelin et al. (2012). The latter work shows that while the algorithms for the determination of aerosol layer heights are nowadays rather efficient, the most difficult task for automated procedures is the attribution to one of the detected heights of the top of the boundary layer, since in many cases residual or advected aerosol layers as well as low aerosol loads may induce errors in this attribution.

For this reason, in the present work a supervised analysis has been performed, and the boundary layer top has been attributed by visual inspection.

Moreover, particular attention must be paid to the afternoon transition between the convective boundary layer and the new stable boundary layer building up after sunset. At that time, in fact, the boundary layer height shows large ambiguity, depending on which criterion is adopted to measure it. When the solar forcing decreases, the convective atmosphere reaches first neutral and then stable temperature lapse rate. Under these conditions, the lower atmosphere still experiences turbulence, but its actual mixing capability is strongly reduced. Aerosols lifted up by daytime turbulence keep aloft and experience slow sedimentation, but new aerosols produced at ground start accumulating in the surface layer. In such conditions Lidar-based estimations of the boundary layer height will keep giving high values, until new aerosol are emitted at ground, thus, enabling the detection of the new shallow stable layer. This happens usually with a very sharp transition, and smooth drops of the PBL heights are rarely observed.

As an example, from Figure 8 to Figure 11 it is shown the daily trend of the signal detected by the ceilometer during the vertical profiles field campaigns. It appears that the trend of PBL along days is represented by a continuous growth until midday followed by decrease until nighttime. The maximum height of the PBL ranges from 500 m to 1000 m.

It is also quite evident the formation of a residual layer during the night that remains suspended in the atmosphere until the next sunrise. The nighttime residual layer formation at high altitude is particularly clear in Figure 8, Figure 9 and Figure 11, as well as the suspended residual layer of the previous day during the first morning hours. In Figure 9 and Figure 10, it is also worth noting a smooth decay of PBL height due to the aerosol falling down after the slackening of solar forcing, although the thermo dynamical situation indicates that turbulence is very low. As a consequence, the comparison between models and observations in this period becomes particularly hard. Indeed, the problem of the afternoon turbulence and PBL decay is still under investigation.

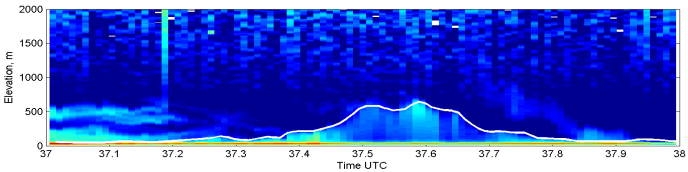

Figure 8 – Corrected ceilometer backscatter signal for 2008-02-06.

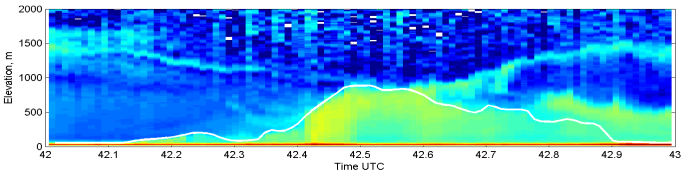

Figure 9 - Corrected ceilometer backscatter signal for 2008-02-11.

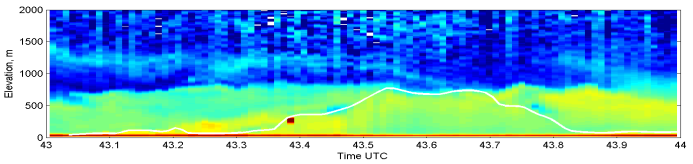

Figure 10 - Corrected ceilometer backscatter signal for 2008-02-12.

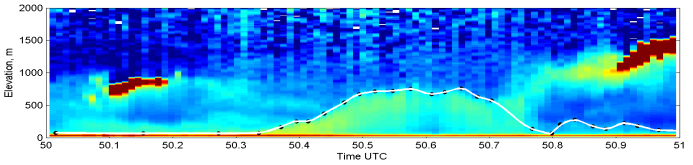

Figure 11 - Corrected ceilometer backscatter signal for 2008-02-19.

2.1.3 Comparison of model and observations

Simulation results were compared to experimental data through the Atmospheric Model Evaluation Tool (AMET 1.1, Appel et al., 2011). Evaluations focus on PBL heights as well as the main meteorological parameters, namely temperature, mixing ratio and wind speed.

Planetary Boundary Layer height was assessed in Torre Sarca using particle vertical profiles by balloon sounding and Lidar data, while

other meteorological fields were evaluated at 63 ground measurement stations located in the Po Valley. Meteorological radio soundings at Milano Linate airport were considered too.
Particle vertical profiles and Lidar data enable to experimentally estimate the magnitude of PBL depth and then the accuracy of different PBL schemes in reconstructing its structure and evolution. Furthermore, Lidar data allow obtaining a greater temporal coverage of measurements.
Finally, meteorological stations and radio-soundings enable to elucidate model capability in reproducing the main meteorological parameters.
Comparisons will be done in terms of temporal variation, vertical profiles, and performance statistics. Several metrics could be included in the analysis (Lin et al., 2008; Zhang et al., 2006). In order to obtain a complete characterization, five statistical parameters were selected (Appendix A2): Mean Obs, Mean Mod, Mean BIAS, Root Mean Square Error (RMSE), and Pearson Correlation (r). BIAS and RMSE enable to consider the accuracy of model schemes in reconstructing the PBL magnitude, while r to characterize the hourly or seasonal evolution.
Modeled and observed data have been corrected removing outliers. Values are analyzed when differences between model and observations are lower than a fixed threshold. For temperature we have chosen a delta value of 20°K, while for mixing ratio a threshold of 10 g/kg is set. Wind speeds lower than 0.5 m/s and higher than 100 m/s are rejected.
The aim of this study is to provide a sensitivity test of PBL scheme in the peculiar area of the Po Valley. For this reason, evaluations consider only the 5 km domain, interpolating model results to measurement sites and hours.

2.2 RESULTS AND DISCUSSION

2.2.1 Temperature, mixing ratio and wind speed

Table 4 displays the performance statistic for 2m-temperature, 2m-mixing ratio and 10-m wind speed at 63 WMO meteorological stations.

Table 4 – Comparison of PBL schemes against 63 ground-based meteorological stations in the Po Valley for 2m-temperature, 2m-mixing ratio and 10m-wind speed. Schemes are indicated as: ACM2 (Asymmetrical Convective Model version 2), MRF (Medium Range Forecast), MYJ (Mellor Yamada Janjic), YSU (Yonsei University), and UW (University of Washington Moist Turbulence). The best performances are highlighted in grey.

Statistic	ACM2	MRF	MYJ	UW	YSU
		Temperature (K)			
Mean Obs	277.487	277.487	277.487	277.487	277.487
Mean Mod	278.088	278.346	278.363	278.398	278.255
MB	0.601	0.859	0.876	0.911	0.767
RMSE	3.501	3.670	3.285	3.360	3.465
r	0.833	0.827	0.840	0.839	0.837
		Mixing Ratio (g/kg)			
Mean Obs	4.577	4.577	4.577	4.577	4.577
Mean Mod	4.618	4.551	4.855	4.842	4.699
MB	0.041	-0.026	0.278	0.265	0.122
RMSE	0.811	0.848	0.966	0.933	0.832
r	0.852	0.842	0.822	0.822	0.850
		Wind Speed (m/s)			
Mean Obs	3.237	3.237	3.237	3.237	3.237
Mean Mod	3.591	3.617	4.013	4.005	3.694
MB	0.354	0.381	0.776	0.768	0.457
RMSE	2.916	2.921	2.870	2.905	2.935
r	0.469	0.465	0.521	0.509	0.471

All simulations produce higher temperatures than the observed values in the lower atmosphere, implying some common errors in all model runs.

The lowest bias is always related to ACM2 scheme (bias = 0.601 °K), while the highest temperature biases are associated to MYJ and UW that use the Janjic Eta Monin–Obukhov surface layer scheme. Indeed, one possible cause of the biases can be related to the heat fluxes delivered by this scheme with respect to Monin–Obukhov surface layer scheme used with YSU, ACM2 and MRF (Hu et al., 2010). In order to verify it, the mean upward sensible heat fluxes at the surface (HFX) are represented in Figure 12.

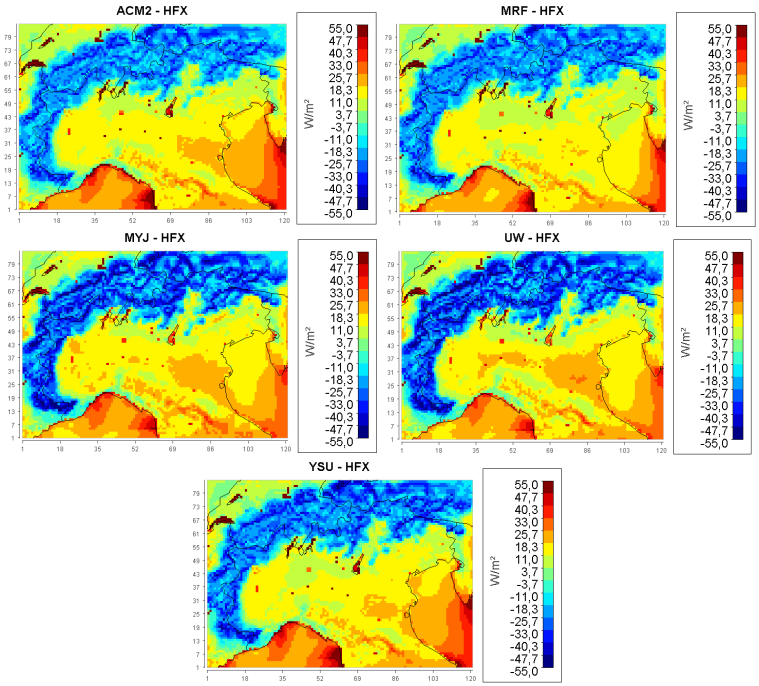

Figure 12 – Monthly mean of upward sensible heat fluxes at the surface (HFX) in the five configurations.

The figure shows that the highest mean heat sensible fluxes are associated to MYJ and UW. In particular UW predicts the largest temperature bias (mean bias=0.911 K) as well as the most pronounced differences of HFX over the Po valley area. However when non-local closure schemes are compared together, it is possible to state that MRF predicts higher temperature then ACM2 and YSU, but lower heat fluxes. Downward flux at the ground surface of shortwave incoming solar radiation (SWDOWN) is represented in Figure 14. All schemes have similar spatial distribution of the incoming solar radiation, even though some discrepancies are detectable on the North-East and South-West regions of the domain because of the differences in the cloud cover (not shown). UW is found to produce an incoming radiation that is on average larger than all other schemes. Indeed, this parameterization has the smallest cloud cover fraction. As discussed later, UW has also the weakest vertical mixing and, thus, low planetary boundary layer heights that tend to trap heat and moisture close to ground reducing the cloud formation at higher atmospheric levels. Looking at Figure 13, in fact, UW has also the highest latent heat flux at the surface (LH).
ACM2 and YSU have a similar mean incoming shortwave radiation which is generally smaller than MRF and MYJ in the North-East of Italy, since the latest schemes have less cloud cover fraction. Non-local closure schemes have quite comparable latent heat fluxes as they use the same surface layer scheme, although in MRF it is slightly higher. Collectively, the comparison shows that discrepancies in temperature performances can be partially explained also with differences in SWDOWN field and latent heat fluxes.

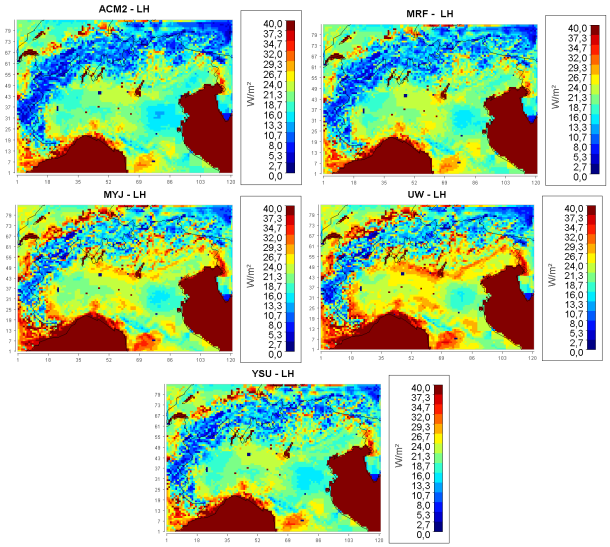

Figure 13 – Monthly mean of latent heat fluxes at the surface (LH) in the five configurations.

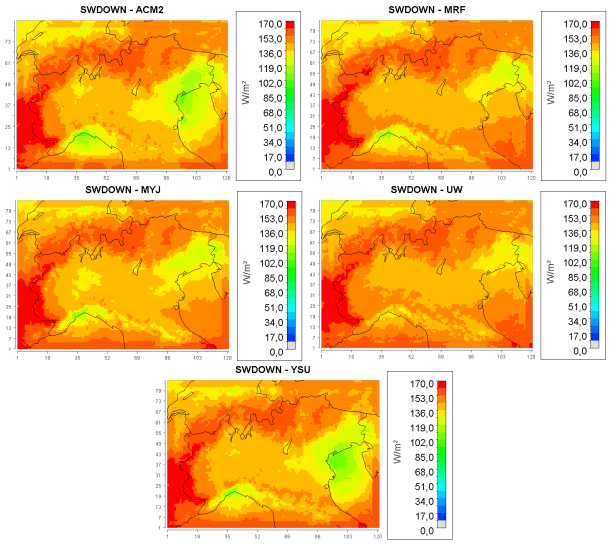

Figure 14 – Monthly mean of downward shortwave flux at the ground surface (SWDOWN) in the five configurations.

Non-local closure schemes (MRF, YSU and ACM2) have also the best performance in terms of mixing ratio. The WRF model predicts a mixing ratio mean bias of -0.026, 0.041, 0.122, 0.265, and 0.278 g/kg with the MRF, ACM2, YSU, UW and MYJ scheme, respectively. Moisture is generally overestimated by all configurations, consistently with temperature overprediction. The only exception is the MRF scheme that slightly under predicts mixing ratio. The overall trend is well reproduced by models, showing a correlation of about 0.8.
As far as wind speed is concerned, performance analysis reveals a model difficulty in reconstructing this meteorological field in terms of both magnitude and time variation. Biases of MRF, YSU and ACM2 are lower than MYJ and UW, and they range from 0.354 (ACM2) to 0.776 m/s (MYJ).

The goal of this work is to focus on the critical area of the Po Valley. For this reason, the following analysis will be performed in the urban city of Milan. The performance indices in Milano Linate station are reported in Table 5.
Runs follow the previous general pattern, over predicting temperature and wind speed, but an underestimation of mixing ratio is observed. Moreover, the five schemes have different relative behavior in the city of Milan.
In order to better analyze those differences, Figure 15 shows the bias diurnal variation of 2-m temperature, 2-m mixing ratio and 10-m wind speed at Milano Linate station.
MRF and YSU produce the highest temperature overestimations (MRF bias = 0.924 °K and YSU bias = 0.981 °K), but all schemes show the same daily trend of the mean bias. In the morning, temperatures predicted with UW have lower bias than the other schemes, while during the day all schemes show positive biases. Discrepancies among the five schemes are mainly related to nighttime hours, especially when YSU parameterization is considered. As reported by Hu et al. (2010), the enhanced stable nighttime vertical mixing included in the YSU scheme (Hong and

Kim, 2008) contributes to stronger downward fluxes that lead to higher temperature and lower moisture near the ground.

Table 5 – Performance statistics of the five configurations at Milano Linate station for 2m-temperature, 2m-mixing ratio and 10m-wind speed. Schemes are indicated as: ACM2 (Asymmetrical Convective Model version 2), MRF (Medium Range Forecast), MYJ (Mellor Yamada Janjic), YSU (Yonsei University), and UW (University of Washington Moist Turbulence). The best performances are highlighted in grey.

	ACM2	MRF	MYJ	UW	YSU
			Temperature (°K)		
Mean Obs	278.980	278.980	278.980	278.980	278.980
Mean Mod	279.586	279.904	279.369	279.189	279.961
MB	0.606	0.924	0.389	0.209	0.981
RMSE	1.972	2.170	1.975	2.110	2.093
r	0.896	0.886	0.885	0.878	0.897
			Mixing Ratio (g/kg)		
Mean Obs	4.735	4.735	4.735	4.735	4.735
Mean Mod	4.527	4.459	4.669	4.620	4.605
MB	-0.208	-0.276	-0.066	-0.115	-0.131
RMSE	0.693	0.729	0.637	0.636	0.688
r	0.874	0.871	0.886	0.888	0.869
			Wind Speed (m/s)		
Mean Obs	1.721	1.721	1.721	1.721	1.721
Mean Mod	2.419	2.536	2.593	2.639	2.699
MB	0.699	0.815	0.873	0.918	0.979
RMSE	1.563	1.702	1.738	1.845	2.092
r	0.331	0.270	0.218	0.407	0.300

Moreover, under nighttime stable conditions, non-local transport of the ACM2 scheme is shut down and the vertical mixing is merely caused to eddy diffusivity as in MYJ (Hu et al., 2010). As a consequence, ACM2 and MYJ have similar magnitudes in

reconstructing temperature and mixing ratio during the night. On the contrary, during daytime ACM2 shows a temperature variation more similar to non-local closure schemes.
Concerning mixing ratio, all runs show good agreement with measurements in the early morning, while a cold biases is observed during the afternoon and the night. The maximum mixing ratio error varies from run to run, with very little positive bias around 6 UTC for YSU and MYJ. A more substantial cold bias is highlighted form 9 to 18 UTC. As discusses later in this work, this is consistent with the bias trend observed in PBL height and it can be partially explained with an enhancing in vertical mixing during these hours. As a consequence, In Milan, all runs produce mixing ratio that are lower than observed. The higher biases are associated to MRF and ACM2, with values of -0.276, -0.208 g/kg, respectively. YSU has a similar behavior, but better overall performances, showing a bias of -0.131 g/kg.
During unstable daytime conditions, MRF, ACM2 and YSU use the same non-local closure approach to simulate mixing inside PBL, and this can lead to the similar behavior in reproducing the temperature and mixing ratio trend.
The diurnal variation of wind speed is analyzed in Figure 15. All schemes confirm a difficulty in reconstructing the daily pattern of wind field. In particular, runs show a positive bias that ranges from 0.699 m/s (ACM2) to 0.979 m/s (YSU), because of an overestimation of the observed values during the early morning and night. YSU scheme is found to generate the highest bias in the nighttime hours. Hong and Kim (2008) demonstrated that the increasing in the critical Richardson number during stable boundary conditions is responsible to the enhanced mixing when winds are generally weak. On the contrary, YSU has the lowest bias in correspondence of midday.
After the sunset ACM2 run produces lower overestimations than runs with MRF, MYJ or YSU. MYJ is also reported in Zhang and Zheng (2004) and Hu et al. (2010) to produce high wind speeds near the ground.

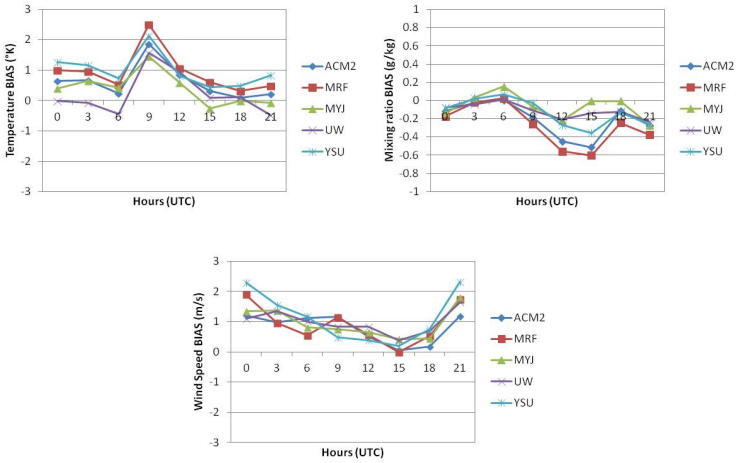

Figure 15 – Diurnal variation of bias index at Milano Linate station.

Finally, the modeled and observed vertical profiles are shown for comparison. Vertical profiles enable to further and better elucidate discrepancies observed in modeled results. From Figure 16 to Figure 21 are depicted the simulated and measured potential temperature, relative humidity and wind speed profiles at Milano Linate station for some days of the PBL experimental campaigns (February 6th and February 12th at 5, 11 and 23 UTC).

The early morning and night profiles show increasing potential temperature (inversion), decreasing humidity and wind shear with height. The local closure schemes have produced more realistic profiles than the non-local schemes.

In the convective conditions during daytime the above parameters are expected to have less pronounced variation with height in the well-mixed boundary layer. Wind speed shows important differences from run to run, but generally non-local closure schemes are closer to observations.

Local closure schemes have similar vertical wind profile on February 6th at 11UTC with higher wind speed in the first 500 m than all other

schemes. Differently, when the vertical profile of February 12th is analyzed, MYJ shows a larger surface wind speed than UW that results more similar to YSU. Both UW and YSU used an explicit term for simulating the entrainment zone, suggesting that either entrainment fluxes or the kind of closure play a key role in determining turbulence in the first meters of atmosphere during unstable conditions.

Moreover, analyzing the vertical profile of February 6th at 11 UTC is quite clear that MYJ an UW have higher moisture and lower potential temperature than the other schemes below 500 m, while schemes are more similar above. Once again this can be partially related by the entrainment fluxes. As extensively discussed by Srinivas et al. (2007) and Hu et al (2010), a possible explanation is a weak entrainment from the free troposphere in local schemes. The air above the PBL has higher potential temperature and less moisture than PBL air. A lack in the entrainment fluxes transport less warmer and drier air into the local PBL schemes with respect to YSU, ACM2 and MRF run, even though different entrainment approaches are used.

Relative humidity profiles can be also analyzed in order to obtain a first validation of PBL height. Since relative humidity is maximum inside the PBL (Seinfred and Pandis, 1998), it is possible to approximately estimate PBL depth looking at the height where relative humidity drops to a lower value. Vertical profiles indicate that relative humidity is characterized by an increasing from the ground level to a layer where a strong negative gradient is present. This layer is generally included in the first 500 m of the lower troposphere. The vertical profiles of February 6th shows that YSU, MYJ and UW predict the lowest PBL values around noon, while MRF and ACM2 overestimates measured profile. On the other hand, the vertical profile of February 12th displays that all schemes overestimate PBL height at 11 UTC.

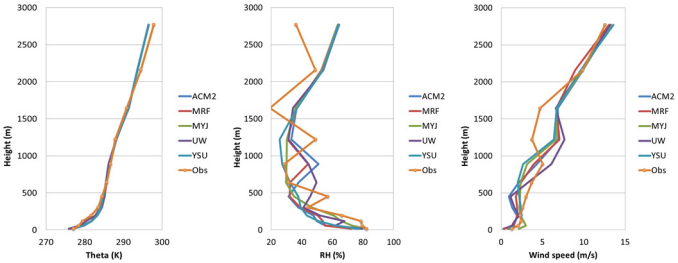

Figure 16 - Vertical profile of potential temperature, relative humidity and wind speed on February 6th at 5.00 UTC.

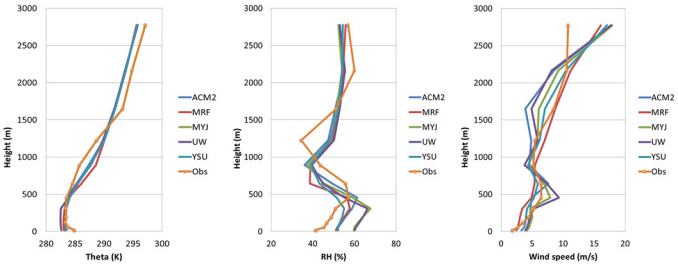

Figure 17 - Vertical profile of potential temperature, relative humidity and wind speed on February 6th at 11.00 UTC.

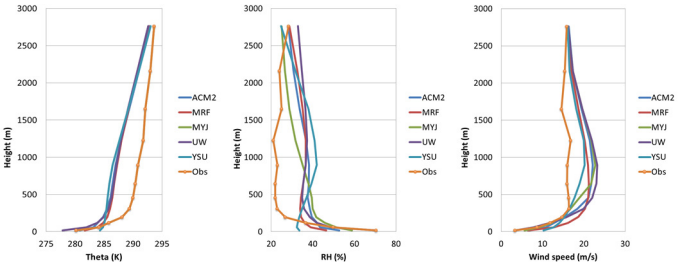

Figure 18 - Vertical profile of potential temperature, relative humidity and wind speed on February 6th at 23.00 UTC.

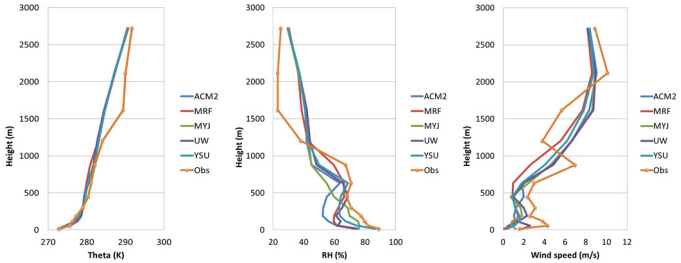

Figure 19 - Vertical profile of potential temperature, relative humidity and wind speed on February 12th at 5.00 UTC.

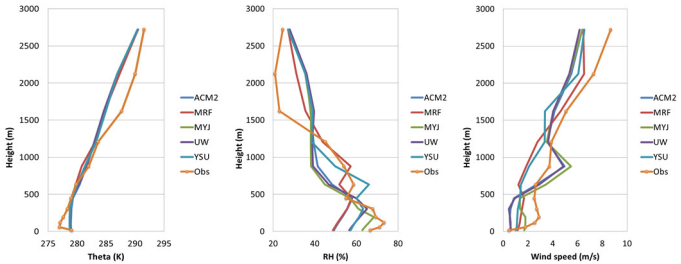

Figure 20 - Vertical profile of potential temperature, relative humidity and wind speed on February 12th at 11.00 UTC.

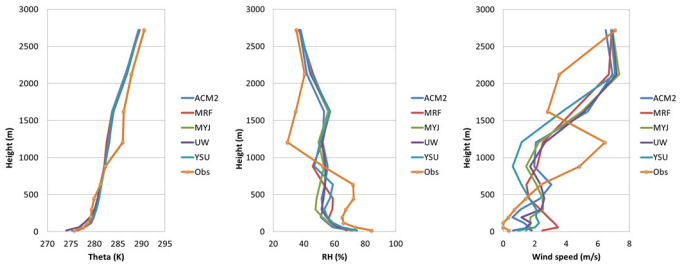

Figure 21 - Vertical profile of potential temperature, relative humidity and wind speed on February 12th at 23.00 UTC.

2.2.2 Planetary Boundary Layer height

Figure 22 depicts the monthly mean variation of the Planetary Boundary Layer height over the Po valley area. MYJ has the highest depths over the region, while UW shows the lowest average values. ACM2 and YSU have a similar general pattern that, in the midst of the valley, it is also close to MRF.

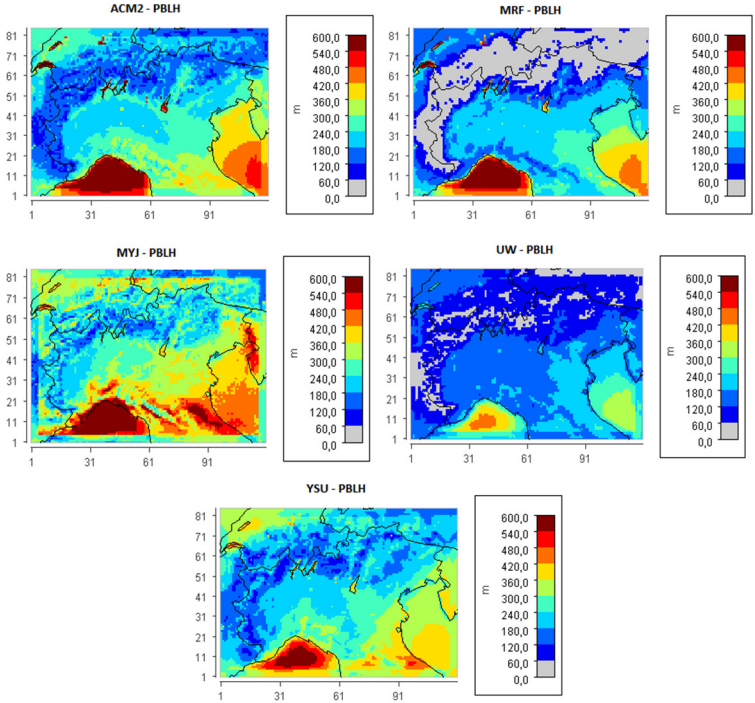

Figure 22 – Monthly mean of Planetary Boundary Layer height (PBLH) in the five parameterizations.

Table 6 shows performance statistics of the five parameterizations for both balloon and Lidar comparisons at Torre Sarca (Milan). It is worth noting that balloon soundings were available only in the morning, making them representative only of the early evolution of the PBL height.

Table 6 – Performance indexes in the five configurations for PBL height. Schemes are indicated as: ACM2 (Asymmetrical Convective Model version 2), MRF (Medium Range Forecast), MYJ (Mellor Yamada Janjic), YSU (Yonsei University), and UW (University of Washington Moist Turbulence). The best performances are highlighted in grey.

	ACM2	MRF	MYJ	UW	YSU
			Balloon		
Count	27	27	27	27	27
Mean Obs (m)	260.88	260.88	260.88	260.88	260.88
Mean Mod (m)	376.22	369.81	360.65	217.06	291.03
MB (m)	115.34	108.93	99.77	-43.82	30.15
RMSE (m)	211.76	186.89	185.17	137.39	104.64
r	0.60	0.71	0.59	0.51	0.76
			Lidar		
Count	219	219	219	219	219
Mean Obs (m)	271.57	271.57	271.57	271.57	271.57
Mean Mod (m)	274.57	222.04	321.60	171.76	244.03
MB (m)	3.00	-49.53	50.04	-99.81	-27.54
RMSE (m)	170.75	189.96	168.82	181.32	156.94
r	0.84	0.84	0.66	0.83	0.68

As discussed previously, in the city of Milan the five parameterizations perform differently.

In the morning, UW and YSU prove to have a quite coherent behavior in reproducing PBL height. Indeed, they have the best performances when compared to balloon data, even though UW is found to underestimate the observation (bias = -43.82 m) while YSU overpredicts the overall morning values (bias = 30.15 m). As discussed before, given the same way they compute the entrainment fluxes into the PBL, this ranking makes sense for these two schemes. Indeed, both differences in reconstructing vertical mixing (non-local and local closure) and entrainment would create differences in the vertical development of the PBL.

Also analyzing the diurnal variation of the mean bias is possible to state that YSU and UW give to lower bias in reconstructing the hourly evolution of PBL until 12.00 UTC (Table 7).

Table 7- Hourly variation of bias index in the five configurations for PBL height balloon campaign. Schemes are indicated as: ACM2 (Asymmetrical Convective Model version 2), MRF (Medium Range Forecast), MYJ (Mellor Yamada Janjic), YSU (Yonsei University), and UW (University of Washington Moist Turbulence). The best performances are highlighted in grey.

BIAS (m)	ACM2	MRF	MYJ	UW	YSU
7:00-8:00	-121.13	-122.97	-78.33	-144.85	-132.27
8:00-9:00	-2.66	38.73	19.21	-81.91	-5.25
9:00-10:00	175.34	159.63	160.85	-82.96	52.10
10:00-11:00	220.27	191.81	169.96	49.82	103.43
11:00-12:00	248.05	200.75	164.44	59.85	78.42

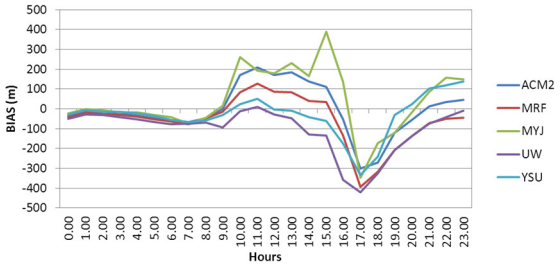

Figure 23 - Diurnal trend of bias index in the five configurations for PBL height Lidar data.

Both parameterizations underpredict balloon measurements from 7.00 to 9.00 UTC and overestimate them from 10.00 to 12.00 UTC. However, the largest overestimations are associated to ACM2 and MRF between 11.00 to 12.00 UTC (ACM2 bias = 248.05 m and MRF bias = 200.75 m). This is consistent with previous studies (Hong et al., 2006) in which it was demonstrated that YSU PBL increases the thermally induced mixing, while decreases the mechnically convection with respect to MRF, thus, partially resolving the problem of early development of PBL before noon.

Comparisons with Lidar measurements allow analyzing the performances over the whole day. It is evident from Figure 23 that all schemes have the same general trend. In the morning, they show small negative biases which slightly increase around 9.00 UTC, reaching the higest values in the afternoon, and then decreasing againg after 15.00 UTC. This general trend implyes some common errors in all runs, such as the overprediction of temperature and wind speed. Indeed the diurnal variations of the performance index is consistent with the bias daily trend of temperature discussed previously. All schemes were found to have the major temperature overestimation from 9.00 to 15.00 UTC when PBL mixing and biases increase. Moreover, the raising in PBL heights can help explaining the consequently deacreasing in mixing ratio observered at that hours.

Table 6 and Figure 23 show that among the five schemes YSU and ACM2 are the most accurate overall. The YSU scheme is especially accurate during midday.

In particular, all schemes underestimate morning values, while MRF, ACM2 and MYJ overpredicted PBL depth around noon. A slight overestimation is also highlighted for YSU from 10.00 to 12.00 UTC, consitent with the balloon observations. On the contrary, UW generally underpredics Lidar data, even though a positive bias is visible around 11.00 UTC.

ACM2 gives the best performances during the evening and night thus improving its overall performances (bias = 3 m).

A further comparison can be done in terms of hourly trend. Figure 24 and Figure 25 depict the hourly modeled PBL height evolution compared to balloon and Lidar data, respectively.

As can be seen from these figures, there are substantial differences among the parameterizations. In the early hours of the day there is closer agreement between models and among these and both Lidar and balloon observations. Deviation between simulated and observed grows with time. Indeed, the daytime development of PBL appears to be too rapid in all simulations. The largest overestimation exists for MRF, MYJ and ACM2 around noon. Under unstable conditions, ACM2 and MRF schemes compute PBL height using a similar

method, and since the simulations with those schemes used the same surface layer, it makes sense that PBL heights are comparable. Moreover ACM2, MYJ and MRF adopt the same approach in reconstructing the entrainment process, influencing the PBL development in a similar way.

The best agreement in reconstructing the PBL height can be shown in the YSU scheme in both Lidar and balloon comparisons, while UW generally under predicted its magnitude.

Moreover all schemes show a too rapid decrease of PBL that collapses to the night-time value by 17.00 UTC, while Lidar data seem to show a smoother profile. The problem of the smooth decay during the afternoon transition of the PBL height during nighttime hours has been discussed previously, making challenging the comparison between model results and Lidar data.

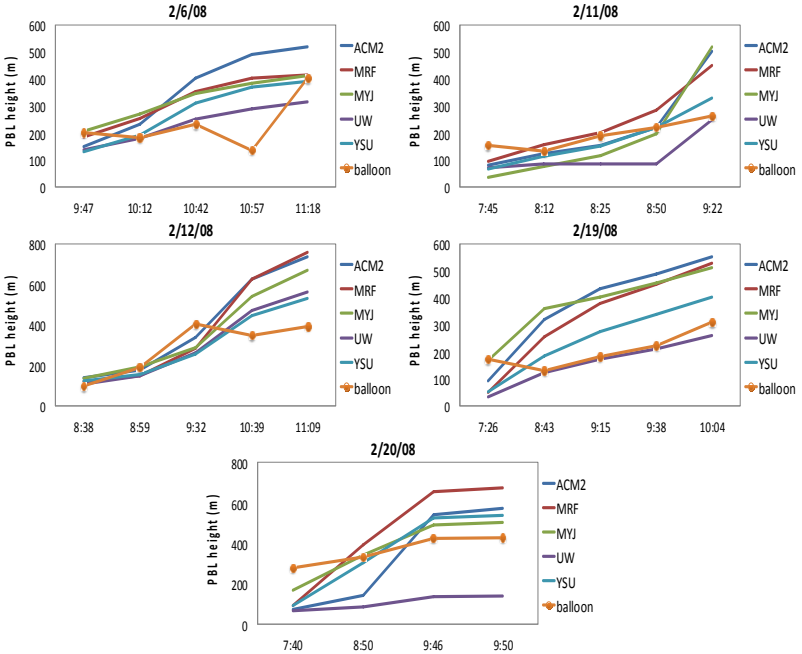

Figure 24 - Comparison of PBL schemes to balloon observations in Torre Sarca. Time is expressed in UTC.

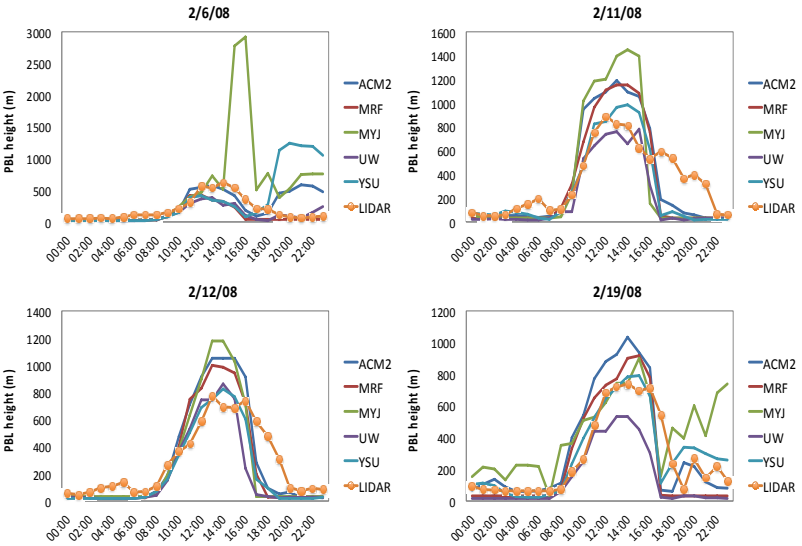

Figure 25 - Comparison of PBL schemes to Lidar measurements in Torre Sarca. Time is expressed in UTC.

2.3 CONCLUSIONS

The WRF model has been applied over the Po Valley area and compared against measurement stations, vertical profiles by balloon soundings and Lidar data in order to assess the skill of the meteorological model in reproducing PBL structure and evolution. Five PBL schemes have been tested for a 5 km simulation. Three non-local closure schemes (ACM2, MRF and YSU) and two local closure parameterizations (MYJ and UW) have been selected.

Vertical profiles of aerosol distribution and Lidar measurements were collected in the area of Milan together with surface temperature, mixing ratio and wind speed of different meteorological sites.

Results show that all five parameterizations produce similar performances, overestimating temperature, mixing ratio and wind speed, implying some common errors in all model runs.

The highest biases are generally associated to MYJ and UW that use the Janjic Eta Monin–Obukhov surface layer scheme that was found to deliver a greater amount of sensible and latent heat fluxes with respect to Monin–Obukhov surface layer scheme. Analyzing only the city of Milan, runs follow the previous general pattern, over predicting temperature and wind speed, but an underestimation of mixing ratio is observed. Moreover, the five schemes have different relative behavior. UW and ACM2 have better performances of temperature, mixing ratio and wind speed than the other schemes. The best performances are related to their ability to predict more reliable results during the morning and evening. Indeed, ACM2 and UW use the same local closure during nighttime conditions that lead to an improving in model performances.

Over predictions of temperature and wind speed are found to cause a general overestimation of mixing during the PBL development in the city of Milan. In the early hours of the day there is a close agreement between models and among these and observations. However, deviation between simulated and observed grows with time. Indeed, the daytime development of PBL appears to be too rapid in all simulations. The largest overestimation exists for MRF, MYJ and ACM2 around noon as they use the same approach in reconstructing the entrainment process. Moreover, under unstable conditions, ACM2 and MRF schemes compute PBL height using the same non-local closure scheme. The best agreement in reconstructing the PBL height was highlighted for YSU. On the contrary, UW generally underpredicted PBL magnitude at all daytime hours.

Results suggest some systematic errors in all PBL schemes, that can be useful to direct other modeling approaches. However, due to the nature of PBL and its extremely spatial variability, it is advised to use this working outcomes for domains with meteorological and geographical situations similar as the Po valley.

PBL hourly evolution is essential to the good reconstruction of the ground concentration fields, especially when stagnant conditions occur. Since all parameterizations produce similar performances over the Po valley in terms of meteorological variables, we have chosen the scheme that gives best results in reconstructing the PBL

development during the day, namely the Yonsei University PBL scheme (YSU). For the aforementioned reason the YSU PBL scheme will be used in the air quality simulations over Italy.

2.4 REFERENCES

Amiridis, V. , Melas, D. , Balis, D.S., Papayannis, A. , Founda, D., Katragkou, E., Giannakaki, E., Mamouri, R.E., Gerasopoulos, E., Zerefos, C., 2007. Aerosol lidar observations and model calculations of the planetary boundary layer evolution over Greece, during the March 2006 total solar eclipse. Atmospheric Chemistry and Physics 7, 6181–6189.

Angelini, F., Barnaba, F., Landi, T. C., Caporaso, L., Gobbi, G. P., 2009. Study of atmospheric aerosols and mixing layer by LIDAR. Radiation Protection Dosimetry 137 (3-4), 275-279, doi: 10.1093/rpd/ncp219.

Appel, K.W., Gilliam, R.C., Davis, N., Zubrow A. and Howard, S.C., 2011. Overview of the atmospheric model evaluation tool (AMET) v1.1 for evaluating meteorological and air quality models. Environmental Modelling & Software 26, 434 – 443, doi: 10.1016/j.envsoft.2010.09.007.

Borge, R., Alexandrov, V., del Vas, J. J., Lumbreras, J., Rodrıguez, E., 2008. A comprehensive sensitivity analysis of the WRF model for air quality applications over the Iberian Peninsula. Atmospheric Environment 42, 8560–8574, doi: 10.1016/j.atmosenv.2008.08.032.

Bretherton, C. S., Park, S., 2009. A New Moisture Parameterization in the Community Atmosphere Model. Journal of Climate 22, 3422-3448, doi: 10.1175/2008JCLI2556.1.

Chen, F., Dudhia, J., 2001. Coupling an Advanced Land Surface–Hydrology Model with the Penn State–NCAR MM5 Modeling System. Part I: Model Implementation and Sensitivity. Monthly Weather Review 129, 569–585.

Chou, M.-D., Suarez, M. J., Ho, C.-H., Yan, M. M.-H., Lee, K.-T., 1998. Parameterizations for cloud overlapping and shortwave single-scattering properties for use in general circulation and cloud ensemble models. J. Clim. 11, 202-214.

Cohn, S.A. , Angevine, W.M., 2000. Boundary layer height and entrainment zone thickness measured by lidars and wind-profiling radars. Journal of Applied Meteorology 39, 1233–1247.

Endlich, R.M., Ludwig, F.L., Uthe, E.E., 1967. An automatic method for determining the mixing depth from lidar observations. Atmospheric Environment 13(7), 1051–1056.

Ferrero, L., Perrone, M. G., Petraccone, S., Sangiorgi, G., Ferrini, B. S., Lo Porto, C., Lazzati, Z., Cocchi, D., Bruno, F., Greco, F., Riccio, A., Bolzacchini, E., 2010. Vertically-resolved particle size distribution within and above the mixing layer over the Milan metropolitan area. Atmos. Chem. Phys. 10, 3915–3932.

Ferrero, L., Riccio, A., Perrone, M.G., Sangiorgi, G., Ferrini, B.S., Bolzacchini, E., 2011. Mixing height determination by tethered balloon-based particle soundings and modeling simulations. Atmospheric Research 102, 145-156, doi:10.1016/j.atmosres.2011.06.016.

Ferrero, L.; Mocnik, G.; Ferrini, B.S.; Perrone, M.G.; Sangiorgi, G.; Bolzacchini, E., 2011. Vertical profiles of aerosol absorption coefficient from micro-Aethalometer data and Mie calculation over Milan. Sci. Total Environ. 409 (14), 2824–2837.

Ferrero, L.; Cappelletti, D.; Moroni, B.; Sangiorgi, G.; Perrone, M.G.; Crocchianti, S.; Bolzacchini, E., 2012. Wintertime aerosol dynamics and chemical composition across the mixing layer over basin valleys. Atmos. Environ. 56, 143-153.

Gandino, C., Leyendecker, W., Sandroni, S., 1990. Northern Foehn and ground-level ozone at Ispra. Il Nuovo Cimento 13 (3), 669–676.

Grell, G. A., Devenyi, D., 2002. A generalized approach to parameterizing convection combining ensemble and data assimilation techniques. Geophys. Res. Lett. 29(14), 1693.

Grell, G., J. Dudhia, and D. Stauffer, 1994. A description of the Fifth-Generation Penn State/NCAR Mesoscale Model (MM5). NCAR Tech. Note. NCAR/TN-3981STR, 117 pp.

Grell, Peckham, Schmitz, McKeen, Frost, Skamarock and Eder, 2005. Fully coupled “online” chemistry within the WRF model. Atmospheric Environment, 39(37), 6957-6975.

Haefflin, M. F. Angelini, Y. Morille, G. Martucci, S.Frey, G.P.Gobbi, S.Lolli, C.D.O'Dowd, L. Sauvage, I. Xueref-Rémy, B. Wastine, D. G. Feist, 2012. Evaluation of Mixing Height Retrievals from Automatic Profiling Lidars and Ceilometers in View of Future Integrated Networks in Europe. Boundary-Layer Meteorology 143(1), 49-75. doi: 10.1007/s10546-011-9643-z.

Hong, S.-Y., Pan, H.-L., 1996. Nonlocal Boundary Layer Vertical Diffusion in a Medium-Range Forecast Model. Monthly Weather Review 124, 2322–2339.

Hong, S.-Y., Noh, Y., Dudhia, J., 2006. A New Vertical Diffusion Package with an Explicit Treatment of Entrainment Processes. Monthly Weather Review 134, 2318-2341.

Hong, S.-Y., Kim, S. K., 2008. Stable boundary layer mixing in a vertical diffusion scheme. Proc. Ninth Annual WRF User's Workshop, Boulder, CO, National Center for Atmospheric Research, 3.3. [Available online at:
http://www.mmm.ucar.edu/wrf/users/workshops/WS2008/abstracts/3-03.pdf.]

Hu, X.-M., Nielsen-Gammon, J. W., 2010. Evaluation of Three Planetary Boundary Layer Schemes in the WRF Model. Journal of Applied Meteorology and Climatology 49, 1831-1844, doi: 10.1175/2010JAMC2432.1.

Janjic, Z. I., 1994. The Step-Mountain Eta Coordinate Model: Further Developments of the Convection, Viscous Sublayer, and Turbulence Closure Schemes. Monthly Weather Review 122, 927-945.

Janjic, Z. I., 2001. Nonsingular implementation of the Mellor-Yamada level 2.5 scheme in the NCEP Meso model. NOAA/NWS/NCEP Office Note 437, 61 pp.

Kim, S.W., Yoon, S.C., Won, J.G., Choi, S.C., 2007. Ground-based remote sensing measurements of aerosol and ozone in an urban area: a case study of mixing height evolution and its effect on ground-level ozone concentrations. Atmospheric Environment 41, 7069–7081.

Laakso, L., Grönholm, T., Kulmala, L., Haapanala, S., Hirsikko, A., Lovejoy, E.R., Kazil, J., Kurtén, T., Boy, M., Nilsson, E.D., Sogachev, A., Riipinen, I., Stratmann, F., Kulmala, M., 2007. Hot-air balloon as a

platform for boundary layer profile measurements during particle formation Boreal. Environment Research 12, 279–294.

Lin, J.-T., Youn, D., Liang, X.-Z., Wuebbles, D. J., 2008. Global model simulation of summertime U.S. ozone diurnal cycle and its sensitivity to PBL mixing, spatial resolution, and emissions. Atmospheric Environment 42 (36), 8470-8483, doi: 10.1016/j.atmosenv.2008.08.012.

Maletto, A., McKendry, Strawbridge, K.B., 2003. Profiles of particulate matter size distributions using a balloon-borne lightweight aerosol spectrometer in the planetary boundary layer. Atmospheric Environment 37, 661-670.

McKendry, I.G., Sturman, A.P., Vergeiner, J., 2004. Vertical profiles of particulate matter size distributions during winter domestic burning in Christchurch, New Zealand. Atmospheric Environment 38, 4805–4813.

Martucci, G., R. Matthey, V. Mitev, H. Richner, 2007. Comparison between Backscatter Lidar and Radiosonde Measurements of the Diurnal and Nocturnal Stratification in the Lower Troposphere. J. Atmos. Oceanic Technol., 24, 1231–1244. doi: http://dx.doi.org/10.1175/JTECH2036.1.

Melfi, S. H., J. D. Spinhirne, S-H. Chou, S. P. Palm, 1985. Lidar Observations of Vertically Organized Convection in the Planetary Boundary Layer over the Ocean. J. Climate Appl. Meteor., 24, 806–821.

Mellor, G. L., Yamada, T., 1982. Development of a Turbulence Closure Model for Geophysical Fluid Problems. Reviews of Geophysics and Space Physics 20 (4), 851-875.

Misenis, C., Zhang, Y., 2010. An examination of sensitivity of WRF/Chem predictions to physical parameterizations, horizontal grid spacing, and nesting options. Atmospheric Research 97, 315–334.

Misenis, C., X.-M. Hu, S. Krishnan, Y. Zhang, and J. Fast, 2006. Sensitivity of WRF/Chem predictions to meteorological schemes. Proc. 86th Annual Conference/14th Joint Conf. on the Applications of Air Pollution Meteorology with the A&WMA, Atlanta, GA, Amer. Meteor. Soc., paper 1.8.

Mlawer, E.J., Taubman, S.J., Brown, P.D., Iacono, M.J., Clough, S.A., 1997. Radiative transfer for inhomogeneous atmospheres: RRTM, a validated correlated-k model for the longwave. Journal of Geophysical Research 102, 16663–16682.

Monin, A. S., Obukhov, A. M., 1954. Basic Laws of Turbulent Mixing in the Ground Layer of the Atmosphere. Trans. Geophys. Inst. Akad. Nauk. USSR 151, 163–187.

Morille, Y., M. Haeffelin, P. Drobinski, J. Pelon, 2007. STRAT: An Automated Algorithm to Retrieve the Vertical Structure of the Atmosphere from Single-Channel Lidar Data. J. Atmos. Oceanic Technol., 24, 761–775. doi: http://dx.doi.org/10.1175/JTECH2008.1

Morrison, H., J. A. Curry, V. I. Khvorostyanov, 2005. A New Double-Moment Microphysics Parameterization for Application in Cloud and Climate Models. Part I: Description. J. Atmos. Sci., 62, 1665–1677. doi: http://dx.doi.org/10.1175/JAS3446.1

Morrison, H., Thompson, G., Tatarskii, V, 2009. Impact of cloud micrpohysics on the development of trailing stratiform precipitation in a simulated squall line: Comparison of one- and two-moment schemes. Monthly Weather Review 137, 991-1007, doi: 10.1175/2008MWR2556.1..

Pleim, J. E., 2007. A Combined Local and Nonlocal Closure Model for the Atmospheric Boundary Layer. Part I: Model Description and Testing. Journal of Applied Meteorology and Climatology 46, 1383-1395, doi: 10.1175/JAM2539.1.

Pleim, J. E., Chang, J. S., 1992. A non-local closure model for vertical mixing in the convective boundary layer. Atmos. Environ. 26A, 965–981.

Rodriguez, S., Van Dingenen, R., Putaud, J.P. , Dell'Acqua, A., Pey, J., Querol, X., Alastuey, A., Chenery, S., Ho, K.F., Harrison, R., Tardivo, R., Scarnato, B., Gemelli, V., 2007. A study on the relationship between mass concentration, chemistry and number size distribution of urban fine aerosol in Milan, Barcelona and London. Atmospheric Chemistry and physics 7, 2217–2232.

Seibert, P, Beyrich, F., Gryning, S.E., Joffre, S., Rasmussen, A., Tercier, P., 2000. Review and intercomparison of operational methods for the determination of the mixing height. Atmospheric Environment 34, 1001-1027.

Seinfeld, J.H., and S.N. Pandis. 1998. Atmospheric Chemistry and Physics, From Air Pollution to Climate Change. John Wiley and Sons, Inc., NY.

Skamarock W.C., Joseph B. Klemp, Jimy Dudhia, David O. Gill, Dale M. Barker, Michael G. Duda, Xiang-Yu Huang, Wei Wang , Jordan G. Powers, 2008. A Description of the Advanced Research WRF Version 3, NCAR Technical Note NCAR/TN-475+STR, Boulder, Colorado.

Srinivas, C. V., R. Venkatesan, and A. Bagavath Singh, 2007. Sensitivity of mesoscale simulations of land-sea breeze to boundary layer turbulence parameterization. Atmos. Environ., 41, 2534–2548.

Stull Roland B., 1989. An introduction to Boundary Layer Meteorology. Kluwer Academic Publishers, ISBN: 90-277-2769-4.

Taubman, B.F., Hains, J.C., Thompson, A.M., Marufu, L.T., Doddridge, B.G., Stehr, J.W., Piety, C.A., Dickerson, R.R., 2006. Aircraft vertical profiles of trace gas and aerosol pollution over the mid-Atlantic United States: statistics and meteorological cluster analysis. Journal of Geophysical Research 111, 1–14 D10S07.

Troen, I., Mahrt, L., 1986. A simple model of the atmospheric boundary layer: Sensitivity to surface evaporation. Bound. Layer Meteor. 37, 129-148.

Wiegner, M., Emeis, S., Freudenthaler, V., Heese, B., Junkermann, W., Münkel, C., Schäfer, K., Seefeldner, M., Vogt, S., 2006. Mixing layer height over Munich, Germany: variability and comparisons of different methodologies. Journal of Geophysical Research 111, D13201.

Yang, Q., Gustafson Jr., W.I., Fast, J.D., Wang, H., Easter, R.C., Morrison, H., 2011. Assessing regional scale predictions of aerosols, marine stratocumulus, and their interactions during VOCALS-REx using WRF-Chem. Atmospheric Chemistry and Physics Discussions 11, 22663e22718. doi:10.5194/acpd-11-22663-2011.

Yerramilli A., Challa V.S., Dodla V.B.R., Dasari H.P., Young J.H., Patrick C., Baham J.M., Hughes R.L., Hardy M.G., and Swanier S.J., 2010. Simulation of Surface Ozone Pollution in the Central Gulf Coast Region Using WRF/ChemModel: Sensitivity to PBL and Land Surface Physics. Advances in Meteorology, 319138, 1-24, doi:10.1155/2010/319138.

Zhang, Y., Liu, P., Pun, B., Seigneur, C., 2006. A comprehensive performance evaluation of MM5-CMAQ for the summer 1999 Southern Oxidants Study Episode - Part I. Evaluation protocols, databases and meteorological predictions. Atmospheric Environment 40, 4825–4838.

Zhang Y, and W.-Z. Zheng, 2004. Diurnal cycles of surface winds and temperatures as simulated by five boundary layer parameterizations. J. Appl. Meteor., 43, 157–169.

Zhong, S., In, H., Clements, C., 2007. Impact of turbulence, land surface, and radiation parameterizations on simulated boundary layer properties in a coastal environment. Journal of Geophysical Research 112, D13110.

3 INVESTIGATING IMPACTS OF CHEMISTRY AND TRANSPORT MODEL FORMULATION ON MODEL PERFORMANCE AT EUROPEAN SCALE

G. Pirovano, A. Balzarini, B. Bessagnet, C. Emery, G. Kallos, F. Meleux, C. Mitsakou, U. Nopmongcol, G.M. Riva, G. Yarwood

Published on Atmospheric Environment 53 (2012), 93-109.

Chemistry and transport models (CTMs) are essential tools to investigate the atmospheric fate of pollutants as well as to design and evaluate effective emission reduction strategies. CTMs include descriptions of the main chemical and physical processes driving air concentration of primary and secondary pollutants, such as sulphur and nitrogen oxides, ozone (Jacobson, 1996, Russell and Dennis, 2000) and particulate matter (Jacobson, 1997; Seigneur, 2001; Vautard et al., 2009).

For regional simulations, present data availability allows computed results to be compared against tens to hundreds of measuring sites in Europe and North America (Tesche et al., 2006; Morris et al., 2006; Van Loon et al., 2007) requiring the development of suitable methodologies, which enable robust findings and conclusions about model performance. In the last decades, several efforts were made to develop a systematic framework for model performance evaluation (MPE, Weil et al., 1992, Chang et Hanna, 2004). More recently Dennis et al. (2010) proposed a rather complete approach identifying

four main components including: operational, diagnostic, dynamical and probabilistic model evaluation.
The Air Quality Modeling International Initiative (AQMEII; http://aqmeii.jrc.ec.europa.eu/) was launched as a joint effort between the North American and the European modeling communities (Rao et al., 2011). In its first phase, it was focused on off-line CTMs in order to create a modeling testbed designed to systematically and objectively evaluate models against large number of stations. In this context, CAMx and CHIMERE models were applied and compared over the European domain for calendar year 2006, in order to obtain a comprehensive evaluation of the validation techniques that will be used for the future coupled simulations with WRF-Chem.
The CAMx and CHIMERE were driven by the same inputs (meteorology, emissions, boundary conditions) provided in the framework of the AQMEII exercise.
Model performance was investigated by sub-dividing the observational data set according to different criteria, such as station classification and geographical features. This effort was made to assess possible differences in model performance within the larger regional domain. In order to objectively evaluate differences between CAMx and CHIMERE, the Wilcoxon test was adopted (Wilks, 2006).

3.1 MODELS AND OBSERVATIONS

CAMx is a widely used three-dimensional photochemical Eulerian model that simulates the atmospheric fate of ozone and PM (ENVIRON, 2010). This study used CAMx version 5.21 with Carbon Bond 2005 (CB05) gas phase chemistry (Yarwood et al., 2005). The CAMx modeling domain was defined in latitude and longitude with 207 by 287 grid cells of resolution of 0.25° longitude by 0.125° latitude and 23 vertical layers. The CAMx surface layer exactly matched the MM5 surface layer and was about 30 m deep.

Further details on the CAMx set up can be found in Nopmongcol et al. (2012).
In this study, the CHIMERE model (Bessagnet et al., 2004; Vautard et al., 2005) was used in a configuration similar to that presented in Bessagnet et al. (2010) with MELCHIOR gas phase chemistry (Latuatti, 1997). In AQMEII, CHIMERE was applied over a domain covering part of the Europe continent (from 15°W to 35.25°E in longitude and from 35°N to 70.25 °N in latitude), with a constant horizontal resolution of 0.25° × 0.25°. The vertical grid contained 9 layers expressed in a hybrid-sigma pressure coordinate system, from the surface to 500 hPa. The first ground layer height was 20 m.
The model documentation is available at http://euler.lmd.polytechnique.fr/chimere. For both ozone and PM_{10} and its components, the model has undergone extensive inter-comparisons with other CTMs at European and urban scales (Bessagnet et al., 2004, 2010; Vautard et al., 2007 and Van Loon et al., 2007).

3.1.1 Input data

AQMEII participants were provided with a meteorological simulation for the year 2006, generated with MM5 model (Dudhia, 1993) for the European domain with resolution of 0.25° × 0.25°. The MM5CAMx preprocessor for CAMx was used to collapse the 32 vertical layers used by MM5 to 23 layers in CAMx and convert from the Mercator grid used by MM5 to a latitude-longitude grid. Both models used the planetary boundary layer (PBL) heights derived from MM5, apart from cloudy days during which the CHIMERE model considers the development of neutral conditions up to the cloud base (Bessagnet et al., 2009). The models adopt different parameterizations of vertical diffusion below the PBL height which, as discussed below, influenced pollutant dispersion under stable conditions (e.g. night-time).
The AQMEII emissions were prepared by TNO (Netherlands Organization for Applied Scientific Research), which provided a gridded emissions database for the year 2005 and 2006 (Pouliot et al., this issue). The dataset consists in European anthropogenic

emissions for the 10 SNAP sectors and international shipping with resolution of 0.125° longitude by 0.0625° latitude. A fire emissions inventory was provided by the Finnish Meteorological Institute (FMI).
The models shared the same emission inventories and the same emission temporal profiles, but the model-ready input files were prepared independently for each model giving rise to some discrepancies (Table 8).

Table 8 - Comparison of CAMx and CHIMERE domain-wide emissions, also split between surface and high level sources (ton/year).

	Surface		High level		Total	
	CAMx	**CHIMERE**	**CAMx**	**CHIMERE**	**CAMx**	**CHIMERE**
CO	51 899 170	35 819 210	29 982 570	27 793 180	81 881 740	63 612 390
NOx	12 986 190	12 377 892	5 282 967	5 115 994	18 269 157	17 493 886
NH_3	5 350 228	5 151 898	492 906	160 960	5 843 134	5 312 858
SO_2	4 396 024	4 318 913	9 657 167	9 291 435	14 053 191	13 610 348
PM10	5 497 295	2 707 733	4 378 300	4 803 718	9 875 595	7 511 451
ISOP	4 920 623	5 817 524	139	-	4 920 762	5 817 524
TERP	2 491 000	2 741 965	433	-	2 491 433	2 741 965
FORM	239 430	67 583	217 245	165 578	456 675	233 161
ETH	1 008 042	357 950	9 456	25 251	1 017 498	383 200
TOL	686 099	609 417	14 561	7 977	700 660	617 394

Particularly:.1) NOx, SO_2 and NH_3 emissions are slightly different because the CAMx computational domain is slightly larger than the CHIMERE domain; 2) the emission vertical distribution was defined from vertical profiles with less detail than the vertical structure of the two models giving rise to discrepancies in the fraction assigned to the surface layer; 3) the models adopted different assumptions to vertically distribute fire emissions which explains why the main differences occur for CO and PM_{10} emissions (Table 8). Biogenic VOC emissions were computed by both models by applying the

MEGAN emission model (Guenther et al., 2006). Sea salt emissions were computed separately using published algorithms (Monahan, 1986 for CHIMERE; de Leeuw et al., 2000 and Gong 2003 for CAMx) driven by MM5 meteorological fields. Boundary conditions for both models were derived from GEMS data (Schere et al., 2012) provided by the European Centre for Medium-Range Weather Forecasts (ECMWF).

3.1.2 Observations

Observed concentrations for calendar year 2006 were provided by the European database of national operational networks (AirBase). Data are available on the AirBase web site for all countries of European Union (http://air-climate.eionet.europa.eu/databases/airbase/). Observations of CO, NO_2, NOx, SO_2, O_3, PM_{10} and $PM_{2.5}$ were selected. Stations were chosen with data availability of 75% and higher. Stations showing outliers in yearly statistics were rejected. Only background stations (rural, suburban and urban) were chosen. A set of 1410 stations were found to fulfill the selection criteria with a total number of 29 countries represented. The station density of the selected dataset was adequate for NO_2, SO_2 O_3 and PM_{10} in Western Europe, while fewer stations were available for Eastern Europe. For NOx, CO and $PM_{2.5}$, monitoring stations were available only for a few countries.

Observations for PM in 2006 from the EMEP (European Monitoring and Evaluation Programme; http://www.emep.int/) database were used too. The PM_{10} measurements were available from 16 countries mostly on daily basis. The $PM_{2.5}$ measurements were available from 11 countries also on daily basis. Sulphate, nitrate and ammonium daily data were available from 24-36 EMEP stations

Four species, namely NO_2, SO_2, O_3 and PM_{10}, were selected for use in model evaluation because they provided a rather homogenous spatial coverage, in contrast to NOx, CO and $PM_{2.5}$. Where necessary, PM_{10} bulk observations data were integrated with $PM_{2.5}$ data as well as with aerosol composition data for nitrate, sulphate and ammonium. NO_2, SO_2 and PM_{10} concentrations were expressed as daily means whereas the daily maximum of the 8-hour running

average was chosen for O_3. The selected metrics for PM_{10} and O_3 are used to establish air quality standard in the European legislation (EU, 2008).

3.2 METHOD

Several concentration statistics and evaluation metrics can be selected to assess model performances (Boylan and Russel, 2006; Schluenzen and Sokhi, 2008; Dennis et al., 2010; Denby, 2011) and to compare results produced by different models (Potempski et al., 2008; Vautard et al., 2009; Thunis et al., 2011). To provide a comprehensive evaluation we selected 7 metrics whose mathematical expression is reported in the Appendix A1: Normalized Mean Bias (NMB), Normalized Mean Error (NME), Mean Fractional Bias (FB), Mean Fractional Error (FE), correlation (r), Index of Agreement (IA), Root Mean Square Error (RMSE). A preliminary analysis of model performance (not shown) revealed that some metrics provided very similar responses; for this reason detailed analysis was limited to a subset of 4 metrics: FB, FE, r and RMSE. One goal of this paper was to investigate the influence of geographical features on model skill. Following the approach of Putuad et al. (2010), the computational domain was split into 3 sub-regions (Figure 26): Southern Europe (SE), Northwestern Europe (NWE) and Eastern Europe (EE).

The SE sub-region is characterized by complex circulation conditions due to coastal areas and complex terrain, it experiences hot summers enhancing photochemical activity (Millán et al., 2000; Gangoiti et al., 2001) and it can be subject to dust episodes more frequently than the rest of Europe (Kallos et al., 2007; Mitsakou et al., 2008). The NWE sub-region is characterized by more homogenous circulation conditions than SE and comparison of PM_{10} composition reveals higher fractions of sea salt and, to a lesser extent, nitrate than other sub-regions (Putaud et al., 2010). The EE sub-region is characterized by a higher PM_{10} fraction of total carbon (Putaud et al., 2010) that could be related to emission characteristics that still distinguish Eastern European countries. Observation sites

were also categorized according to station type, following the official classification proposed by the European Environment Agency (EU, 1997): rural background stations (RB), suburban background stations (SB) and urban background stations (UB).

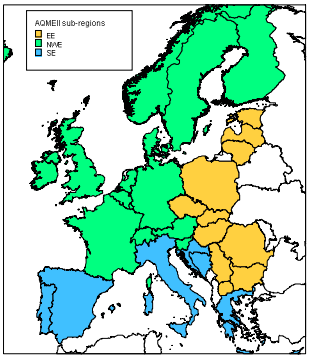

Figure 26 - Regions identified within the computational domain: Southern Europe (SE), North-Western Europe (NWE), Eastern Europe (EE). Countries without available observations are in white.

The Wilcoxon matched-pairs rank test (WMP, Wilks, 2006) was applied to perform the comparison between CAMx and CHIMERE skill. The WMP test is the non-parametric counterpart of the matched-pairs Student t-test. Being non-parametric, the test relaxes the constraint on normality of the underlying distributions (Gego et al., 2006). Firstly observation sites were categorized in subsets according to sub-region and stations type. For each subset, the pairs of metrics computed by CAMx and CHIMERE were submitted to the WMP to investigate whether the null hypothesis (i.e. the two series of metrics are not different) could be rejected or not. The probability level (p) of rejecting the hypothesis was set to 5%. In case of rejection (i.e. $p < 5\%$), model performance could be considered significantly different and a better performing model was identified.
The Wilcoxon-Mann-Witney test for unpaired series (WMU, Wilks, 2006) was applied to investigate differences in model performance within subsets of either region or station type. Subsets of metrics

were compared by using an index computed as follows: The WMU test was applied to each possible combination of subsets (e.g. NWE versus SE; NWE versus EE and SE versus EE, in case of regional comparison) of the 7 metrics previously described and then summing the total number of "non-negative scores"(NNS) of each subset. A non-negative score takes place when a subset performs not worse than the other one. The score ranges between 0 (the subset is always worse than the others for each metric) and 14 (the subset is always better or not significantly different than the others). NNS were computed for each model separately; for each station type in case of regional comparison and, conversely, for each region in case of station type comparison.

3.3 RESULTS AND DISCUSSION

3.3.1 Nitrogen dioxide

Figure 27 provides a concise comparison of model performance for NO_2 for each sub-region and station type. CHIMERE and CAMx showed a rather coherent behavior, meaning that in most cases they provided their best or worst performance in the same region or for the same kind of station. Best performance usually occurred at rural stations in the NWE sub-region. Model estimates show FB very close to 0, absolute errors (FE) lower than 50% on average and a small spread of the distribution for all metrics, suggesting that the level of performance is fairly homogenous in the whole region. In contrast, NO_2 performance in the SE sub-region was systematically worse than for other sub-regions) due to circulation conditions that are strongly influenced by local scale features, such as sea-land interface and complex terrain, often associated with low wind speeds and stable conditions. In all 3 sub-regions, both models showed a worsening in performance moving from rural to urban stations, driven by the growing influence of local scale emissions.

Correlation was less sensitive to station type and, quite surprisingly, displayed better performances at urban or suburban stations than rural ones for SE and EE regions. This is probably due to the

stronger variability at urban sites, between winter and summer observed concentrations, slightly enhancing correlation score.

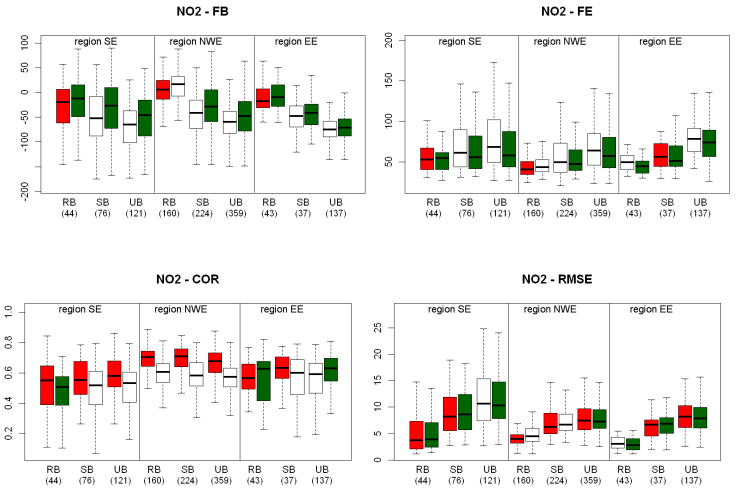

a)

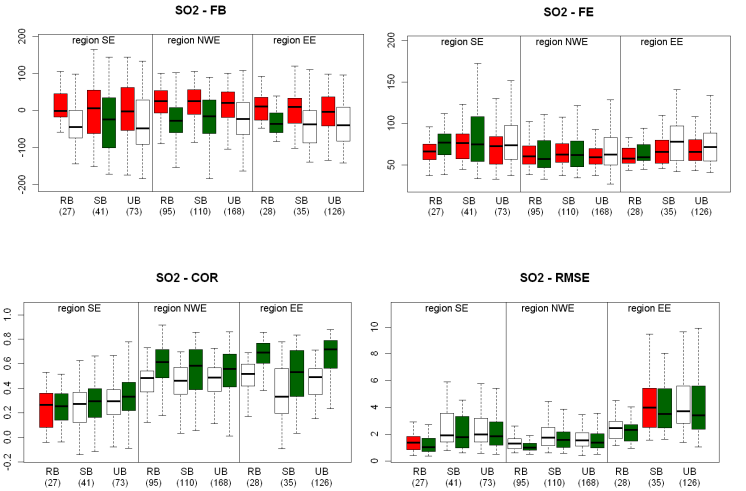

b)

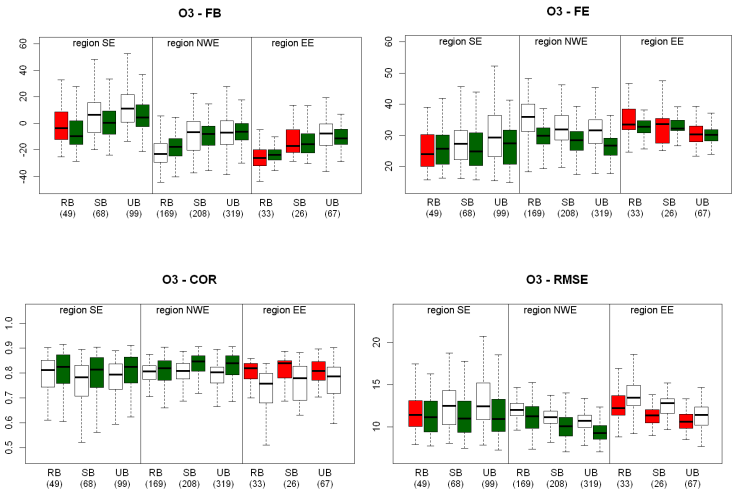

c)

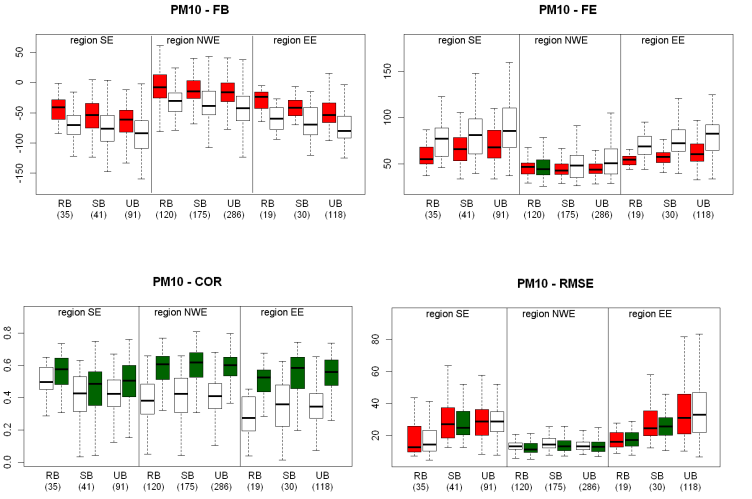

d)

Figure 27 - Box-whisker plots of the distribution of the different metrics computed for CAMx (red) and CHIMERE (green) in each region and for each kind of station. The number of stations is reported in brackets. The plot is unfilled for the worst model.

The WMP test was used to discriminate when CAMx and CHIMERE performance can be considered significantly different ($p < 5\%$). As illustrated in Figure 27, CAMx performed significantly better than CHIMERE in terms of correlation, while CHIMERE performed better than CAMx, when assessed by FB and FE.
The WMP test also allowed detection of differences in model performance that are not obvious from box-whisker plots. As an example, RMSE distribution at SB and UB sites of SE region seems to show comparable performance for CAMx and CHIMERE at both station types. However, the WMP test reveals statistically significant difference between the two models. This result stems from the WMP approach that takes into account the number of times that one model performs better than the other one. In this case, this means that CHIMERE is slightly but systematically more skillful than CAMx at UB stations.
Figure 28 shows the daily Box-whisker plots of the distribution of the observed and computed NO_2 concentration at SB sites of NWE and SE region. CHIMERE concentrations are almost always higher than CAMx, thus explaining the better score in FB and FE. Conversely, CAMx seems to better reproduce the weekly cycle of NO_2 concentrations, giving rise to a higher correlation skill. As discussed below, such differences are related to the different assumptions underlying the reconstruction of the vertical diffusion and the first layer wind speed in the two models.

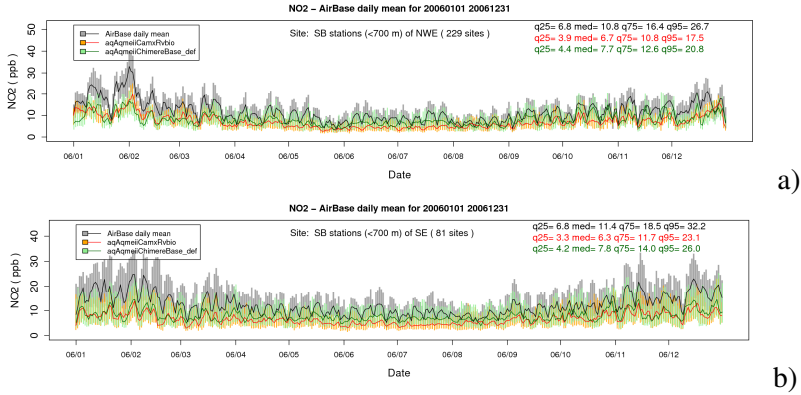

Figure 29 - Daily Box-whisker plots of the observed and computed NO_2 concentration at Suburban Background sites of NWE (a) and SE (b) regions. Observations are in black/grey; CAMx in red/orange and CHIMERE in dark green/light green. Bars show the 25th-75th quantile interval, while the median is displayed by the continuous line. The 25th, 50th, 75th, and 95th quantile of the yearly series are reported too.

3.3.2 Sulphur dioxide

Figure 27 compares CAMx and CHIMERE performance in simulating SO_2 concentrations. Concerning FB, CAMx performs better than CHIMERE showing a slight overestimation, whereas CHIMERE concentrations are underestimated. In contrast, CHIMERE shows better skill than CAMx in capturing temporal variability of observed concentrations, as shown by the correlation values. There is a clear worsening in model performance in the SE sub-region as discussed above for NO_2. Overall, geographical region is less important for SO_2 in CAMx but CHIMERE performance is clearly worst in the SE sub-region. Station type is less influential for SO_2 model skill because SO_2 emissions mainly come from aloft sources (Table 8) which disperse emissions widely. An exception is presented by RMSE for UB and SB stations in the EE region that show a clear worsening, increasing from 2 to 4 ppb, on average (Figure 27). This happens because surface level sources of SO_2 are still relevant in the EE region and they influence the observed concentrations at UB and SB sites (Hjellbrekke and Fjæraa, 2008).

Figure 30 shows the box-whisker time-series of SO_2 daily concentrations at SB stations for the EE and SE regions.
CAMx computes higher concentrations that result in better performance for FB but without reproducing the time series variability. Indeed, it can be noted that over EE stations, CAMx overestimates the lowest quantiles of the yearly series, while underestimating the highest ones. Moreover, the model tends to underestimate January-March concentrations, whereas the October-December period is overestimated. Similar conclusions can be drawn for SE stations where the spread of the observed distribution is well reproduced by both models, but not the temporal variability. Moreover, the seasonal cycle at SE stations is very smooth, causing further worsening in correlation estimates. Because point source stack parameters were lacking from the emission inventory both models were forced to assume static vertical profiles to distribute point source emission rather than calculating time-varying plume rise based on meteorological conditions.

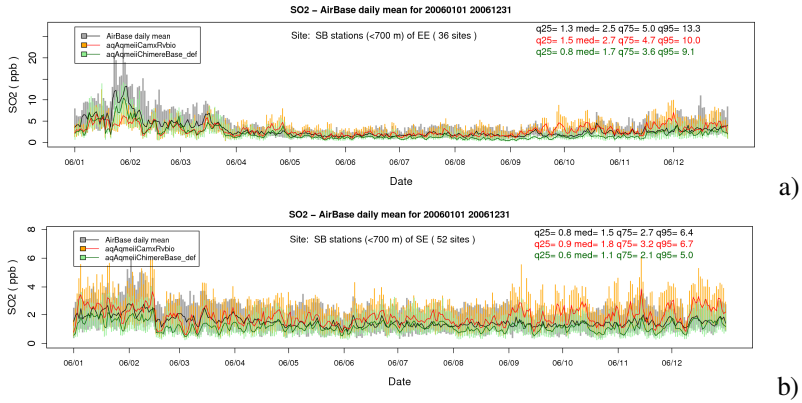

Figure 30 - Daily Box-whisker plots of the observed and computed SO_2 concentration at Suburban Background sites of EE (a) and SE (b) regions. Observations are in black/grey; CAMx in red/orange and CHIMERE in dark green/light green. Bars show the 25th-75th quantile interval, while the median is displayed by the continuous line. The 25th, 50th, 75th, and 95th quantile of the yearly series are reported too.

Figure 31 compares the daily mean SO_2 concentration computed by CAMx and CHIMERE for October 10th, 2006.
CAMx ground level concentrations are always higher than CHIMERE, above all urban and industrialized areas.

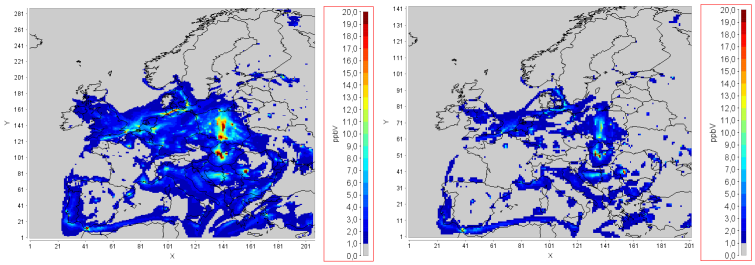

Figure 31– SO_2 daily mean concentration computed by CAMx (left) and CHIMERE (right) for October 10th, 2006.

To investigate the differences between the two models, Figure 32 compares the NO_2 and SO_2 vertical profiles computed by CAMx and CHIMERE from October 9th to October 11th at an industrial area close to Katowice (Poland), where SO_2 maximum concentrations are found.
NO_2 concentrations display a rather typical hourly profile driven by emissions and the Planetary Boundary layer (PBL) evolution and the models show similar behavior, although CAMx concentrations are higher than CHIMERE. Maximum ground level NO_2 concentrations are observed late in the evening due to ozone-NO titration combined with low PBL height. The latter also creates a sharp vertical gradient in NO_2 concentrations dropping from 20-30 ppb for CHIMERE and 25-35 ppb for CAMx at ground level to less than 12 ppb at 100 m above ground level (agl). Conversely, minimum values (around 6 ppb) are observed during daytime, due to chemical removal of NO_2 and a deeper PBL. SO_2 shows a relatively different profile, especially on October 10th and 11th when the highest concentrations are observed for both models. Both models show comparable profiles at noon on October 9th, but when the PBL collapses the models behave very differently: Both models display a concentration peak between

250 and 500 m agl, confirming the importance of aloft sources for SO_2 but CAMx has higher concentrations in the surface layer than aloft whereas CHIMERE has lower concentrations in the surface layer than aloft. Similar behavior, even enhanced, is shown on October 11th. Differences in the models results can be explained noting that: a) CAMx displays a sharp gradient close to ground level during stable conditions, while CHIMERE maxima take place mostly at higher altitude; b) CAMx concentrations are usually higher than CHIMERE inside the PBL, while at higher altitude (over 1000 m agl) CHIMERE values can be greater than CAMx. Considering that the models: a) shared the same emission inventory b) adopted the same vertical distribution for point source emissions c) showed similar dry deposition fields, the differences showed by the models can be ascribed to different assumptions in the description of the PBL processes for stable conditions.

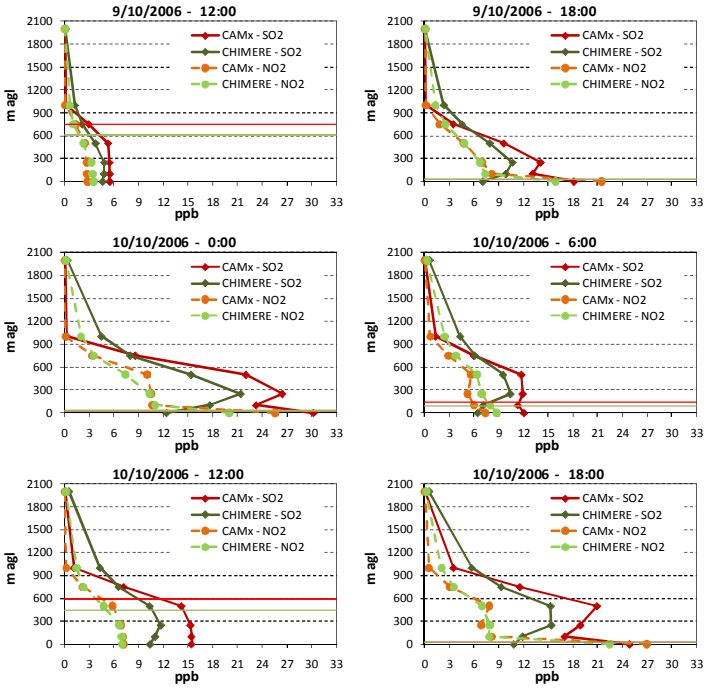

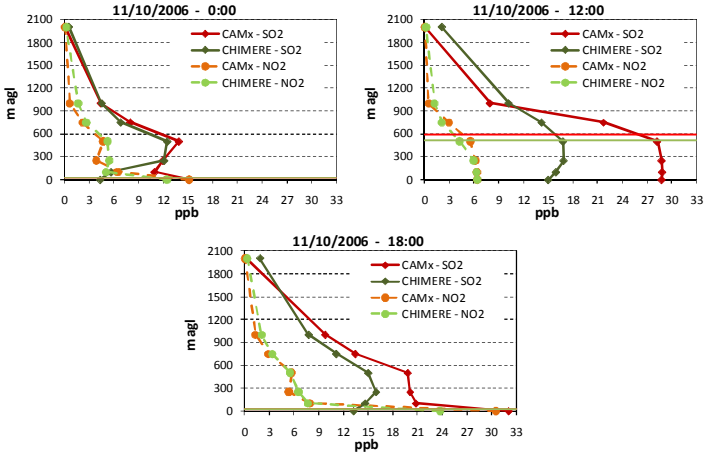

Figure 32 – Selection of hourly vertical profiles of NO_2 and SO_2 computed by CHIMERE (light and dark green) and CAMx (orange and red) at a site belonging to the industrial area of Katowice (Poland), between October 9th and 11th, 2006. Plots also display PBL height adopted by CAMx (red) and CHIMERE (green) at the same site.

3.3.3 Ozone

CAMx and CHIMERE also present coherent behavior for secondary pollutants.

The best performance for ozone (Figure 27) takes place in the SE sub-region, with FB values close to 0, whereas NWE and EE are characterized by a negative bias ranging from 10 to 30 %. Rather surprisingly, model performance clearly improves moving from rural to urban stations, where FB is close to 0. By examining the FE distribution conclusions similar to FB can be extracted, with values ranging, on average, from 20 to 30% in SE region and being greater than 30% in Eastern Europe. In contrast to NO_2, CHIMERE and CAMx did not show any statistically significant difference from region to region. For both metrics, CHIMERE skills are significantly better than CAMx for most subsets. Both models present a noticeable skill in terms of correlation. CHIMERE performed very well in SE and NWE regions showing correlation values higher than 0.8 at more than 50% of the selected sites and being significantly better than

CAMx. Conversely, CAMx performed better at EE sites, whereas CHIMERE correlation drops to values lower than 0.8 at most sites.
A clear worsening in CAMx performance is presented only for UB stations for the SE sub-region. This happens because O_3 concentrations at urban stations are rather influenced by local scale effects (e.g. titration) that are not well captured in the SE sub-region, because of the coarse resolution as well as the circulation characteristics of the area. Indeed, in the SE sub-region were included quite complex circulation areas (e.g. Italy and Greece) that were characterized by more frequent stagnant conditions than in NWE and EE sub-regions.
CHIMERE displays a very different behavior in the EE region where performance is always the worst. Such a discrepancy is driven by correlation at EE sites, which is clearly lower than the other regions.
Comparing O_3 model estimates for different station types showed a rather surprising outcome, where rural stations are usually worse than others. Such unexpected behavior could be driven by an error compensation or it could indicate that station classification is not correctly identified.
Figure 33 presents the box-whisker plots for daily maximum 8-hour O_3 for a few station subsets. Generally speaking, both models are able to follow the seasonal cycle of daily maximum ozone also reproducing most of the episodes taking place in the summer season. Simulated concentrations are slightly underestimated by both models, as shown by comparing the quantiles. CHIMERE performed better in reproducing the low concentrations, while CAMx better reproduced the median and high quantiles.
The analysis of the temporal evolution shows that model bias is mainly driven by a strong underestimation taking place during the first part of the year in the NWE and EE regions when both models show the strongest discrepancy. This feature is very clear at EE stations, thus explaining the significant differences in correlation. This underestimation of ozone during the first part of the year results from a lack of ozone in the northern boundary conditions, as explained through sensitivity simulations by Nopmongcol et al. (2012).

To investigate differences in model behavior, Figure 34 displays the temporal evolution of selected variables at a rural site in the EE region (PL0014A). The 5 day period, from February 28th to March 3rd, is characterized by the development of a spring ozone episode, with observed concentrations reaching 60 ppb. Observed wind speed ranges between 1 and 6 m/s. The models are able to capture the hourly evolution of wind speed but CHIMERE has lower wind speeds than CAMx because CHIMERE has a shallower surface layer (20 m) than MM5 (30 m) and therefore adjusted down the MM5 wind speeds, whereas CAMx has the same surface layer depth as MM5 and used the MM5 winds directly. CAMx and CHIMERE PBL heights are both derived from MM5, but the influence of the CHIMERE modification to PBL height during cloudy days is clearly evident for example on NOx and NO_2 concentrations at night on March 2nd. Conversely, when the PBL is very low in both models, the NOx and NO_2 concentrations simulated by CHIMERE are often higher than CAMx (e.g. evening hours of March 2-4). These differences result from the wind speed and the minimum value of the vertical dispersion coefficient (Kz) adopted by the models. The influence of these differences in meteorological fields is rather systematic as it can be inferred from the computed quantiles, better reproduced by CHIMERE than CAMx (Figure 34).

The differences in the reconstruction of wind and vertical diffusion aim in explaining the resulting differences in the night-time ozone concentrations. However comparing ozone time series, it can be noted that models differ in the reconstruction of the daytime build-up too, being stronger in CAMx than CHIMERE. Higher ozone concentrations can be also observed along the vertical profile, as shown in Figure 35, which illustrates the increase of CAMx concentrations from February 28th to March 4th. This difference could be attributed to the chemical mechanism, suggesting that CB05 is more effective than MELCHIOR in producing ozone. This behavior is clearly displayed by the increasing discrepancy between CAMx and CHIMERE daytime vertical profiles, inside the PBL. Moreover, ozone produced during daytime is accumulated in upper layers, enhancing the differences between the two models along the

development of the episode. As a final result, CAMx performed better than CHIMERE, because the stronger ozone production in CAMx compensated for underestimation in the background ozone caused by the boundary conditions.

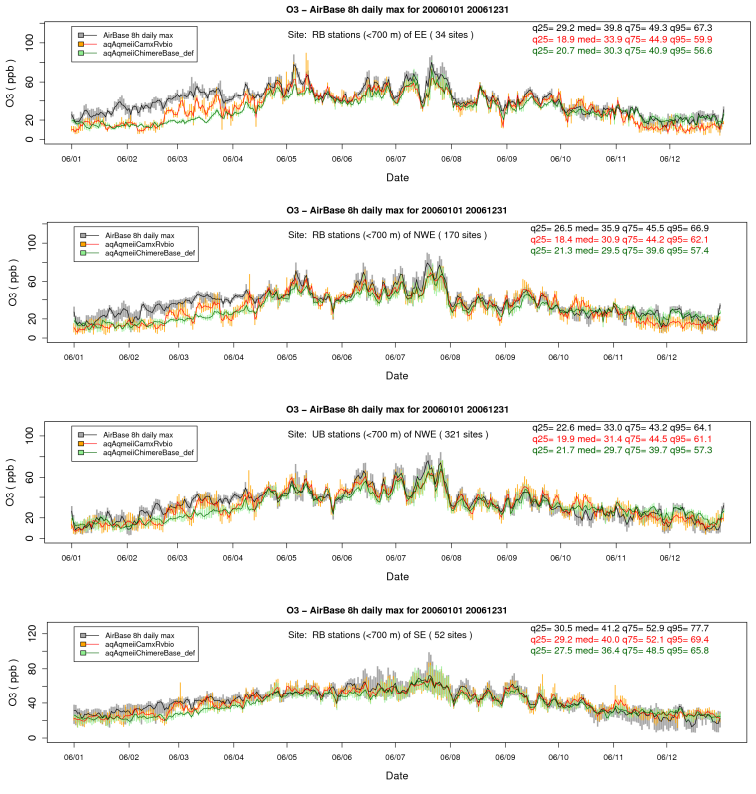

Figure 33– Daily Box-whisker plots of the observed and computed O_3 concentration at RB sites of EE (a), NWE (b) SE (d) regions and at UB sites of NWE region (c). Observations are in black/grey; CAMx in red/orange and CHIMERE in dark green/light green. Bars show the 25th-75th quantile interval. The median is displayed by the continuous line. The 25th,50th, 75th, and 95th quantile of the yearly series are reported too.

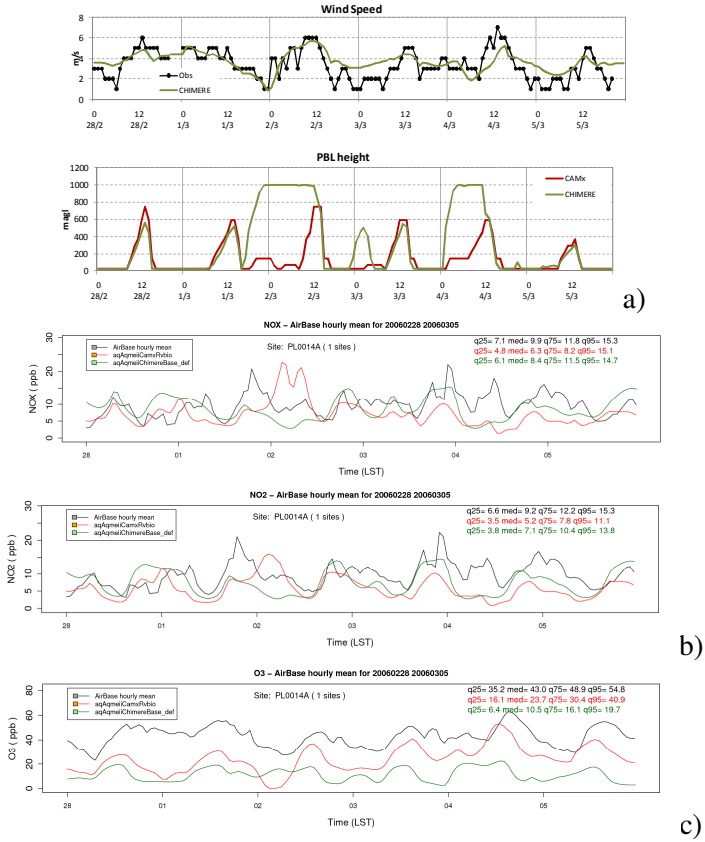

Figure 34 - Hourly time series of observed and computed fields at PL0014A site from 2/28/2006 to 3/5/2006: wind speed and PBL height (a); NOx and NO_2 concentrations (b); ozone concentration (c). Observations are in black; CAMx in red and CHIMERE in green. As for chemical species, the 25th, 50th, 75th and 95th quantile of the hourly series are reported too.

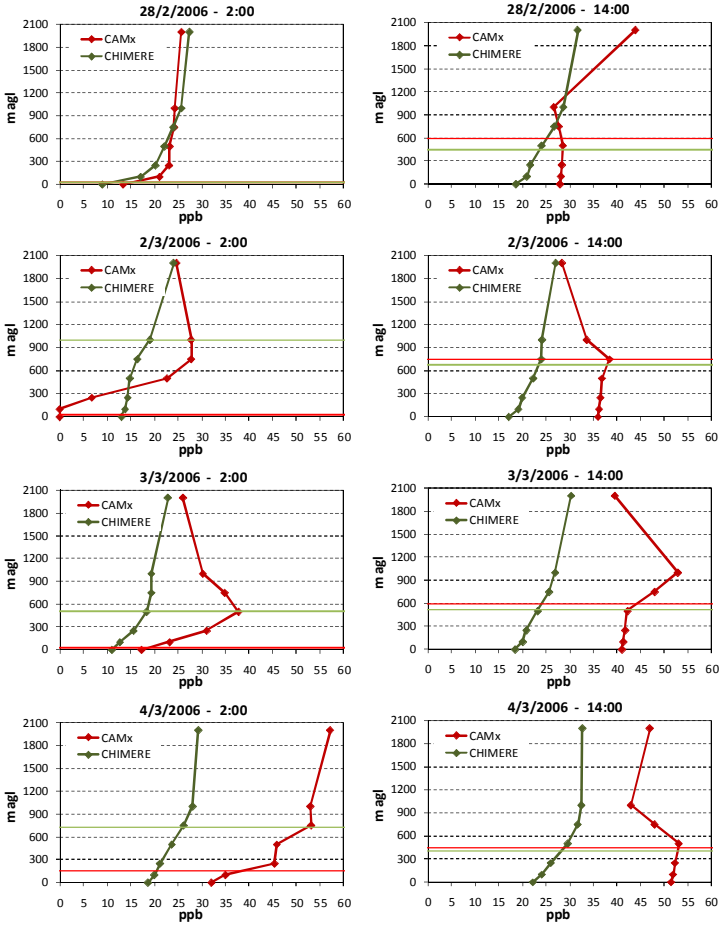

Figure 35 - Selection of hourly ozone vertical profiles computed by CHIMERE (green) and CAMx (red) at site PL0014A, between February 28th and March 4th. Plots also display PBL height adopted by CAMx (red) and CHIMERE (green) at the same site.

To better investigate possible differences in photochemistry, the ozone mean day concentrations from April to September are compared in Figure 36.

The seasonal analysis confirms that the increase in the daytime concentration is systematically higher in CAMx than CHIMERE. Discrepancies are stronger during the first part of the daytime period, supporting the hypothesis that CB05 produces more ozone than MELCHIOR. This finding seems to be confirmed also by the spread of the computed concentrations that is higher in CAMx than CHIMERE. CAMx skills show better in terms of hourly ozone peak, but not over the whole daytime period. This result could provide an explanation for the more accurate CHIMERE performance with respect to the daily maximum 8-hour ozone.

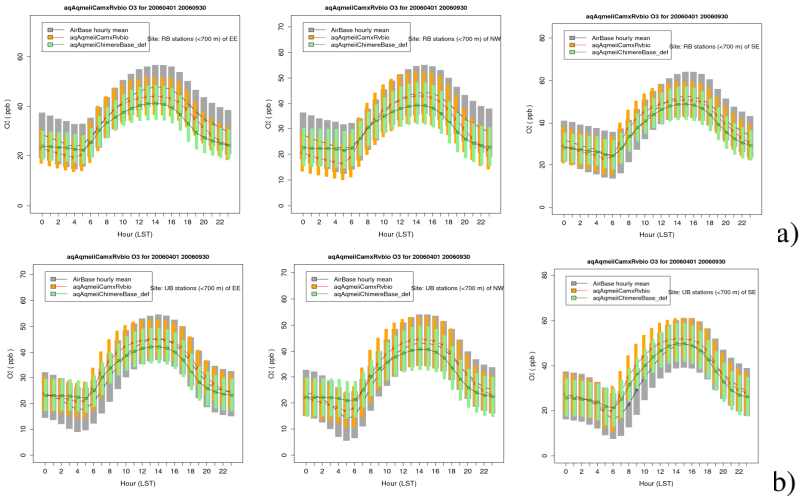

Figure 36 - Ozone mean day concentration at RB (a) and UB (b) stations of EE, NWE and SE regions. Each bar represents 25th-75th quantile interval of the distribution of the concentrations at all stations for the same hour. Lines display the median of the distribution. Observations are in black/grey; CAMx in red/orange and CHIMERE in dark green/light green.

3.3.4 Particulate matter (PM_{10} and $PM_{2.5}$)

In analyzing PM_{10} performance, shown in Figure 27, it appears once again that the models provided a coherent answer both comparing

different regions as well as considering different types of station. Similar to NO_2, the best PM_{10} performance take place in NWE region and for RB stations. The WMP test shows that CAMx systematically provided better FB and FE scores than CHIMERE. CAMx bias is close to 0 in NWE region, whereas SE and EE stations display a negative bias. CHIMERE presents a similar pattern but characterized by a stronger negative bias. Similar findings can be derived by FE scores. Analyzing the WMP results for correlation displays a very different pattern, with CHIMERE performing always better than CAMx.

Differences among regions depend neither on the model nor the station type, confirming the strong influence of geographical features on PM_{10} simulations (Figure 38). Differences in region to region skill are mainly driven by bias, which ranges around 0 in the NWE area, dropping down to -100% in the SE region. Discrepancies in PM_{10} FB and FE are stronger than NO_2 (Figure 27), indicating that there is inaccuracy in the reconstruction of either emission sources or aerosol processes or both, influencing PM_{10} concentration in the EE and SE regions.

To investigate the differences in PM model performances, Figure 37 compares the yearly mean concentration of primary and secondary PM_{10} computed by both models. The spatial patterns look similar, but CAMx concentrations are generally higher than CHIMERE, mainly for primary PM_{10}, thus helping to explain the stronger bias exhibited by CHIMERE. The discrepancies between the two models can be ascribed to: a lower contribution of dust at boundaries in CHIMERE due to a smoothing filter applied to peak events; a lower emission of PM_{10} at ground level (Table 8); more efficient wet deposition scavenging in CHIMERE.

As a further step in evaluating PM performance, $PM_{2.5}$ concentrations at RB sites were compared. Due to the lower number of $PM_{2.5}$ stations, the results shown in Figure 39 cannot be strictly compared to Figure 38. However, available stations show that $PM_{2.5}$ modeled concentrations are closer to observations than PM_{10}. A clear improvement in model performance can be observed for CHIMERE at NWE sites and for CAMx at SE sites.

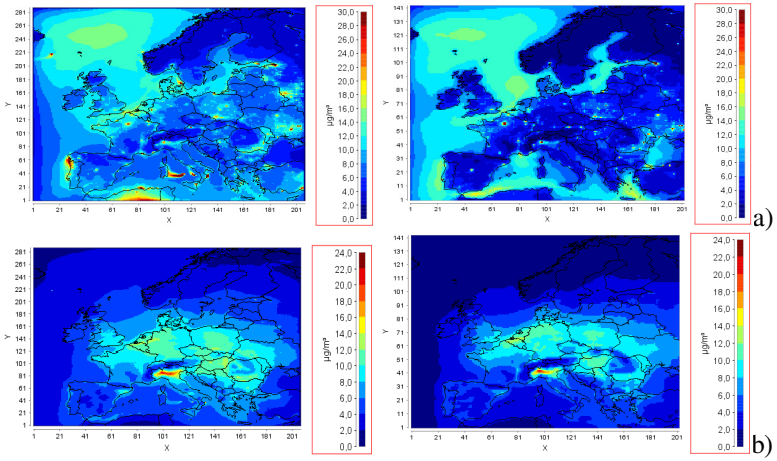

Figure 37 - Primary (a) and secondary (b) PM_{10} yearly mean concentration computed by CAMx (left) and CHIMERE (right).

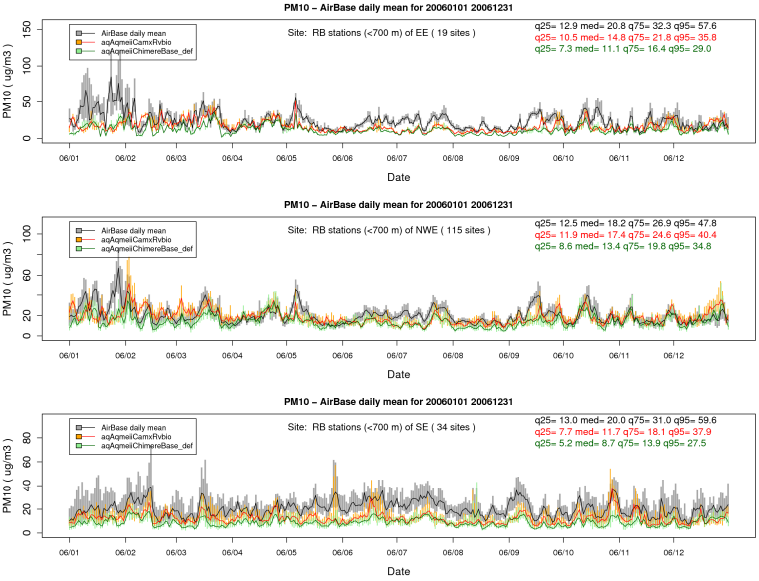

Figure 38 - Daily Box-whisker plots of the observed and computed PM_{10} concentration at RB sites of EE (a), NWE (b) SE (c) regions. Observations are in black/grey; CAMx in red/orange and CHIMERE

in dark green/light green. Bars show the 25th-75th quantile interval, while the median is displayed by the continuous line. The 25th, 50th, 75th, and 95th quantile of the yearly series are reported too.

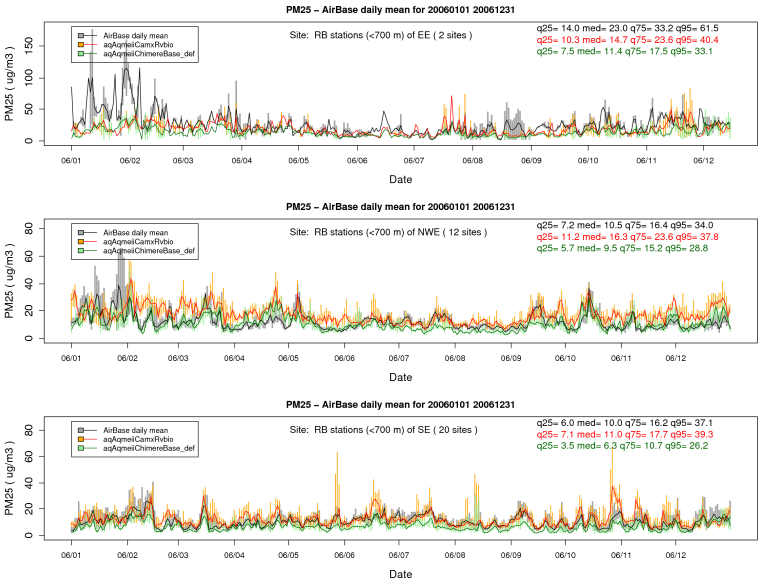

Figure 39 - Daily Box-whisker plots of the observed and computed PM_{10} concentration at RB sites of EE (a), NWE (b) SE (c) regions. Observations are in black/grey; CAMx in red/orange and CHIMERE in dark green/light green. Bars show the 25th -75th quantile interval, while the median is displayed by the continuous line. The 25th,50th, 75th, and 95th quantile of the yearly series are reported too.

Comparing $PM_{2.5}$ and PM_{10} shows that, as expected, observed concentrations clearly decrease when just the fine PM fraction is considered. However, the quantiles of the modeled concentration distributions are rather constant. This result suggests that emissions of coarse PM are missing from both models.

Finally, it is worth noting that CAMx overestimated the $PM_{2.5}$ concentration at NWE sites. This behavior was investigated further.

Figure 40 provides an overview of CAMx and CHIMERE performance in reproducing the three main inorganic aerosol

compounds at RB sites, the only type of stations available in the EMEP dataset. Comparing sulphate performance shows that CAMx provided better FB and FE scores, whereas the model was clearly worse than CHIMERE for correlation. CAMx concentrations were higher than CHIMERE (see Figure 41), due to the corresponding higher availability of SO_2, as discussed previously.

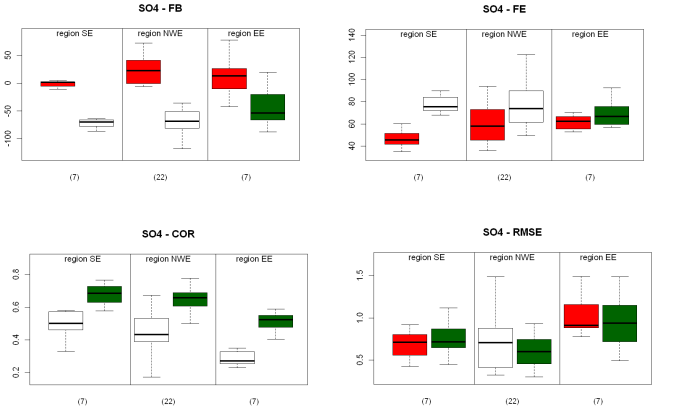

a)

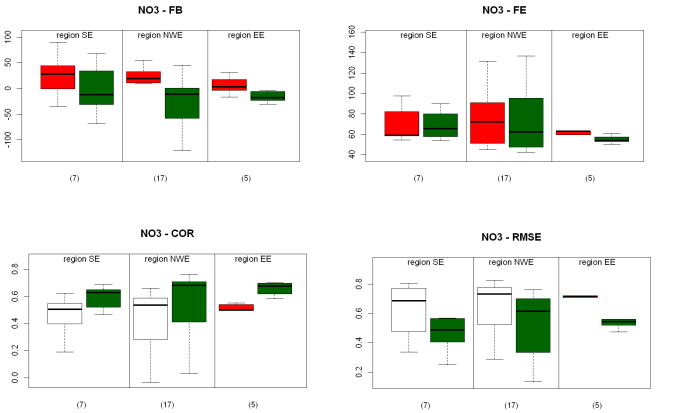

b)

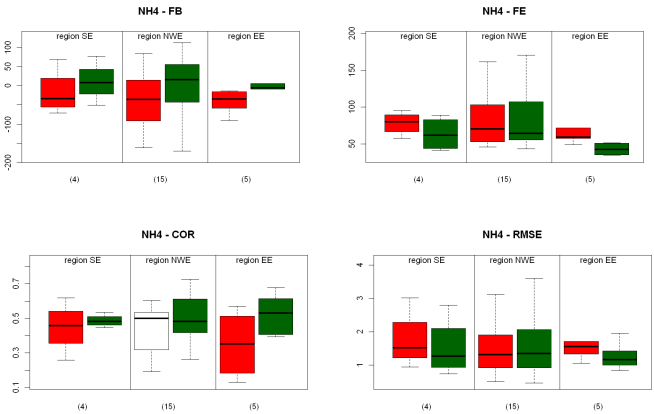

c)

Figure 40 - Box-whisker plots of the distribution of the different metrics computed for CAMx (red) and CHIMERE (green) in each region and for EMEP RB stations. The number of stations included is reported in brackets. The plot is unfilled for the worst model.

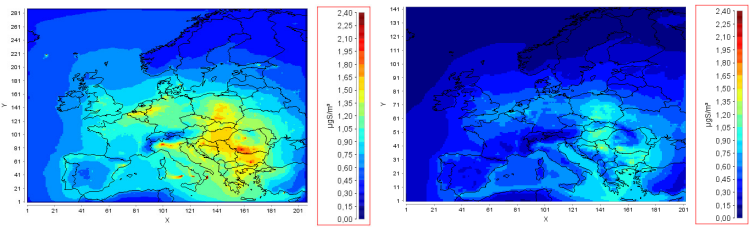

Figure 41 - Sulphate yearly mean concentration computed by CAMx (left) and CHIMERE (right).

Both models presented comparable FB and FE scores for both nitrate and ammonium. Similar to PM_{10}, CHIMERE correlation estimates are generally better than CAMx, especially for sulphate and nitrate. Also in this case, the worsening in CAMx performances is due an overestimation of the variability of computed concentrations, both in space and time. Figure 42 provides an example of such behavior. Differences between the models can be clearly detected by analyzing

the episode that occurred between September 27th and October 2nd, where CAMx overestimates both sulphate and nitrate concentrations.

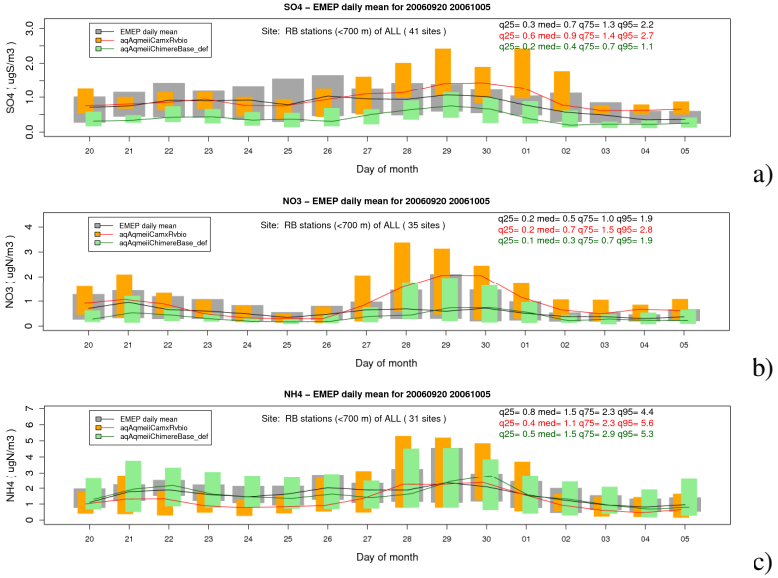

Figure 42 - Daily Box-whisker plots of the distribution of the observed and computed concentration of sulpahte (a), Nitrate (b) and ammonium (c) at EMEP sites. Observations are in black/grey; CAMx in red/orange and CHIMERE in dark green/light green. Bars show the 25th -75th quantile interval, while the median is displayed by the continuous line. The 25th,50th, 75th, and 95th quantile of the whole period are reported too.

Figure 43 helps in explaining model discrepancies. Panels (a) show the nitrate hourly concentrations on September 29th at 07:00, when CAMx concentrations are higher than CHIMERE, above all in a large area across France and Germany. Differences in nitrate concentrations can be related to a higher availability of nitric acid, whose concentration is higher in CAMx, starting from the day before (as shown in Figure 43.b). The increase in HNO_3 concentration that takes place during daytime hours is caused by the development of the

PBL that favor the vertical mixing of pollutants produced by high level sources. Between 250 and 500 m agl, CAMx exhibits HNO_3 night-time concentrations higher than 12 ppb, while CHIMERE is lower than 3 ppb. As soon as the PBL starts growing a downward mixing takes place, giving rise to a strong increase in ground level concentrations. This result suggests that, similar to SO_2, the discrepancies between the two models are driven by different assumptions in simulating PBL processes.

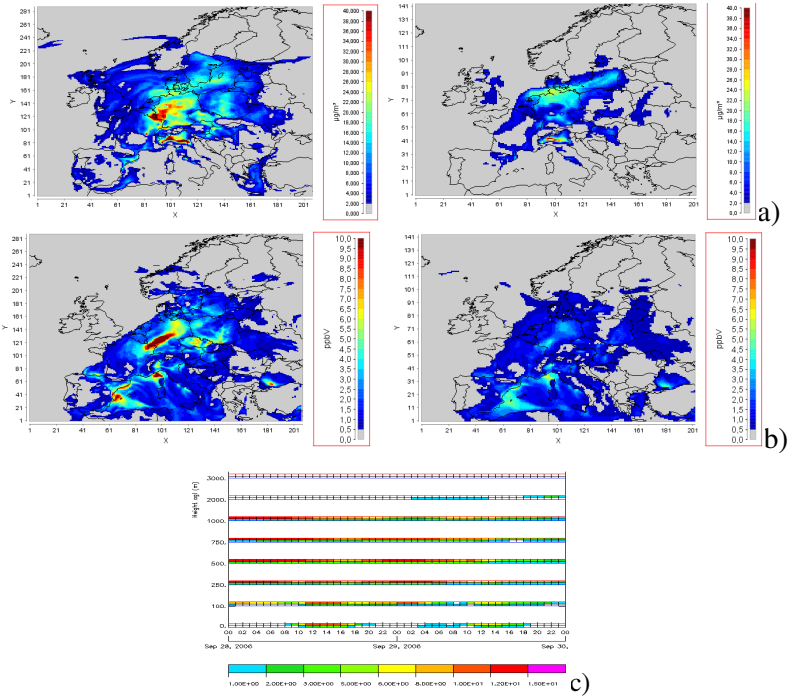

Figure 43 - (a) Nitrate hourly mean concentration computed by CAMx (left) and CHIMERE (right) on September 29th at 07:00; (b) Nitric acid hourly mean concentration computed by CAMx (left) and CHIMERE (right) on September 28th at 12:00; (c) Hourly time series of nitric acid vertical profiles computed by CHIMERE (lower band) and CAMx (upper band) at site (8.00E, 50.00N).

3.4 CONCLUSIONS

Two CTMs were evaluated and compared over Europe for calendar year 2006 in the framework of the AQMEII project. The analysis sub-setted the observational sites according to geographical region and station type. Performance statistics were compared objectively by application of a non-parametric statistical test of matched pairs rank.

The models demonstrated similar geographical variations in model performance with just a few exceptions: for SO_2 in the SE sub-region and O_3 in the EE sub-region. Both models displayed great performance variability from region to region and within the same region for NO_2 and PM_{10}. Station type is relevant mainly for pollutants directly influenced by low level emission sources, such as NO_2 and PM_{10}, while station type is not influential for region to region comparisons.

Investigation of model performance differences showed that FB (or NMB) and FE (or NME) metrics together with correlation index (or index of agreement) often highlighted significant differences in model scores, usefully guiding model users to further analysis of model behavior.

A more detailed analysis of the likely causes of the differences between CAMx and CHIMERE results revealed that:

- Differences in the reconstruction of vertical diffusion coefficients (Kz) and wind speed in the first model layers can affect the surface concentration of primary compounds, especially for stable conditions. Lower threshold for minimum Kz could enhance NO_2 peaks in CHIMERE, improving FB. Also, taking into account the influence of clouds on PBL height can modify the reconstruction of the daily variability yielding different correlation values.
- Differences in the vertical profiles of Kz strongly influenced the impact of aloft sources on ground level concentrations of both primary pollutants such as SO_2 as well as PM_{10} compounds such as sulphate and nitrate. CAMx vertical mixing proved to be more efficient than CHIMERE (note that

since CAMx vertical mixing is determined by input Kv profiles this finding may be specific to this application). As a consequence, CAMx often performed better in terms of bias, while CHIMERE was better than CAMx for correlation. This happened because the stronger mixing produced a general increase of ground level concentrations, but also caused the overestimation of several episodes.

- CAMx showed stronger photochemistry than CHIMERE giving rise, on average, to higher ozone concentrations that agreed better with observations, as shown by analysis of the diurnal variation during the summer season. However, CHIMERE performance on daily basis was better than CAMx because the greater variability of the CAMx concentrations yielded worsening bias and correlation. The only exception was for the EE region where CAMx estimates were more accurate. Nonetheless, this result seems to be due to an error compensation, where the more effective photochemistry showed by CAMx compensated for an underestimation in the background concentration.
- PM_{10} performance was rather poor for both models, except for the NWE region. Model results were sensitive to geographical features and station type similar to NO_2. However, differences in model performance between the NWE region and the other two areas were stronger than for NO_2, suggesting that either further emission sources, or processes, or both are missing for PM_{10} in the SE and EE regions. Moreover, PM_{10} performance was very different between regions, while secondary inorganic aerosol scores were relatively homogenous. This suggests that PM_{10} underestimation has to be ascribed to other compounds (e.g. PM coarse, Particulate Organic Matter and dust). This finding has been confirmed by comparing $PM_{2.5}$ stations, which exhibited a lower bias than PM_{10} sites. This result proved that coarse PM sources are still missing from emission inventories. Beside these shared features, comparing the two models displayed a rather unexpected result, with CAMx performing always better than CHIMERE in terms of bias,

while CHIMERE score for correlation was always higher than CAMx. As already mentioned, vertical mixing is one cause of such discrepancies.

3.5 REFERENCES

Bessagnet, B., Hodzic, A., Vautard, R., Beekmann, M., Cheinet, S., Honoré, C., Liousse, C., Rouïl, L., 2004. Aerosol modeling with CHIMERE: preliminary evaluation at the continental scale. Atmos. Environ. 38, pp. 2803–2817

Bessagnet, B., Khvorostyanov, D., Menut, L., Monge, J.L., Vautard, R., 2009. Documentaion of the chemistry transport model CHIMERE. http://www.lmd.polytechnique.fr/chimere/docs/CHIMEREdoc2008.pdf

Bessagnet, B., Seigneur, C., Menut, L., 2010. Impact of dry deposition of semi-volatile organic compounds on secondary organic aerosols. Atmospheric Environment, 44, Issue 14, Pages 1781-1787, ISSN 1352-2310, DOI: 10.1016/j.atmosenv.2010.01.027.

Boylan, J., and Russel, A., 2006. PM and light extinction model performance metrics, goals, and criteria for three-dimensional air quality models. Atmospheric environment, 40, 4946-4959.

Chang, J.C., Hanna, S.R., 2004. Air quality model performance. Meteorol Atmos Phys 87, 167–196.

Cuvelier, C., Thunis, P., Vautard, R., Amann, M., Bessagnet, B., Bedogni, M., Berkowicz, R., Brandt, J., Brocheton, F., Builtjes, P., Carnevale, C., Copalle, A., Denby, B., Douros, J., Graf, A., Hellmuth, O., Honoré, C., Hodzic, A., Jonson, J., Kerschbaumer, A., de Leeuw, F., Minguzzi, E., Moussiopoulos, N., Pertot, C., Peuch, V.H., Pirovano, G., Rouil, L., Sauter, F., Schaap, M., Stern, R., Tarrason, L., Vignati, E., Volta, M., White, L., Wind, P., Zuber, A., 2007. CityDelta: A model intercomparison study to explore the impact of emission reductions in European cities in 2010. Atmospheric Environment 41, issue 1, 189-207.

de Leeuw, G, Neele, F.P., Hill, M., Smith, M.H., Vignati, E., 2000. Production of sea spray aerosol in the surf zone. J. Geophys. Res. 105 (29),397-29,409.

Denby, B. (ed), 2011. Guidance on the use of models for the European Air Quality Directive (A FAIRMODE working Document). ETC/ACC report, ver 6.2. http://fairmode.ew.eea.europa.eu/

Dennis, R., Fox, T., Fuentes, M., Gilliland, A., Hanna, S., Hogrefe, C., Irwin, J., Rao, S.T., Scheffe, R., Schere, K., Steyn, D., Venkatram, A., 2010. A framework for evaluating regional-scale numerical photochemical modeling systems. Environ Fluid Mech, doi: 10.1007/s10652-009-9163-2.

Dudhia, J., 1993. A nonhydrostatic version of the Penn State / NCAR mesoscale model: Validation tests and simulation of an Atlantic cyclone and cold front. Mon. Wea. Rev. 121 1493-1513.

ENVIRON, 2010. User's Guide to the Comprehensive Air Quality Model with Extensions (CAMx). Version 5.20. Report prepared by ENVIRON International Corporation Novato, CA.

EU, 1997. Council Decision of 27 January 1997 establishing a reciprocal exchange of information and data from networks and individual stations measuring ambient air pollution within the Member States (Exchange of Information (97/101/EC)). Official Journal L 035, 05/02/1997, pp. 14-22. See http://ec.europa.eu/environment/air/quality/legislation/reporting.htm

EU, 2008. Directive 2008/50/EC of the European Parliament and of the Council of 21 May 2008 on ambient air quality and cleaner air for Europe. Official Journal L 152, 11.6.2008, p. 1–44 http://eur-lex.europa.eu/LexUriServ/LexUriServ.do?uri=OJ:L:2008:152:0001:0044:EN:PDF

Gangoiti, G., Millán, M., Salvador, R., Mantilla, E., 2001. Long-range transport and re-circulation of pollutants in the western Mediterranean during the project Regional Cycles of Air Pollution in the West-Central Mediterranean Area. Atmospheric Environment 35, 6267-6276.

Gego, E., Porter, P.S., Hogrefe, C., Irwin, J. S., 2006. An objective comparison of CMAQ and REMSAD performances, Atmospheric Environment, Volume 40, Issue 26, Pages 4920-4934.

Gong, S. L., 2003. A parameterization of sea-salt aerosol source function for sub- and super-micron particles. Global Biogeochemical Cycles 17: 1097-1104.

Guenther, A., Karl, T., Harley, P., Wiedinmyer, C., Palmer, P., Geron, C., 2006. Estimates of global terrestrial isoprene emissions using MEGAN (Model of Emissions of Gases and Aerosols from Nature), Atmos. Chem Phys., 6, 3181-3210.

Hjellbrekke, A.-G., Fjæraa, A.M., 2008, Data Report 2006. Acidifying and eutrophying compounds. EMEP/CCC-Report 1/2008, Norwegian Institute for Air Research.

Jacobson, M.Z., Lu, R., Turco, R.P., and Toon, O.B., 1996. Development and application of a new air pollution model system – Part I: Gas-phase simulations. Atmos. Environ., 30, 1939- 1963.

Jacobson, M.Z., 1997. Development and application of a new air pollution modeling system. Part III:Aerosol-phase simulations, Atmos. Environ., 31A, 587-608.

Kallos, G., Astitha, M., Katsafados, P., Spyrou, C., 2007. Long-range transport of anthropogenically and naturally produced particulate matter in the Mediterranean and North Atlantic: Current status of knowledge. Journal of Applied Meteorology and Climatology 46, 1230-1251.

Latuatti, M.: Contribution `a l'étude du bilan de l'ozone troposphérique `a l'interface de l'Europe et de l'Atlantique Nord: Modélisation lagrangienne et mesures en altitide, PhD thesis, Université de Paris 6, Paris, 1997.

Millán, M., Mantilla, E., Salvador, R., Carratalá, A., Sanz, M. J., Alonso, L., Gangoiti, G., Navazo, M., 2000. Ozone Cycles in the Western Mediterranean Basin: Interpretation of Monitoring Data in Complex Coastal Terrain. J. Appl. Meteor. 39, 487–508.

Mitsakou, C., Kallos, G., Papantoniou, N., Spyrou, C., Solomos, S., Astitha, M., Housiadas, C., 2008. Saharan dust levels in Greece and received inhalation doses. Atmos. Chem. Phys. 8, 7181-7192.

Monahan, E. C., 1986. The ocean as a source for atmospheric particles. The Role of Air–Sea Exchange in Geochemical Cycling, P. Buat-Menard, Ed., D. Reidel, 129–163.

Morris, R.E., G. Yarwood, C.A. Emery, G. Wilson and B. Koo, 2006. Regional Modeling using One-Atmospheric Models to Address Regional Haze, 8-Hour Ozone and PM2.5 Air Quality. Presented at the

99th A&WMA Annual Conference, New Orleans, LA, (Paper # 06-A-503-AWMA). June

Murphy, A.H., 1988. Skill Scores Based on the Mean Square Error and Their Relationships to the Correlation Coefficient. Monthly Weather Review, Vol 116, 2417-2424. doi:10.1175/1520-0493(1988)116<2417:SSBOTM>2.0.CO.

Nopmongcol, U., Koo, B., Tai, R., Jung, J., Piyachaturawat, P., Emery, C., Yarwood, G., Pirovano, G., Mitsakou, C., Kallos, G., 2012. Modeling Europe with CAMx for the Air Quality Model Evaluation International Initiative (AQMEII). Atmospheric Environment 53, 177-185.

Potempski, S., Galmarini, S., Addis, R., Astrup, P., Bader, S., Bellasio, R., Bianconi, R., Bonnardo,t F., Buckley, R., D'Amours, R., van Dijk, A., Geertsema, G., Jones, A., Kaufmann, P., Pechinger, U., Persson, C., Polreich, E., Prodanova, M., Robertson, L., Sorensen, J., Syrakov, D., 2008. Multi-model ensemble analysis of the ETEX-2 experiment, Atmospheric Environment, Volume 42, 7250-7265, doi: 10.1016/j.atmosenv.2008.07.027.

Pouliot G., Pierce T., Denier van der Gon H., Schaap M., Moran M., Nopmongcol U. 2012. Comparing Emission Inventories and Model-Ready Emission Datasets between Europe and North America for the AQMEII Project. Submitted to Atmospheric Environment 53, 4-14.

Putaud, J.-P., Van Dingenen, R., Alastuey, A., Bauer, H., Birmili, W., Cyrys, J., Flentje, H., Fuzzi, S., Gehrig, R., Hansson, H.C., Harrison, R.M., Herrmann, H., Hitzenberger, R., Hüglin, C., Jones, A.M., Kasper-Giebl, A., Kiss, G., Kousa, A., Kuhlbusch, T.A.J., Löschau, G., Maenhaut, W., Molnar, A., Moreno, T., Pekkanen, J., Perrino, C., Pitz, M., Puxbaum, H., Querol, X., Rodriguez, S., Salma, I., Schwarz, J., Smolik, J., Schneider, J., Spindler, G., ten Brink, H., Tursic, J., Viana, M., Wiedensohler, A., Raes, F., 2010. A European aerosol phenomenology - 3: Physical and chemical characteristics of particulate matter from 60 rural, urban, and kerbside sites across Europe, Atmospheric Environment, Volume 44, 1352-2310, doi: DOI: 10.1016/j.atmosenv.2009.12.011.

Rao, S. T., Galmarini, S., Puckett, K., 2011. Air Quality Model Evaluation International Initiative (AQMEII): Advancing the State of the Science in Regional Photochemical Modeling and Its Applications. BAMS, Volume 92, Issue 1, 23-30.

Russell, A., Dennis, R., 2000. NARSTO critical review of photochemical models and modeling. Atmospheric Environment 34, 2283-2324.

Schere, K., J. Flemming, R. Vautard, C. Chemel, A. Colette, C. Hogrefe, B. Bessagnet, F. Meleux, R. Mathur, S. Roselle, R.-M. Hu, R.S. Sokhi, S.T. Rao, and S. Galmarini. 2012. Trace gas/aerosol boundary concentrations and their impacts on continental-scale AQMEII modeling domains. Atmospheric Environment, 53, 38–50.

Schluenzen, K.H. and Sokhi, R.S. (eds), 2008. Overview of tools and methods for meteorological and air pollution meso-scale model evaluation and user training, Joint Report of COST Action 728 and GURME, WMO/TD-No.1457, ISBN 978-1-905313-59-4.

Seigneur, C., 2001. Current status of air quality models for particulate matter. Journal of the Air and Waste Management Association, 51(11), 1508-1521.

Solazzo, E., Bianconi, R., Pirovano, G., Volker, M., Vautard, R., and et al., 2012. Operational model evaluation for particulate matter in Europe and North America in the context of AQMEII. Atmospheric Environment 53, 75-92, doi:10.1016/j.atmosenv.2012.02.045.

Tesche, T.W., Morris, R., Tonnesen, G., McNally, D., Boylan, J., Brewer, P., 2006. CMAQ/CAMx annual 2002 performance evaluation over the eastern US. Atmospheric Environment, 40, 4906-4919 DOI: 10.1016/j.atmosenv.2005.08.046.

Thunis, P., Georgieva, E., Galmarini, S., 2011. A procedure for air quality models benchmarking. FAIRMODE document, URL: http://fairmode.ew.eea.europa.eu/models-benchmarking-sg4

Van Loon, M., Vautard, R., Schaap, M., Bergstrom, R., Bessagnet, B., Brandt, J., Builtjes, P., Christensen, J.H., Cuvelier, K., Graf, A., Jonson, J., Krol, M., Langner, J., Roberts, P., Rouil, L., Stern, R., Tarrason, L., Thunis, P., Vignati, E., White, L., Wind, P., 2007. Evaluation of long-term ozone simulations from seven regional air quality models and their ensemble average. Atmos. Environ. 41, 2083–2097.

Vautard, R., Bessagnet, B., Chin, M., Menut, L., 2005. On the contribution of natural aeolian sources to particulate matter concentrations in Europe: testing hypotheses with a modelling approach. Atmos. Environ. 39: 3291–3303.

Vautard, R., Builties, P.H.J., Thunis, P., Cuvelier, C., Bedogni, M., Bessagnet, B., Honore, C., Moussiopoulos, N., Pirovano, G., Schaap, M., Stern, R., Tarrason, L.,Wind, P., 2007. Evaluation and intercomparison of ozone and PM10 simulations by several chemistry transport models over four European cities within the CityDelta project. Atmos Environ 41:173–188.

Vautard, R., Schaap, M., Bergstrom, R., Bessagnet, B., Brandt, J., Builtjes, P.J.H., Christensen, J.H., Cuvelier, C., Foltescu, V., Graff, A., Kerschbaumer, A., Krol, M., Roberts, P., Rouil, L., Stern, R., Tarrason, L., Thunis, P., Vignati, E., Wind, P., 2009. Skill and uncertainty of a regional air quality model ensemble. Atmospheric Environment, Volume 43, 4822-4832, DOI: 10.1016/j.atmosenv.2008.09.083.

Weil, J.C., Sykes, R.I., Venkatram, A., 1992. Evaluating air quality models: review and outlook. J Appl Meteorol 31, 1121–1145.

Wilks, D.S., 2006. Statistical Methods in the Atmospheric Sciences, 2nd Ed. International Geophysics Series, Vol. 59, Academic Press, 627 pp.

Yarwood, G., Rao, S., Yocke, M., Whitten, G., 2005. Updates to the Carbon Bond Chemical mechanism: CB05, report, Rpt. RT-0400675, US EPA, Res. Tri. Park.

4 COMPARING WRF-CHEM AND CAMX OVER ITALY: ONLINE VERSUS OFFLINE APPROACH

A. Balzarini, G. Pirovano and G.M. Riva

Submitted manuscript

As models are becoming important tools for air quality management and the evaluation of emission control strategies, it is essential to assess their ability in simulating air concentrations.
During the past decades, many modeling inter-comparison experiences have been proposed to investigate model predictions from traditional Chemistry and Transport Models (CTMs, Cuvelier et la., 2007; van Loon et al, 2007; Pernigotti et al., 2013; Rao et al., 2011), achieving a comprehensive evaluation of the main gaps and phenomena driving the regional-scale numerical estimations.
Studies reveal a large variability among models in reconstructing the main atmospheric pollutants. However, Solazzo et al. (2012) have demonstrated a systematical tendency through underestimation of particulate matter as well as its main precursors for several CTMs over Europe. Many Chemistry and Transport Models (CTMs) have been tested. Some examples are EMEP (Simpson et al., 2003), CAMx (ENVIRON, 2011), CHIMERE (Bessagnet et al., 2009) and LOTOS (Schaap et al., 2008).

All these CTMs are implemented "*offline"* (e.g. chemical and meteorological fields are simulated by two independent models). Moreover, they do not allow the estimation of the coupled interactions between meteorology and air quality ("*un-coupled*"). Decoupling between meteorology and chemistry leads to a loss of information about atmospheric processes that have a time scale smaller than the output time of the meteorological model (usually 1 hour), e.g. wind speed and wind direction, rainfall, and cloud formation (Grell et al., 2005; Zhang, 2008).
As discussed before, in recent years the atmospheric modeling community is moving toward an integrated method that aims at incorporating chemistry and meteorology in the same regional model with a full modular approach ("*on-line*"). In principle, the step towards the on-line approach should introduce an improvement in model performance, whose relevance, anyhow, need to be proved and quantified, through the examination of the various physical and chemical processes included in regional-scale integrated meteorology-chemistry models.
On this contest, the comparison to well-known systems, such as CTMs, represents an important step to improve their knowledge as well as to investigate the effect of on-line approach on air quality simulations.
The Weather Research and Forecasting model coupled with chemistry (WRF-Chem; Grell et al., 2005) is a state-of-the-art on-line model, in which chemistry transformations are completely embedded into the meteorological model WRF (Skamarock et al., 2008). In addition, it allows considering the complex aerosol-cloud-radiation feedback mechanisms ("*coupled*").
In this study WRF-Chem model was compared to the off-line chemistry and transport model CAMx (Comprehensive Air quality Model with eXtension; ENVIRON 2011) over Italy for January and February 2005, in order to evaluate the effect of on-line and off-line approaches on air quality simulations.
To this aim, WRF-Chem was implemented without the full coupling of aerosol and radiation-cloud processes, because feedbacks may

complicate the interpretation of results on gas and aerosol (Tuccella et al., 2012).
CAMx is an Eulerian chemistry and transport model widely applied in several modeling inter-comparison exercises over Europe (Pirovano et al., 2012; Vautard et al., 2007) and Italy (Pernigotti et al., 2013). As presented previously in this study (Chapter 3), CAMx was demonstrated to reconstruct the main pollutant events over Europe with similar performances to other frequently used chemistry and transport models (CHIMERE), thus representing an interesting benchmark for the WRF-Chem application.
Whether possible the simulation design was identically defined in the two model runs to make more comparable the modeling approaches. In particular, modeling configurations were in line with the outcomes of previous studies and sensitivity tests. As discussed in Chapter 2, we chose the meteorological parameterizations that were found to give the best performances over Italy and the Po valley area. Moreover, statistical evaluations presented in Chapter 3 were adopted here.
Of particular interest for air quality studies is the fate of particulate matter, as the PM_{10} limit values of the European Directive are exceeded in many areas of Italy especially during the winter (Directive 2008/50/EC). For this reason, results were focused on particulate matter and its main precursors and components. Results were also compared against measurement data.

4.1 WRF-CHEM MODEL APPLICATION

4.1.1 Models description and set up

In this study WRF-Chem model (version 3.3.1; September, 2011) has been applied and compared to CAMx (version 5.4; ENVIRON 2011) over the Italian domain for January and February 2005.
WRF-Chem is the chemical extension of the fully compressible and non-hydrostatic Advanced Research WRF model, and it was developed jointly by NOAA, NCAR, PNNL and other research institutes. As well as WRF, it uses terrain-following hydrostatic

pressure as the vertical coordinate, and Arakawa-C grid for grid staggering. The model implements the Runge-Kutta second and third order time integration schemes and second to sixth order advection schemes in both the horizontal and vertical directions.

WRF-Chem enables a variety of chemical and physical-dynamical parameterizations. The physics options applied in this study are: the Rapid Radiative Transfer Model (RRTM) longwave radiation scheme (Mlawer et al., 1997), the Goddard shortwave radiation scheme (Chou et al., 1998), the Noah land surface model (Chen and Dudhia, 2001), the Morrison double moment microphysics scheme (Morrison et al., 2009) and the Grell 3D ensemble cumulus parameterization (Grell and Devenyi, 2002). The PBL scheme adopted here is based on previous studies and includes the Yonsei University Planetary Boundary Layer (Hong et al., 2006) and the MM5 surface model based on Monin and Obukhov (1954). Sensitivity tests indicate that the combination of schemes for surface layer and PBL adopted in this work produces the best results over Italy (Chapter 2).

The chemical mechanisms included in the analysis are CBM-Z for gas-phase chemistry (Carbond Bond Mechanism version Z, Zaveri and Peters, 1999) and MOSAIC for aerosol formation (Model for Simulating Aerosol Interactions and Chemistry, Zaveri et al., 2008).

This combination of chemical mechanism was selected because of the similarity of the photochemical scheme (CBM-Z) with the CAMx one (Carbon Bond 2005, CB05; Yarwood et al., 2005) that will be used to compare model results.

CBM-Z is a fairly popular mechanism in the atmospheric chemistry modeling community that derives from the CBM-IV scheme (Gery et al., 1989). The major modification involved the explicit treatment of lesser reactive paraffines, such as methane and ethane; revised parameterizations of more effective paraffines, olefins and aromatics. The resulting mechanism contains 52 prognostics species grouped according to the types of bonds present in the molecular structure and 132 gas-phase reactions.

Aerosol reactions are reconstructed by means of Model for Simulating Aerosol Interactions and Chemistry. MOSAIC scheme

treats major aerosol species including sulphate (SO_4), nitrate (NO_3), chloride (Cl), ammonium (NH_4), sodium (Na), black carbon (BC), primary organic mass (OC) and other inorganic mass (OIN) (e.g., trace metals, silica and other inert minerals). It includes the main aerosol processes e.g. inorganic aerosol thermodynamic equilibrium, binary nucleation, coagulation, condensation, PM formation due to aqueous-phase chemistry, and dry and wet deposition. In particular, Wexler et al. (1994) and Jacobson et al. (1994) approaches are used for simulating nucleation and coagulation, respectively.
MOSAIC reproduces aerosol size distribution using a sectional method, in which both mass and number are predicted for each size bin. The size bins are defined by their lower and upper dry particle diameters (Table 9). Furthermore, each bin is assumed to have the same chemical composition within a bin (internally mixed), while particles are externally mixed between different bins.
For this investigation four size bins are used, ranging from 0.04 μm (lower bound) to 10 μm (upper bound).

Table 9 – Size bin distributions used in the study.

	Bin 1	**Bin 2**	**Bin 3**	**Bin 4**
Minimum diameter (μm)	0.04	0.156	0.625	2.5
Maximum diameter (μm)	0.156	0.625	2.5	10.0
Particle center (μm)	0.078	0.313	1.250	5.0

The current implementation of MOSAIC does not take into account for the gas-phase photochemical reactions that lead to the Secondary Organic Aerosols (SOA) formation, whereas the bulk aqueous phase chemistry of Fahey e Pandis (2001) is used, which includes 147 aqueous reactions that involve 50 chemical species.
The photolysis frequencies are calculated with the Fast-J scheme (Barnard et al., 2004) under clear and cloudy sky conditions. This code employs the conventional "*plane-parallel assumption*", so that the optical properties are constant in any horizontal plane, and the radiative transfer equations are functions only of the vertical coordinate (Barnard et al., 2004).

The WRF-Chem meteorological simulation has driven CAMx model. CAMx is an Eulerian chemical and transport model that allows simulating emission, dispersion, chemical reaction and removal processes of pollutants in the troposphere. In the present work, it implements the Carbon Bond 2005 gas phase chemistry (CB05; Yarwood et al., 2005), and the ISORROPIA scheme to simulate the thermodynamic equilibrium of inorganic particles (Nenes et al., 1998; Nenes et al., 1999).

CB05 is a condensed mechanism of atmospheric oxidant chemistry that updates the earlier CBIV (Gery et al., 1989). The main differences include an explicit organic chemistry for methane and ethane, the addition of higher aldehyde (e.g. peroxyacyl radicals, peroxynitrates and carboxylic acids) and internal olefin species such as 2-butenes. CB05 treats 51 lumped species and 156 gas-phase reactions.

ISORROPIA predicts ammonium, sodium, chloride, nitrate, sulfate and water, which are partitioned between gas, liquid and solid phases. The aerosol particles are assumed to be internally mixed, meaning that all particles of the same size have the same composition.

The aqueous chemistry of the RADM-AQ mechanism (Chang et al., 1987) was employed. It consists of 77 reactions among 36 species. Furthermore, the SOAP algorithm was adopted in order to simulate the organic species partitioning (Strader et al., 1999).

The aerosols dynamic follows a coarse/fine approach that divides the size distribution in two modes. Primary species can be modeled as fine or coarse particles, while all secondary species are associated to the fine particles only. Moreover particles do not move from the fine mode into the coarse mode due to dynamic processes.

The rates for the primary photolysis reactions are generated using the Tropospheric Ultra-violet Visible (TUV) radiative transfer model (NCAR, 2011).

Wet scavenging coefficient is determined differently for gas and aerosols, based upon the relationship described in Seinfeld and Pandis (1998).

Finally, Wesely (1989) dry deposition is included in both modeling applications.
The main physics and chemistry options adopted in this study are listed in Table 10.

Table 10 - Chemistry and physics options.

		WRF-Chem	WRF - CAMx
Physics options	Cumulus parameterization	Grell 3D	Grell 3D
	Microphysics	Morrison 2-moment	Morrison 2-moment
	Planetary Boundary Layer	YSU	YSU
	Surface layer	MM5	MM5
	Land Surface Model	Noah LSM	Noah LSM
	Shortwave radiation	Goddard	Goddard
	Longwave radiation	RRTM	RRTM
	PBL grid nudging	on	on
Chemistry options	Gas phase chemistry	CBM-Z	CB05
	Aerosol chemistry	MOSAIC	ISORROPIA
	SOA formation	-	SOAP
	Aqueous chemistry	Fahey and Pandis	RADM-AQ
	Aerosol dynamic	4bin sectional approach	Coarse/Fine
	Photolysis	Fast-J	TUV
	Dry deposition	Wesely	Wesely
	Wet deposition	Included	Included

Models shared the same computational domain that extends over a 1290x1470 km^2 area and it was defined in Conical Conformal Lambert projection with 86x96 grid cells of 15 km horizontal resolution (Table 11 and Figure 44). Differently, vertical grid varied between the two modeling applications. WRF-Chem considers 27 vertical layers, from the surface to about 18 km (50 hPa), while CAMx includes 14 vertical layers up to 11 km. However, in order to preserve consistency as much as possible, CAMx shared exactly the same vertical structure of WRF-Chem within the first 1000 m agl, whereas aloft CAMx layers were defined collapsing each two WRF-Chem layers into a CAMx one. Moreover, models adopt different parameterizations of vertical diffusion below the PBL height which, as discussed below, influenced pollutant dispersion in the atmosphere.

Table 11 - Domain characteristics.

	u.m.	**D01**
SW X corner	[km]	-604.5
SW Y corner	[km]	-1023.5
NE X corner	[km]	685.5
NE Y corner	[km]	446.5
DX-DY	[km]	15
NX	[n]	86
NY	[n]	98

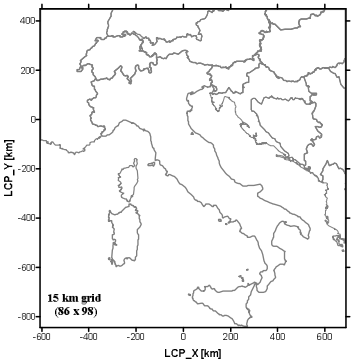

Figure 44 – Computational domain

4.1.2 Emissions

Emissions fields were externally generated for both anthropogenic and natural emissions.

Anthropogenic emissions were taken from two different emission inventories for the year 2005: (1) Inventario Nazionale delle Emissioni Provinciali, and (2) EMEP database (http://webdab.emep.int). The first one is the Italian official emission inventory provided by ISPRA (Istituto Superiore per la Protezione e la Ricerca Ambientale, 2009) which contains both area and point emissions for the whole Italian peninsula with provincial coverage, while the second one provides European emissions over a 50 km grid resolution domain. EMEP inventory was employed to estimate emissions from neighboring countries.

Emission inventories provide data for each chemical species: nitrogen oxides (NOx), carbon monoxide (CO), sulphur dioxide (SO_2), ammonia (NH_3), Non-Methane Volatile Organic Compounds (NMVOC), and particulate matter ($PM_{2.5}$ and PM_{10}). Emissions are split in 11 source types denoted by so-called European SNAP codes (Selected Nomenclature for sources of Air Pollution). SNAP sectors considered 10 anthropogenic sources, as shown in Table 12, and an eleventh source-sector, "Other sources and sinks" that consists

almost entirely of emissions from natural and biogenic sources. Officially submitted emissions from such source are not used in this modeling work, except for those from volcanoes and fires.

Table 12 – SNAP codes.

SNAP code	Description
01	Combustion in energy and transformation industries
02	Non-industrial combustion plants
03	Combustion in manufacturing industry
04	Production processes
05	Extraction and distribution of fossil fuels and geothermal energy
06	Solvent and other product use
07	Road transport
08	Other mobile sources and machinery
09	Waste treatment and disposal
10	Agriculture
11	Other sources and sink

The procedure followed to build in anthropogenic emission fields includes the SMOKE processor (Sparse Matrix Operator Kernel Emissions, version 2.6), developed by the University of North Carolina (www.smoke-model.org). It allows spatial and temporal disaggregation of emission inventories as well as the speciation of the inventory pollutants into model compounds.
The main SMOKE settings were defined by Pirovano et al. (2011) and Balzarini et al. (2012) during previous studies.
For the spatial disaggregation different proxy variables are used (e.g. length of highways and roads, land use, railway network, and rivers), in order to spatially distribute emissions to the computational grid.
Time variability is calculated by means of statistical time functions for species and source category dependent on monthly, daily and hourly cycles. These functions are provided by CHIMERE (Bessagnet et al., 2009) and EMEP-GENEMIS (http://webdab.emep.int).
Chemical speciation was made through speciation profiles, for both VOCs and PM, which are specific for each emission sector. Total

amount of NMVOC was split into 427 chemical compounds of the SAROAD classification (Storage and Retrieval of Aerometric Data) using UK speciation profiles (Passant, 2002), and then aggregated into the gas species of the two models.
However, since WRF-Chem was first developed for RADM2 gas-phase chemical mechanism, the NMVOC emissions obtained from Passant speciation are first lumped into 15 RADM2 chemical species following the procedure proposed by Carter (2001), and then added to some ad-hoc CBMZ chemical species (CH_3OH, C_2H_5OH). Moreover, paraffins are totally assigned to HC5, accordingly to CBM-Z code.
PM_{10} and $PM_{2.5}$ were assigned respectively to PM coarse and PM fine and disaggregated into the chemical components of the aerosol modules using POMI profiles (http://aqm.jrc.it/POMI). Nevertheless, WRF-Chem requires a PM speciation in MADE species. In this way Elemental Carbon, Organic Carbon, SO_4, NO_3 and NH_4 emissions of the fine fraction were assumed to be included into the accumulation mode, accordingly to model equations.
Model ready emission fields were prepared independently in the two applications because of the different approach for aloft sources. In WRF-Chem a plume rise calculation was included in the pre-processing phase for both Italian and EMEP emissions, while CAMx has its own plume rise algorithm embedded in the main code. The algorithm follows the multi-layer stability-dependent theory of Turner et al. (1986) that calculates the effective emission height according to the meteorological conditions of the stack hosting layer and the layers above. This approach was employed to estimate the anthropogenic plume growth for the Italian point sources, whereas EMEP data were split between surface and height accordingly to EMEP profiles for each SNAP sector (Table 13) and, then, vertically injected using an effective stack height at which the plume is emitted (Vestreng, 2003).

Table 13 – Emission vertical distribution as a function of the effective height.

	Level	1	2	3	4	5	6
	Effective height (m)	-	138	254	423	652	944
SNAP CODE	01	0	0	8	46	29	17
	02	50	50	0	0	0	0
	03	0	4	19	41	30	6
	04	90	10	0	0	0	0
	05	90	10	0	0	0	0
	06	100	0	0	0	0	0
	07	100	0	0	0	0	0
	08	100	0	0	0	0	0
	09	10	15	40	35	0	0
	10	100	0	0	0	0	0

In WRF-Chem the plume rise was calculated by means of the SMOKE module *Laypoint*, that uses gridded hourly meteorological data and stack parameters to calculate the plume rise for all point-source emissions. The program's approach is based on the Briggs algorithm (Briggs, 1965), and provides the effective emission height as well as the top and bottom heights of the plume. *Laypoint* uses these heights to compute the plume distribution into the vertical layers that the plume intersects, using the pressure difference across each layer over the pressure difference across the entire plume as a weighting factor. Only 11 layers were included in the calculation, from the surface up to 2500 m.

Italian emission inventory provides both low-level and point emissions as well as stack parameter for each aloft source (e.g. stack height, stack diameter, gas exit velocity and gas exit temperature). On the contrary, this information is not included in EMEP data. To this aim EMEP emissions were firstly distributed between surface and height according to EMEP profiles and depending on SNAP sectors (Table 14; Vestreng, 2003). Combustion and industrial emissions from SNAP sector 1, 2, 3, 4, 5 and 9 were treated as elevated sources, while it was assumed that the leftover sectors were only surface emitted. Data of stack height, stack diameter, gas exit velocity and gas exit temperature were applied using average stack

values depending on SNAP sector (personal communication of G. M. Riva).
Meteorological fields needed for the plume rise algorithm are provided by MCIP processor (Meteorology-Chemistry Interface Processor; Otte and Pleim, 2010) and a previous WRF simulation performed with the same meteorological configuration.

Table 14 – Distribution between surface and height for 11 SNAP sectors of EMEP emissions.

SNAP	01	02	03	04	05	06	07	08	09	10	11
surface	0.	50.	0.	90.	90.	100.	100.	100.	10.	100.	100.
height	100.	50.	100.	10.	10.	0.	0.	0.	90.	0.	0.

As an example, annual emissions processed by SMOKE are reported in Table 15. WRF-Chem VOC emissions show a slightly decrease of -2% with respect to CAMx because of the different approach in their speciation. It is worth noting that this variation concerns the whole domain and the entire year 2005.

Table 15 –Emissions processed by SMOKE for the whole Italian domain.

Data base	CO [Mg/year]	NOx [Mg/year]	VOCs [Mg/year]	NH_3 [Mg/year]	SO_2 [Mg/year]	$PM_{2.5}$ [Mg/year]	PM Coarse [Mg/year]
ISPRA	3.08E+06	8.88E+05	1.18E+06	4.14E+05	7.49E+04	1.15E+05	3.05E+04
EMEP	3.23E+06	1.59E+06	1.12E+06	5.24E+05	6.70E+05	1.97E+05	9.32E+04
Total	**6.30E+06**	**2.48E+06**	**2.31E+06**	**9.38E+05**	**7.45E+05**	**3.12E+05**	**1.24E+05**

Natural emissions were treated separately, although their on-line calculation is allowed in WRF-Chem. In the current version of the code, the MEGAN (Model of Emissions and Gases from Nature) biogenic emission model is completely embedded in the code as well as the sea salt algorithm of Gong et al. (2003). Nevertheless, in this application MEGAN model (version 2.04, Guenther et al., 2006) and SeaSalt code (Gong et al., 2003) were applied off-line in both

modeling systems in order to obtain more comparable emission fields.
In WRF-Chem the natural fields are added to SMOKE outputs using unit and species conversion factors. Concerning VOC species the molar ratio was calculated using the number of isoprenic unit in each molecule and then multiplied for the unit conversion form g/s to moles/h. One to one aggregation was done for PM.

4.1.3 Boundary conditions

Initial and boundary conditions for chemistry were derived from the same CHIMERE model run at European scale (Bessagnet et al., 2004).
CHIMERE provides chemical fields for 142 species over Europe with horizontal resolution of 0.5 degrees and temporal resolution of one hour. The vertical grid extends from the ground up to 8000 m. It uses MELCHIOR (Derognat et al., 2003) gas-phase mechanism and ISORROPIA aerosol scheme (Nenes et al., 1998) that treat gas and aerosol compounds differently than the chemical mechanisms adopted in CAMx and WRF-Chem.
Boundary conditions were prepared using some ad hoc codes that were developed in order to: (1) vertically interpolate the 8-layers CHIMERE grid to WRF-Chem and CAMx vertical levels; (2) spatially interpolate CHIMERE fields onto the computational domain; (3) link CHIMERE species to WRF-Chem and CAMx ones.
Meteorological initial and boundary condition were provided by the 6-hourly ECMWF analysis fields (European Centre for Medium-Range Weather Forecasts; http://www.ecmwf.int) with 0.5 degrees of horizontal resolution and the 24-land use categories of the U.S. Geological Survey (USGS).

4.2 METHODS

WRF-Chem and CAMx simulations were compared against chemical and meteorological observations using AMET (*Atmospheric Model Evaluation Tool*, version 1.1; Appel et al., 2011).
Ground-based concentrations for the calendar year 2005 have been taken from the European network AirBase. Data are available on the AirBase web site for a large number of stations for all countries of European Union (http://air-climate.eionet.europa.eu/databases/airbase/), but with heterogeneous quality and mostly at rather polluted locations not representative for the model grid size of 15 km.
Indeed, only NO_2, NOx, SO_2, PM_{10} and $PM_{2.5}$ observation were selected. Stations were chosen with data annual coverage of 75% and higher, with the exception of PM_{10} and $PM_{2.5}$ for which a less restrictive threshold of 40% is applied. Stations showing outliers in yearly statistics were rejected and only background stations (rural, suburban and urban) were included in the analysis. A set of 300 stations was found to fulfill the selection criteria over the whole domain.
In addition, PM composition was analyzed against EMEP observations (European Monitoring and Evaluation Programme). In the EMEP programme a number of stations throughout Europe report quality-controlled, long-term measurements of gaseous precursor substances and aerosol variables. Suphate, nitrate and ammonium daily data at 12 stations belonging to the modeling domain were selected, while elemental carbon (EC) and organic carbon (OC) were available only at Ispra station. PM_{10} and $PM_{2.5}$ observations were integrated where necessary.
Meteorological observations are archived from the WMO measurement network (World Meteorological Organization). Surface data have 3-hours temporal coverage and they are available for temperature, dew point temperature, pressure, relative humidity, wind speed, wind direction and precipitation. A set of 114 meteorological stations were found over the computational domain for the year 2005.

Results were examined as monthly averages, time series, cross vertical sections and performance statistics.
Measurement stations of chemical compounds were divided in three different regions of the computational domain: Po valley area, Center-South of Italy and foreign countries. Moreover sites were grouped according to their location in rural background (RB) and urban-suburban background (UBSB). PM_{10}, $PM_{2.5}$ and PM composition data has been analyzed together with the main gaseous precursors (NO_2 and SO_2). Concentrations were expressed as daily means.
As described in Pirovano et al. (2012), the following metrics are considered in the analysis (Appendix A1): mean observed and mean modeled, Normalized Mean Bias (NMB), Normalized Mean Error (NME), Root Mean Square Error (RMSE) and Pearson Correlation (r). The first five indices enable to elucidate the accuracy of the models in reproducing gas and aerosol concentrations, while the other to characterize the daily or monthly evolution.
Since WRF-Chem and CAMx shared the same meteorology, meteorological outcomes are only analyzed for the first model. Modeled and observed data are corrected from the presence of outliers. Temperature is investigated when the difference between model and observation is lower than 20 °K, while a threshold of 10 g/kg is set for mixing ratio. Wind speeds lower than 0.5 m/s and higher than 100 m/s are rejected.
As for meteorology, different metrics were selected (Appendix A2): mean observed and mean modeled, Mean Bias (MB), Mean Absolute Error (MAE), Root Mean Square Error (RMSE) and Pearson Correlation (r).

4.3 RESULTS AND DISCUSSION

4.3.1 Meteorology

WRF performances have been extensively analyzed in Chapter 2 for the current modeling configuration. Therefore meteorological evaluation has been limited here to surface parameters.

Table 16 shows the statistical indices averaged at all stations, while in Figure 45 we reported the diurnal statistics trend for all stations.
The comparison of simulated 2m-temperature, 2m-mixing ratio and 10m-wind speed shows very good agreement with WMO measurement data both in terms of temporal variability and average values.
The means of temperature and wind speed are well reproduced. Also relative humidity is realistically represented.
All meteorological variables are overpredicted by the model. Temperature is simulated with a correlation of 0.82, a positive mean bias of 0.82°K and mean absolute error of 2.85°K, due to overestimation of daily minima during early morning.
The model reproduces relative humidity with a correlation of 0.80 and a small bias of 0.37 g/kg, due to maximum values in the morning, consistently with the temperature overestimation.
Finally, the model systematically overestimates wind speeds by about 0.42 m/s. Nevertheless, the diurnal cycle is well reproduced, showing a correlation of 0.5.

Table 16 – Performance statistics for 2m-temperature, 2m-mixing ratio and 10m-wind speed.

Parameter	Mean Observed	WRF Mean	MB	MAE	RMSE	r
Temperature (°K)	277.58	278.40	0.82	2.85	3.72	0.82
Mixing ratio (g/kg)	4.36	4.73	0.37	0.80	1.05	0.80
Wind speed (m/s)	4.07	4.48	0.42	2.14	2.93	0.55

Overall, meteorology is well represented but the errors in temperature and wind speed simulation may affect chemical transformation rates and aerosol formation processes.

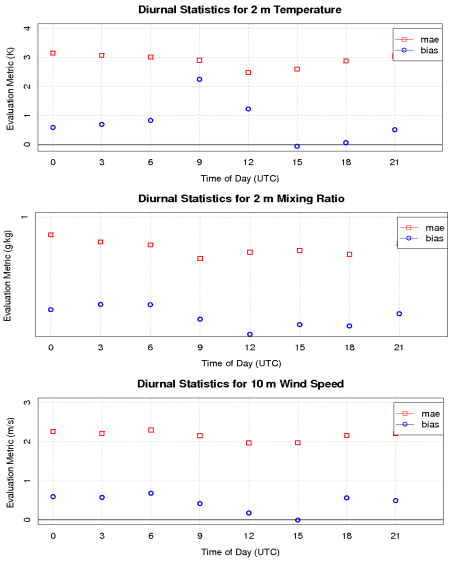

Figure 45 – Diurnal variation of Bias and MAE statistics for 2m-temperature, 2m-mixing ration and 10m-wind speed averaged at all stations.

4.3.2 Chemistry

Performance indices of model results are reported in Table 17 at all measurement stations. In the following sections we will discuss the performance results for each compound.

4.3.2.1 Gas species

Gas-phase precursors which lead to the secondary aerosol part of Particulate Matter are analyzed here. The simulated concentration of these species is regulated mainly by the transport, diffusion and removal properties of a CTM and the way in which the emissions are distributed within the grid (Sten et al., 2008).

Figure 46 shows SO_2 concentrations over Italy. WRF-Chem and CAMx are able to reconstruct the main emission areas of the Po Valley region (Milan and Bologna), where the mean concentrations

yield up to 8-10 ppb. In this region, CAMx is generally higher than WRF-Chem. On the contrary, in the Eastern area of the modeling domain WRF-Chem reproduces the highest values.
Finally, international shipping provides an important contribution only in the South-West Mediterranean Sea, beyond Sicily region.
Concerning the overall performances, models are found to underestimate SO_2 concentration in all measurement stations, because of the underestimation observed to a large extent in foreign countries and North-West of Italy (Figure 50). WRF-Chem estimations show a NMB of -29.5%, whereas for CAMx is -33.0%. The averaged statistics for NME ranges from 74.2% (CAMx) to 74.4% (WRF-Chem).
Differences in model results might in part be related to the different plume rise assumption inside models and the different reconstruction of the vertical diffusion. Particularly, the first assumption can explain higher WRF-Chem concentrations outside the Italian boundaries, where the major differences in the treatment of point emissions are located. On the contrary, the second one can elucidate the discrepancies over the Italian region.

Table 17 – Performance statistics of daily data at all measurement stations.

Compound	Network	Mean observed	WRF-Chem					CAMx				
			Mean	NMB (%)	NME (%)	RMSE	r	Mean	NMB (%)	NME (%)	RMSE	r
SO_2 (ppb)	AirBase	3.28	2.31	-29.5	74.4	6.6	0.21	2.20	-33.0	74.2	6.7	0.17
NO_2 (ppb)	AirBase	17.81	9.74	-45.3	52.2	12.3	0.57	8.59	-51.8	56.3	13.0	0.57
NOx (ppb)	AirBase	47.17	20.19	-57.2	64.7	52.0	0.40	17.62	-62.7	67.1	53.0	0.41
PM_{10} ($\mu g/m^3$)	AirBase	38.12	16.61	-56.4	60.1	33.9	0.46	16.51	-56.7	61.5	35.1	0.34
PM_{25} ($\mu g /m^3$)	AirBase	29.58	15.38	-48.0	53.1	23.7	0.58	15.20	-48.6	55.3	25.1	0.46
NH_4 ($\mu g\ N/m^3$)	EMEP	4.15	4.08	-1.7	69.5	3.8	0.31	3.84	-7.5	70.7	3.9	0.25
NO_3 ($\mu g\ N/m^3$)	EMEP	1.85	1.12	-39.7	57.5	1.8	0.50	0.89	-52.1	63.8	2.0	0.39
SO_4 ($\mu g\ S/m^3$)	EMEP	1.31	0.65	-50.2	55.8	1.2	0.64	0.99	-24.8	52.9	1.2	0.43

Figure 47, Figure 48 and Figure 49 compare the daily mean SO_2 concentrations computed by WRF-Chem and CAMx. The observed trend is well reproduced by the models. Best performances generally occur in rural background stations outside the Italian region, with the exception of an episode taking place from 8 to 10 of February. There is also a worsening in model performances moving from North to Central-South of Italy.

CAMx produce slightly higher concentrations than WRF-Chem in the Po valley area. As shown below, this can be ascribed to a stronger vertical mixing in CAMx than WRF-Chem favoring a downward flux of aloft emissions. The different behavior of SO_2 concentrations was well captured at both rural (median observed = 1.2 ppb; median WRF-Chem = 1.0 ppb; median CAMx = 1.1. ppb) and urban-suburban background stations (median observed = 2.3 ppb; median WRF-Chem = 1.9 ppb; median CAMx = 2.1 ppb). Differently, both models overestimate measured concentrations in Center-South of Italy. Overpredictions are generally associated to coastal stations (Figure 50) where the main emitting sites are located (e.g. industrial and shipping areas). A possible overestimation of the principal emitting sources in the emission inventory can contribute to the observed mismatch, together with too low vertical dispersion at the interface between land and sea. Uncertainties in emission inventories for SO_2 have been shown to be generally large (de Meij et al., 2006; Endresen et al., 2005) and even more so for their strongest contributor, international shipping (Endresen et al., 2005), consistent with the stronger overestimation at coastal stations.

Moreover, inefficiency in aqueous phase oxidation of SO_2 to particulate SO_4 can partially explain this overestimation (Tuccella et al., 2012).

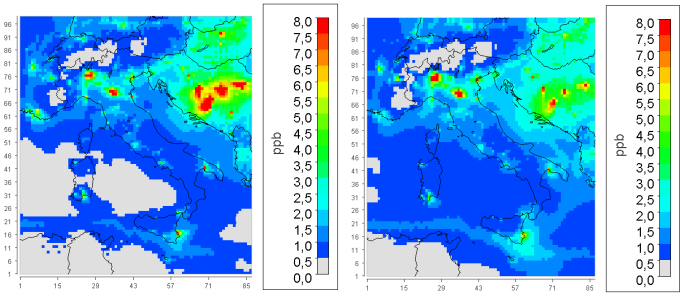

Figure 46 – SO_2 mean concentrations for WRF-Chem (left) and CAMx (right).

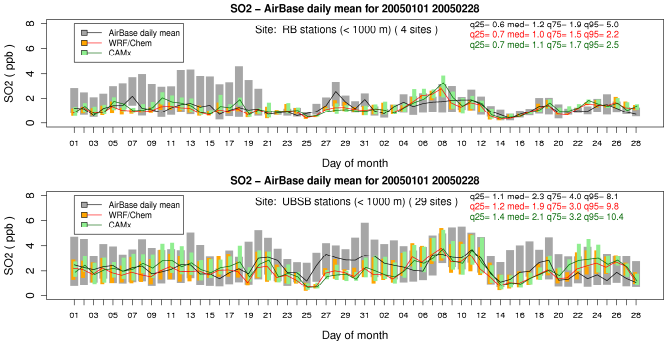

Figure 47 – SO_2 time series of daily data at all measurement stations of the Po Valley.

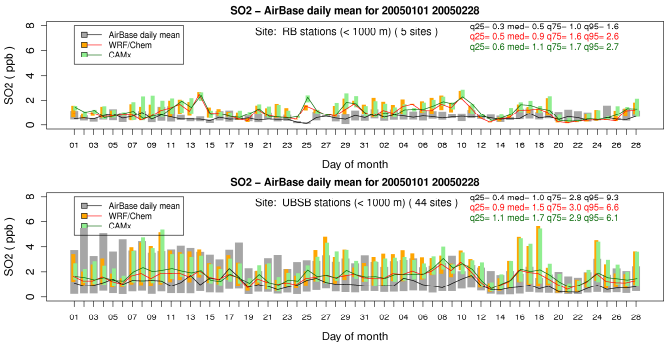

Figure 48 – SO_2 time series of daily data at all measurement stations of Center-South of Italy.

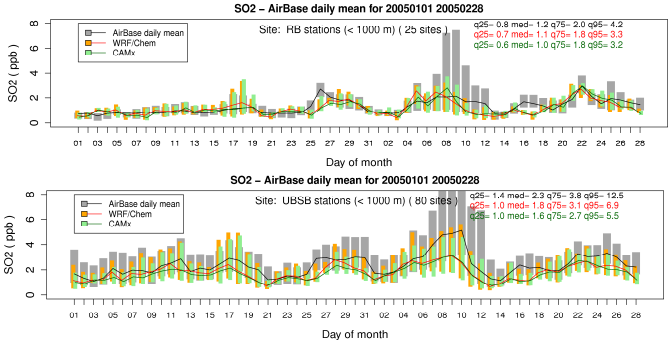

Figure 49 – SO_2 time series of daily data at all measurement stations of foreign countries.

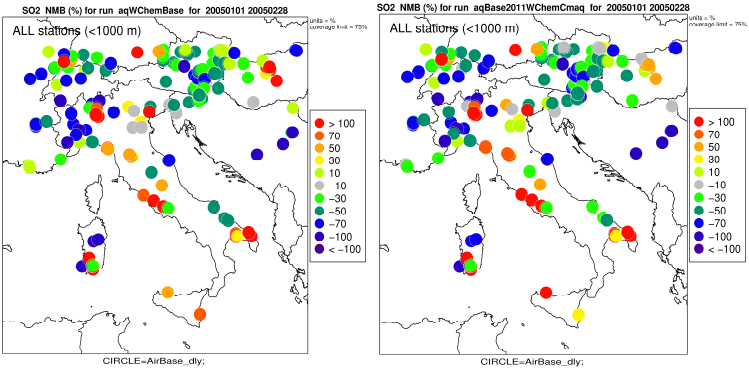

Figure 50 – Normalized Mean Bias distribution at all measurement stations in the computational domain for SO_2. *aqWChemBase* indicates the WRF-Chem simulation (left), while *aqBase2011WChemCmaq* is used for CAMx (right).

NO_2 and NOx concentrations are reported in Figure 51 and Figure 52, respectively. Nitrogen Oxides are emitted predominantly by fossil fuel combustion processes, as road transport, domestic heating and energy production. They are emitted largely as NO, but very quickly converted to NO_2. Therefore, NO_2 can be considered as a good marker of the correct reconstruction of the emissions distribution and strength. The highest concentrations of Nitrogen

Dioxide were found in Milan, Turin and Naples, showing NO_2 average concentrations close to 30 ppb in both modeling applications. Such high concentrations are also observed near the major cities and along the major transit route, where NO_2 computed values range between 6 and 20 ppb. NOx mean concentration can raise up to 70 ppb in Milan and Turin, but it generally shows a smooth difference between the two models.

In the main emitting areas WRF-Chem computes higher concentrations for both NO_2 and NOx, that result in better performances in terms of NMB and NME.

Models reproduced NO_2 concentrations with a Normalized Mean Bias that range from -45.3% (WRF-Chem) to -51.8% ppb (CAMx) whereas for NOx concentrations NMB is between -57.2% (WRF-Chem) and -62.7% (CAMx). The correlation is 0.57 for NO_2 and 0.4 for NOx in both modeling applications.

Indeed, WRF-Chem and CAMx show a rather coherent behavior in reconstructing the daily concentration trend of Nitrogen Oxides in all station type and areas, but they underestimate the observed values (Figure 53, Figure 54 and Figure 55). The major underestimations are associated to urban-suburban stations, because of the 15 km horizontal resolution that is more representative of a rural environment.

The quite homogeneous level of NO_2 performances in the two applications suggested that the observed underestimation cannot be related mainly to the influence of the model structure, but it need to be related either to a lack in NOx emission inventories or to an overestimation of dispersion processes, as well as to the limited model resolution.

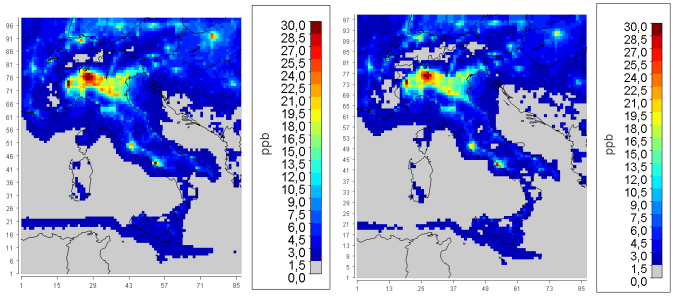

Figure 51 – NO_2 mean concentrations for WRF-Chem (left) and CAMx (right).

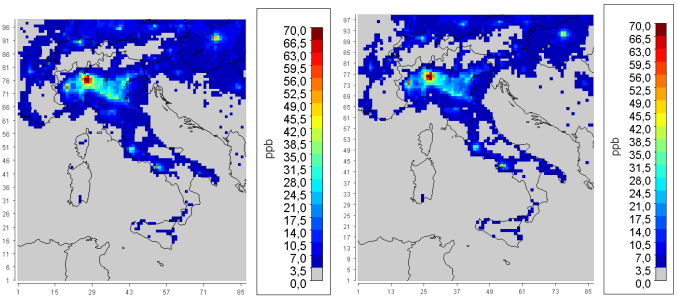

Figure 52 - NOx mean concentrations for WRF-Chem (left) and CAMx (right).

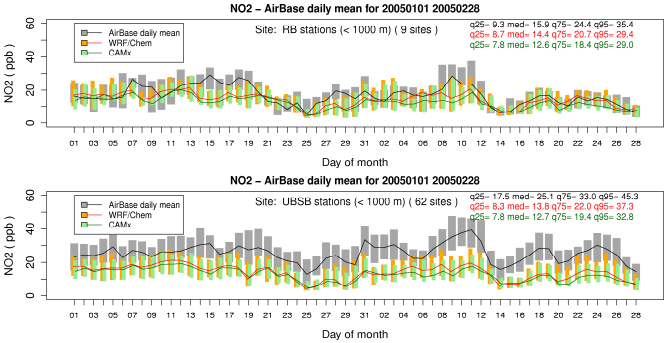

Figure 53 – NO_2 time series of daily data at all measurement stations of the Po Valley.

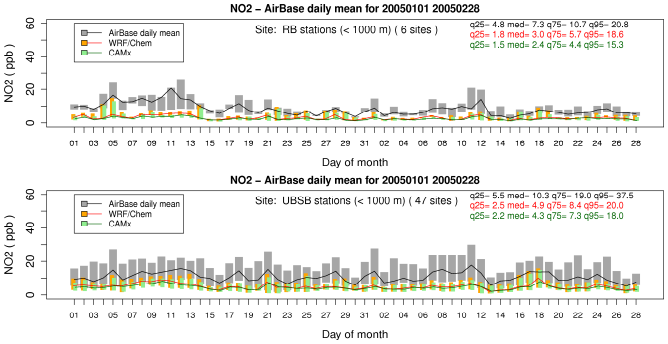

Figure 54 – NO_2 time series of daily data at all measurement stations of Center-South of Italy.

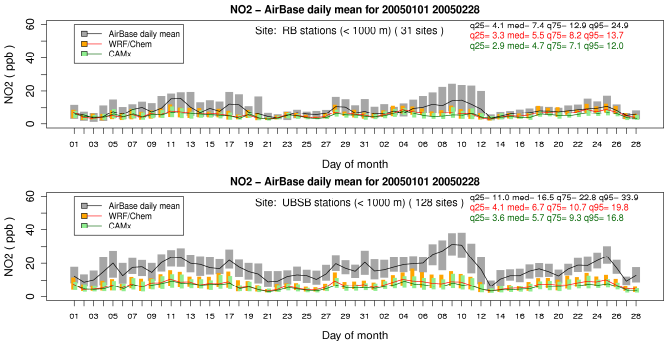

Figure 55 – NO_2 time series of daily data at all measurement stations of foreign countries.

Though they were not particularly relevant, the models showed some systematic differences.

The previous outcomes have shown that in the Po valley WRF-Chem has higher concentrations of ground-emitted compounds (NOx and NO_2), whereas CAMx has higher values of aloft-emitted species (SO_2).

One possible cause of this behavior would be the different vertical profile of Kz. Indeed, Kz is calculated differently in the two model

applications. In WRF-Chem it is computed directly inside the model; while in CAMx Kz is calculated externally by means of the WRFCAMx preprocessor (release 2.3; www.environcorp.com/) which includes several algorithms to determine its value. In this work the CMAQ algorithm was adopted (Byun et al., 1999).

To check this possibility, cross sections of NOx and SO_2 are analyzed on February 21st at 9 UTC.

Figure 56 highlights that CAMx is characterized by a stronger vertical diffusion below the PBL. NOx concentrations are well mixed in the first model layers affecting the surface concentration of primary compounds, especially for stable conditions. At the same time, differences in vertical profiles of Kz strongly influenced the impact of aloft sources on ground level concentrations. Aloft emitted compounds are down welled by vertical fluxes, increasing ground level concentrations of primary pollutants such as SO_2. This is also consistent with previous studies (Pirovano et al., 2012).

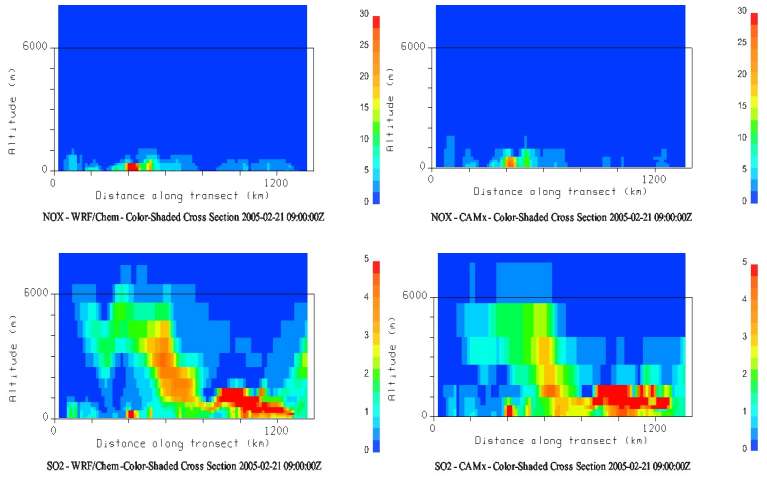

Figure 56 – NOx (top) and SO_2 (bottom) vertical cross sections at 45.5 °N on February 21st at 9.00 UTC.

4.3.2.2 Aerosols compounds

The spatial distribution of PM_{10} concentration is represented in Figure 57. The highest concentrations have been found near urbanized regions. Particularly, Po valley is a densely populated, highly industrialized area and it is known to have a relatively high level of anthropogenic pollution. In this site the concentration are always higher than 25 $\mu g/m^3$ in both modeling systems. Some discrepancies are found in the city of Milan, where WRF-Chem simulates PM_{10} concentrations of 40 $\mu g/m^3$ while CAMx is generally lower (32-36 $\mu g/m^3$). This confirms the previous hypothesis of higher vertical diffusion in CAMx application which generates lower concentrations of primary ground-emitted pollutants.
However the concentrations decrease sharply as one moves from urban and suburban to rural site and then to remote sites. In different rural sites the simulated average concentration is quite similar and ranges between 8 to 16 $\mu g/m^3$. The striking difference between urban-suburban areas and remote locations evidences the dominant role of anthropogenic emissions to PM_{10} concentrations. PM is produced mainly by vehicles and domestic heating emissions; as a result the average distribution of particular matter has a similar pattern to NOx.
WRF-Chem and CAMx have comparable performances for PM_{10}, showing a NMB of -56.4% and -56.7%, respectively. Correlation varies between 0.34 (CAMx) and 0.46 (WRF-Chem).
Figure 58, Figure 59 and Figure 60 compare the monthly time series of PM_{10} daily values in different station types and areas. Models capture the daily trend but they underestimate the magnitude of observed values. We found systematic negative biases through the season, especially in the Po valley and in both rural and urban-suburban background stations.
Rural stations are deemed the most representative for a model evaluation, but analyzing the measured trend in the Po valley region is possible to observe some quite unusual high values which models cannot reproduce. Henne el al. (2010) and Joly and Peuch (2012) noticed that measurement stations are often categorized based on

subjective criteria that are not uniformly applied by the European atmospheric community, yielding an inconsistent site classification. Moreover, Po valley is known to be a problematic area with respect to pollution from PM_{10}, with a number of daily exceedances of the limit value (50 $\mu g/m^3$) which is by far beyond the 35 days/year allowed by the air quality directive (Directive 2008/50/EC).
Indeed, moving from North to Center-South of Italy and, then, to neighboring countries, model performances improve, but the underestimation persists.
PM_{10} underestimation can have multiple reasons including: (1) missing sources (e.g. resuspension and local mineral dust sources) that contribute mainly to the coarse fraction (Hendriks, 2009; Hodzic et al., 2007; Vautard et al., 2005); (2) lacking in aerosol processes; (3) overestimation of either wind speed or vertical dispersion in the first model layers.
Discrepancies in PM_{10} NFB and NFE are similar to NO_2 and NOx, confirming that there is inaccuracy in the reconstruction of emission sources inside emission inventories. Indeed, the characterization of PM sources is an area of active research as many gaps in our knowledge are reported by different studies (Solazzo et al., 2012; Simpson et al., 2007 and Whyatt et al., 2007). The underestimation could also be an artefact of the limited model resolution.
On the other hand, differences between models are mainly related to chemical mechanisms and, once againg, to vertical dispersion coefficient (Kz).

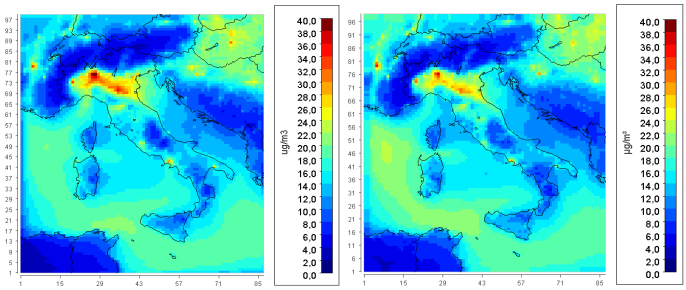

Figure 57 – Winter mean of PM_{10} concentrations for WRF-Chem (left) and CAMx (right).

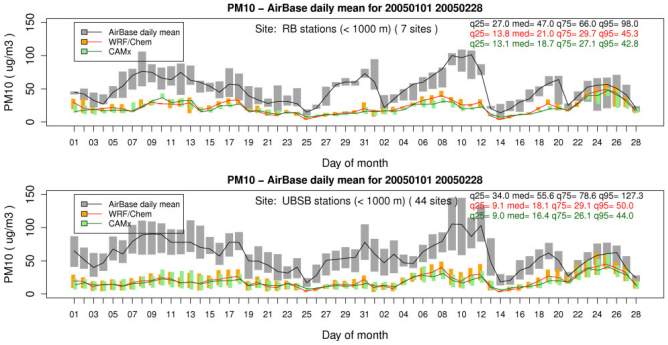

Figure 58 – PM_{10} time series of daily data at all measurement stations of the Po Valley.

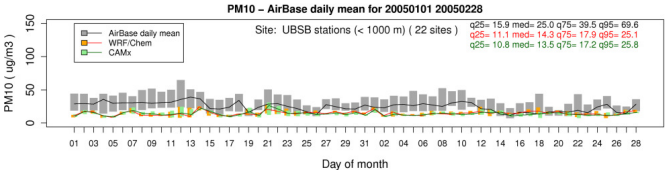

Figure 59 – PM_{10} time series of daily data at all measurement stations of Center-South of Italy.

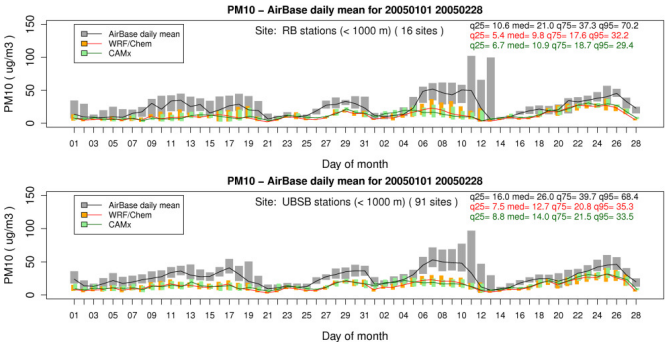

Figure 60 – PM_{10} time series of daily data at all measurement stations of foreign countries.

The $PM_{2.5}$ spatial pattern is represented in Figure 61. As for PM_{10}, WRF-Chem exhibits higher concentrations than CAMx, particularly in the Po valley area.
Comparing $PM_{2.5}$ and PM_{10} shows that model performances improve when just the fine fraction is considered. This result suggests that emissions of coarse PM are missing from both models.
CAMx correlation (0.46) is smaller than WRF-Chem correlation (0.58), indicating that WRF-Chem follows the observed time pattern better than CAMx. Conversely the two models showed a very similar NMB, equal to -48.6% for CAMx and to -48.0% for WRF-Chem. Model performances correspond in magnitude, even though WRF-Chem is slightly better than CAMx because of the different efficiency in reconstructing secondary inorganic aerosols (SIA) fraction, as detailed in the following paragraph.
The overall $PM_{2.5}$ has a tendency towards negative biases. As discussed later in this work, this is caused by an underestimation of all components. As reported by Stern et al. (2008), gaps in the knowledge of many of the physical and chemical processes constitute important sources of error in $PM_{2.5}$ estimations.
$PM_{2.5}$ monthly time series of daily concentrations are analyzed in Figure 62. Since only 13 sites were available for this compound, stations were grouped simply by station type.
Surprisingly, the best performances are in urban-suburban background stations, suggesting a possible incorrect classification of some measurement sites on the Italian Peninsula.

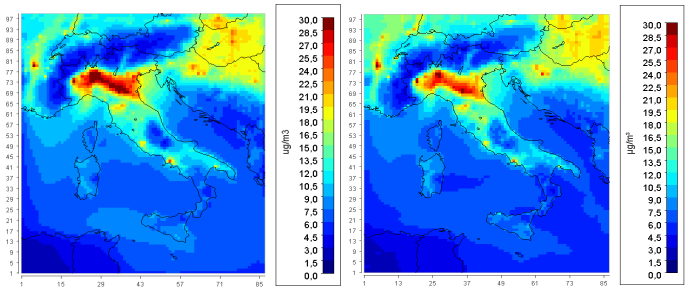

Figure 61 – Winter mean of $PM_{2.5}$ concentrations for WRF-Chem (left) and CAMx (right).

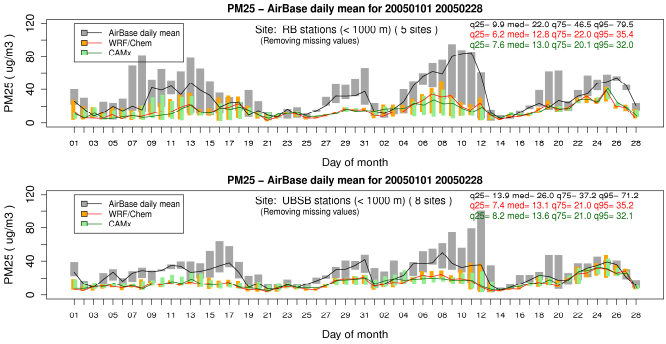

Figure 62 – $PM_{2.5}$ time series of daily data at all measurement stations over the whole domain.

4.3.2.3 Secondary Inorganic Aerosols

To investigate the causes of $PM_{2.5}$ underestimation and differences in model performances, the aerosol chemical composition was evaluated by comparison with EMEP data. As an example, Figure 63 and Figure 64 show a comparison with observations of the $PM_{2.5}$ speciation in Ispra (IT) and Payerne (CH).

Analyzing the time series of Ispra station is quite clear that the underprediction of $PM_{2.5}$ is due to a wrong reconstruction of the main aerosol primary components.

The aerosol composition showed a significant underestimation of EC and OC in Ispra station for both models (median observed=3.9 $\mu g/m^3$; median WRF-Chem and CAMx=0.8 $\mu g/m^3$). The underestimation of EC is well documented in literature, especially in the Po valley (Tuccella et al., 2012; Yttri et al., 2007), and is mainly related to a lack in the main emission sources i.e. transportation and domestic heating.

On the contrary, OC underestimation of CAMx model can be due to an inefficient transformation of gaseous precursor during the Secondary Organic Aerosol (SOA) formation process. However, it is worth noting that CAMx concentrations of OC are identical to WRF-Chem which does not account for any SOA in the current application.

As reported in Gilardoni et al. (2011) more than 50% of the OM measured at this site is related to local biomass burning (i.e. wood burning from domestic heating). This fraction reaches 63% in the cold season. Those arguments suggest that the underestimation of the winter OC is due to a deficiency in emissions rather than in SOA formation (Pernigotti et al., 2013).

Secondary Inorganic Aerosols (SIA) at Ispra site are slightly better reconstructed by the two models than carbonaceous compounds, at least during February. Differently, the time evolution is well represented by our simulations both in Ispra and Payerne. Single events with higher aerosol concentrations correspond in time with the observations. However, several model deficiencies can be seen throughout the comparison, namely an overestimation of ammonium in Payerne and an underestimation of nitrate and sulphate. The overestimation of ammonium is occurring only at Payerne station and it is caused by an overestimation of the total ammonia (not shown); while the underestimation of sulphate supports the previous hypothesis of an inefficient aqueous phase conversion of SO_2 to SO_4.

Investigating $PM_{2.5}$ total mass with respect to SO_4, NO_3 and NH_4, it is possible to state that secondary inorganic aerosols are generally better reproduced by the models than total $PM_{2.5}$, confirming that large errors exist in the simulation of the other components of $PM_{2.5}$ such as unspeciated $PM_{2.5}$.

Simulated NH_4 has a normalized mean bias of -1.7% (WRF-Chem) and -7.5% (CAMx), NO_3 is underestimated by -39.7% (WRF-Chem) and -52.1% (CAMx). Finally, SO_4 shows a NMB of -50.2% and -24.8% for WRF-Chem and CAMx, respectively.

CAMx has higher SO_4 concentrations than WRF-Chem due to the corresponding higher availability of SO_2. Consequently, WRF-Chem has higher NH_4 and NO_3 concentrations because lower ammonia is consumed by sulphate thus favoring the formation of ammonium nitrate (NH_4NO_3) (Meng et al., 1997; Seinfeld and Pandis, 1998).

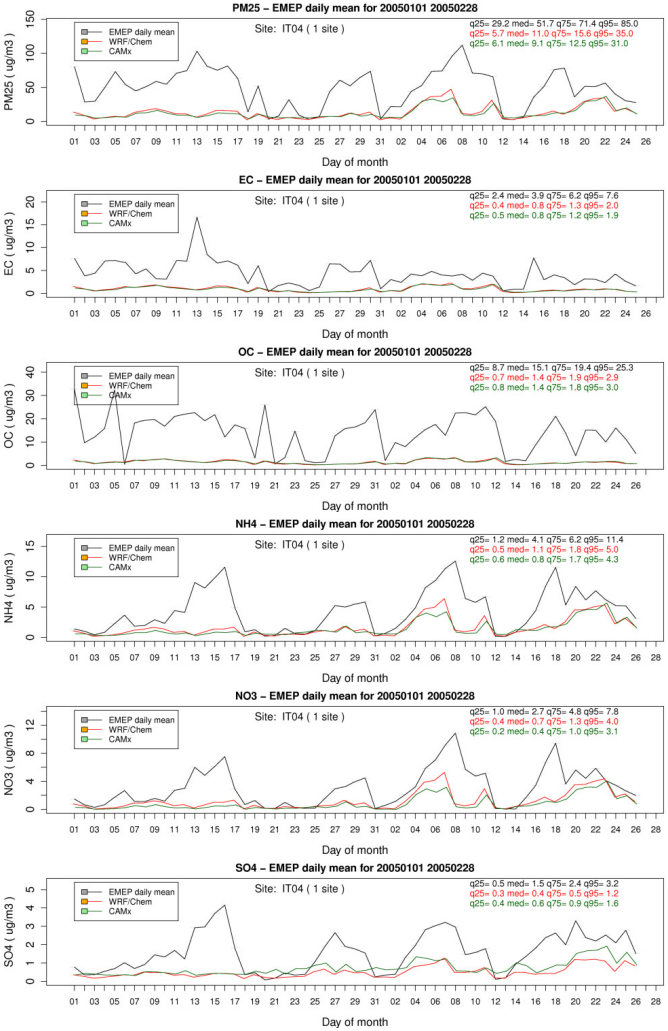

Figure 63 – Time series of $PM_{2.5}$ and its main components at Ispra station (Italy).

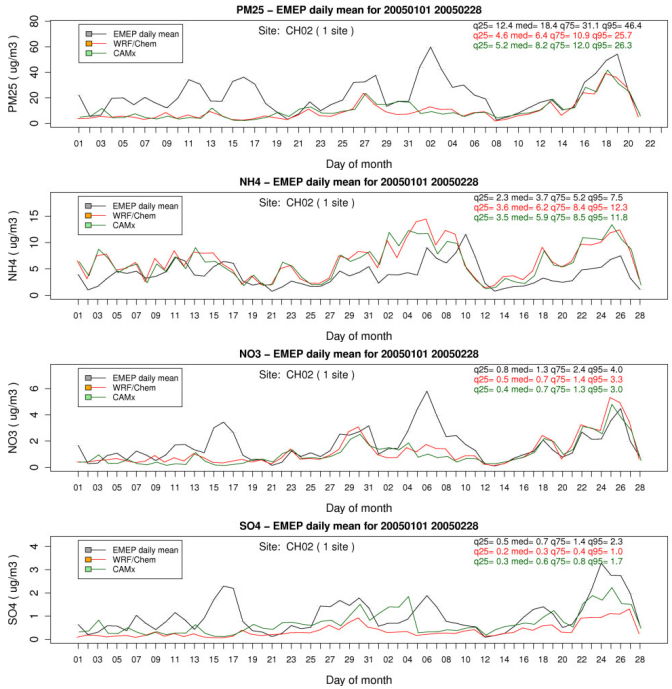

Figure 64 – Time series of $PM_{2.5}$ and its main components at Payerne station (Switzerland).

4.4 CONCLUSIONS

A modeling comparison has been performed over Italy for January and February 2005 in order to investigate the effect of on-line approach on air quality simulations. To this aim, the on-line Weather Research and Forecasting model coupled with chemistry (WRF-Chem) has been evaluated against the CAMx off-line Eulerian chemistry and transport model. WRF-Chem and CAMx shared the same computational domain, emissions, boundary conditions and meteorology. However, they use different gas and aerosol chemistry.

WRF-Chem implements CBM-Z gas-phase reactions and MOSAIC for aerosol formation, whereas CAMx includes CB05 gas mechanism and ISORROPIA aerosol scheme.
Results were analyzed subdividing the computational domain in three regions: Po valley, Center-South of Italy and foreign countries.
Model demonstrated similar geographical variation in reproducing gaseous compounds, even though WRF-Chem is generally closer to observations. Particularly, in the Po valley WRF-Chem has higher concentrations of ground-emitted compounds (NOx and NO_2), whereas CAMx has higher values of aloft-emitted species (SO_2). Differences in the reconstruction of vertical diffusion coefficients (Kz) and wind speed in the first model layers can affect those surface concentrations of primary compounds, especially for stable conditions. CAMx vertical mixing proved to be more efficient than WRF-Chem. As a consequence, CAMx has better performances for SO_2 in the Po valley, while WRF-Chem improves the performances for NO_2 and NOx. On the contrary, outside the Italian boundaries WRF-Chem reproduces better SO_2 concentrations, because of the different plume rise assumption in the two applications.
Models underestimated PM_{10} and $PM_{2.5}$ concentrations. PM_{10} model performances are similar to NO_2 and NOx, suggesting that there is inaccuracy in the reconstruction of emission sources inside emission inventories for both NOx and PM_{10}. Moreover comparing $PM_{2.5}$ and PM_{10} shows that model performances improve when just the fine fraction is considered. This result suggests that emissions of coarse PM are missing from both models. The aerosol composition showed a significant underestimation of EC and OC that can be related to the underestimation of $PM_{2.5}$.
PM performances were rather poor for both models, but WRF-Chem model improves the overall results. Differences in vertical diffusion might cause differences between models in reproducing PM_{10} concentrations, while different efficiency in reconstructing secondary inorganic aerosols fraction can explain model discrepancies for $PM_{2.5}$. CAMx has higher SO_4 concentrations than WRF-Chem due to the corresponding higher availability of SO_2. Consequently, WRF-

Chem has higher NH_4 and NO_3 concentrations, improving the general performances of $PM_{2.5}$.

4.5 REFERENCES

Appel K.,W., R.C. Gilliam, N. Davis, A. Zubrow, S.C. Howard, 2011. Overview of the atmospheric model evaluation tool (AMET) v1.1 for evaluating meteorological and air quality models. Environmental Modelling & Software, 26, 434-443, doi: 10.1016/j.envsoft.2010.09.007.

Balzarini, A., Pirovano, G., Riva, G.M., Toppetti, A., 2012. Prime valutazioni delle interazioni clima-qualità dell'aria mediante l'applicazione del modello accoppiato meteorologico-chimico WRF-Chem. Rapporto RSE n°12001041.

Barnard J., Chapman E.G., Fast J., Schmelzer J.R., Slusser J.R., Shetter R.E., 2004. An evaluation of the FAST-Jphotolysis algorithm for predicting nitrogen dioxide photolysis rates under clear and cloudy sky conditions. Atmospheric Environment 38, 3393–3403. doi:10.1016/j.atmosenv.2004.03.034.

Bessagnet B., A. Hodzic, R. Vautard, M. Beekmann, S. Cheinet, C. Honore, C. Liousse, L. Rouil., 2004. Aerosol modeling with CHIMERE-preliminary evaluation at the continental scale. Atmospheric Environment, 38, 2803-2817.

Bessagnet, B., Khvorostyanov, D., Menut, L., Monge, J.L., Vautard, R., 2009. Documentaion of the chemistry transport model CHIMERE. http://www.lmd.polytechnique.fr/chimere/docs/CHIMEREdoc2008.pdf

Briggs G.A., 1965. A plume rise model compared with observations, Journal of Air Pollution Control Association, 15:9, 433-438, doi: 10.1080/00022470.1965.10468404.

Byun, D. W. and Ching, J. K. S., 1999. Science algorithms of the EPA Models-3 Community Multiscale Air Quality (CMAQ) Modeling System. US Environmental Protection Agency Report,EPA-600/R-99/030, 727.

Carter W., 2011. SAROAD assignment, http://www.cert.ucr.edu/~carter/emitdb

Chang, J.S., R.A. Brost, I.S.A. Isaksen, S. Madronich, P. Middleton, W.R. Stockwell, and C.J, Walcek., 1987. A Threedimensional Eulerian Acid Deposition Model: Physical Concepts and Formulation. J. Geophys. Res., 92, 14,68114,700.

Chen, F., Dudhia, J., 2001. Coupling an Advanced Land Surface–Hydrology Model with the Penn State–NCAR MM5 Modeling System. Part I: Model Implementation and Sensitivity. Monthly Weather Review 129, 569–585.

Chou, M.-D., Suarez, M. J., Ho, C.-H., Yan, M. M.-H., Lee, K.-T., 1998. Parameterizations for cloud overlapping and shortwave single-scattering properties for use in general circulation and cloud ensemble models. J. Clim. 11, 202-214.

Cuvelier, C., Thunis, P., Vautard, R., Amann, M., Bessagnet, B., Bedogni, M., Berkowicz, R., Brandt, J., Brocheton, F., Builtjes, P., Carnevale, C., Copalle, A., Denby, B., Douros, J., Graf, A., Hellmuth, O., Honoré, C., Hodzic, A., Jonson, J., Kerschbaumer, A., de Leeuw, F., Minguzzi, E., Moussiopoulos, N., Pertot, C., Peuch, V.H., Pirovano, G., Rouil, L., Sauter, F., Schaap, M., Stern, R., Tarrason, L., Vignati, E., Volta, M., White, L., Wind, P., Zuber, A., 2007. CityDelta: A model intercomparison study to explore the impact of emission reductions in European cities in 2010. Atmospheric Environment 41, issue 1, 189-207.

de Meij, A., M. Krol, F. Dentener, E. Vignati, C. Cuvelier, and P. Thunis, 2006. The sensitivity of aerosol in Europe to two different emission inventories and temporal distribution of emissions. Atmos. Chem.Phys., 6, 4287-4309.

Derognat, C., Beekmann, M., Baeumle, M., Martin, D., and Schmidt, H., 2003. Effect of biogenic volatile organic compound emissions on tropospheric chemistry during the Atmospheric Pollution Over the Paris Area(ESQUIF) campaign in the Ile-de-France region. J. of Geophys. Res., 108(D17):8560.

Endresen, O., J. Bakke, E. Sorgard, T. Flatlandsmo Berglen, and P. Holmvang, 2005. Improved modeling of ship SO2 emissions a fuel-based approach. Atmos. Environ., 39 (20), 3621-3628.

ENVIRON, 2011. User's Guide to the Comprehensive Air Quality Model with Extensions (CAMx). Version 5.4. Report prepared by ENVIRON International Corporation Novato, CA.

EU, 2008. Directive 2008/50/EC of the European Parliament and of the Council of 21 May 2008 on ambient air quality and cleaner air for Europe. Official Journal L 152, 11.6.2008, p. 1–44 http://eur-lex.europa.eu/LexUriServ/LexUriServ.do?uri=OJ:L:2008:152:0001:0044:EN:PDF.

Fahey K.M. and Pandis, S.N., 2001. Optimizing model performance: variable size resolution in cloud chemistry modeling. Atmospheric Environment, 35, 4471-4478.

Gery, M.W., Whitten G.Z., Killus J.P., Dodge M.C., 1989. A Photochemical Kinetics Mechanism for Urban and Regional Scale Computer Modeling. J. Geophys. Res., 94, 925-956.

Gilardoni, S., Vignati, E., Cavalli, F., Putaud, J.P., Larsen, B.R., Karl, M., Stenström, K., Genberg, J., Henne, S., Dentener, F., 2011. Better constraints on sources of carbonaceous aerosols using a combined 14C – macro tracer analysis in a European rural background site. Atmospheric Chemistry and Physics Discussions 11, 2503–2547.

Gong, S. L., 2003. A parameterization of sea-salt aerosol source function for sub- and super-micron particles. Global Biogeochemical Cycles 17: 1097-1104.

Grell, G. A., Devenyi, D., 2002. A generalized approach to parameterizing convection combining ensemble and data assimilation techniques. Geophys. Res. Lett. 29(14), 1693.

Grell, Peckham, Schmitz, McKeen, Frost, Skamarock and Eder, 2005. Fully coupled "online" chemistry within the WRF model. Atmospheric Environment, 39(37), 6957-6975.

Guenther, A., Karl, T., Harley, P., Wiedinmyer, C., Palmer, P., Geron, C., 2006. Estimates of global terrestrial isoprene emissions using MEGAN (Model of Emissions of Gases and Aerosols from Nature). Atmos. Chem Phys., 6, 3181-3210.

Hendriks E.C.J., H.A.C. Denier van der Gon, M. Schaap, 2009. Constraining the potential source strength of various soil dust sources contributing to atmospheric PM10 concentrations in Europe. Proceedings of the 30th NATO/CCMS ITM conference, San Francisco, U.S.A.

Henne, S., D. Brunner, D. Folini, S. Solberg, J. Klausen, and B. Buchmann, 2010. Assessment of parameters describing representativeness of air quality in-situ measurement sites. Atmos. Chem. Phys., 10 (8), 3561-3581.

Hodzic, A., Madronich, S., Bohn, B., Massie, S., Menut, L., Wiedinmyer, C., 2007. Wildfire particulate matter in Europe during summer 2003: meso-scale modeling of smoke emissions, transport and radiative effects. Atmospheric Chemistry and Physics 7, 4043–4064.

Hong, S.-Y., Noh, Y., Dudhia, J., 2006. A New Vertical Diffusion Package with an Explicit Treatment of Entrainment Processes. Monthly Weather Review 134, 2318-2341.

ISPRA, 2009, La disaggregazione a livello provinciale dell'inventario nazionale delle emissioni. Rapporto 92/2009.

Jacobson, M. Z., R. P. Turco, E. J. Jensen, and O. B. Toon, 1994. Modeling coagulation among particles of different composition and size. Atmos. Environ., 28, 1327–1338.

Joly M., Peuch V.-H., 2012. Objective classification of air quality monitoring sites over Europe. Atmospheric Environment 47, 111-123. doi:10.1016/j.atmosenv.2011.11.025.

Mlawer, E.J., Taubman, S.J., Brown, P.D., Iacono, M.J., Clough, S.A., 1997. Radiative transfer for inhomogeneous atmospheres: RRTM, a validated correlated-k model for the longwave. Journal of Geophysical Research 102, 16663–16682.

Meng, Z., D. Dabdud, and J. H. Seinfeld, 1997. Chemical coupling between atmospheric ozone and particulate matter. Science, 277, 116–119, doi:10.1126/science.277.5322.116.

Monin, A. S., Obukhov, A. M., 1954. Basic Laws of Turbulent Mixing in the Ground Layer of the Atmosphere. Trans. Geophys. Inst. Akad. Nauk. USSR 151, 163–187.

Morrison, H., Thompson, G., Tatarskii, V, 2009. Impact of cloud micrpohysics on the development of trailing stratiform precipitation in a simulated squall line: Comparison of one- and two-moment schemes. Monthly Weather Review 137, 991-1007, doi: 10.1175/2008MWR2556.1.

Nenes, A., Pandis, S. N., Pilinis, C., 1999. Continued development and testing of a new thermodynamic aerosol module for urban and regional air quality models. Atmospheric Environment 33, 1553-1560.

Nenes, A., Pilinis, C., Pandis, S.N., 1998. ISORROPIA: A new thermodynamic model for inorganic multicomponent atmospheric aerosols. Aquatic Geochemistry 4, 123-152.

NCAR, 2011. The Tropospheric Visible and Ultraviolet (TUV) Radiation Model web page. National Center for Atmospheric Research, Atmospheric Chemistry Division, Boulder, Colorado, http://cprm.acd.ucar.edu/Models/TUV/index.shtml.

Otte T. L. and Pleim J. E., 2010. The Meteorology-Chemistry Interface Processor (MCIP) for the CMAQ modeling system: updates through MCIPv3.4.1. Geosci. Model Dev., 3, 243–256.

Passant, N., 2002. Speciation of UK emissions of NMVOC, AEAT/ENV/0545, AEA Technology, London.

Pernigotti D., Thunis P., Cuvelier C., Georgieva E., Gsella A., De Meij A., Pirovano G., Balzarini A., Riva G.M., Carnevale C., Pisoni E., Volta M.,Bessagnet B., Kerschbaumer A., Viaene P., De Ridder K., Nyiri A., Wind P., 2013. POMI: a model inter-comparison exercise over the Po Valley. Air Qual Atmos Health 6(4), 701-715. doi: 10.1007/s11869-013-0211-1.

Pirovano G., Balzarini A., Bessagnet B., Emery C., Kallos G., Meleux F., Mitsakou C.,Nopmongcol U., Riva G.M., Yarwood G., 2012. Investigating impacts of chemistry and transport model formulation on model performance at European scale. Atmospheric Environment 53, 93-109. doi:10.1016/j.atmosenv.2011.12.052.

Pirovano G, Toppetti A.M., Balzarini A., 2011. Aggiornamento del sistema modellistico per la valutazione della qualità dell'aria a scala nazionale e di bacino. Rapporto aggiuntivo RSE n° 1100124.

Rao, S. T., Galmarini, S., Puckett, K., 2011. Air Quality Model Evaluation International Initiative (AQMEII): Advancing the State of the Science in Regional Photochemical Modeling and Its Applications. BAMS, Volume 92, Issue 1, 23-30.

Schaap, M., F. Sauter, R. Timmermans, M. Roemer, G. Velders, J. Beck, and P. Builtjes, 2008. The LOTOS-EUROS model: description,

validation and latest developments. Int. J. Environ. Pollut., 32(2), 270–290, doi:10.1504/IJEP.2008.017106.

Seinfeld, J.H., and S.N. Pandis, 1998. Atmospheric Chemistry and Physics, From Air Pollution to Climate Change. John Wiley and Sons, Inc., NY.

Simpson, D., H. Fagerli, J. E. Jonson, S. Tsyro, P. Wind, and J.-P. Tuovinen, 2003. Transboundary acidification, eutrophication and ground level ozone in Europe. Part I: Unified EMEP model description. EMEP Rep.1/2003, 104 pp., Norw. Meteorol. Inst., Oslo.

Skamarock W.C., Joseph B. Klemp, Jimy Dudhia, David O. Gill, Dale M. Barker, Michael G. Duda, Xiang-Yu Huang, Wei Wang , Jordan G. Powers, 2008. A Description of the Advanced Research WRF Version 3. NCAR Technical Note NCAR/TN-475+STR, Boulder, Colorado.

Solazzo, E., Bianconi, R., Pirovano, G., Volker, M., Vautard, R., and et al., 2012. Operational model evaluation for particulate matter in Europe and North America in the context of AQMEII. Atmospheric Environment 53, 75-92, doi:10.1016/j.atmosenv.2012.02.045.

Stern R., P. Builtjes, M. Schaap, R. Timmermans, R. Vautard, A. Hodzic, M. Memmesheimer, H. Feldmann, E. Renner, R. Wolke, A. Kerschbaumer, 2008. A model inter-comparison study focussing on episodes with elevated PM10 concentrations. Atmospheric Environment 42, 4567–4588. doi:10.1016/j.atmosenv.2008.01.068.

Strader, R., Lurmann, F., Pandis, S.N., 1999. Evaluation of secondary organic aerosol formation in winter. Atmospheric Environment 33, 4849-4863.

Tuccella, P., G. Curci, G. Visconti, B. Bessagnet, L. Menut, and R. J. Park, 2012. Modeling of gas and aerosol with WRF/Chem over Europe: Evaluation and sensitivity study. J. Geophys. Res., 117, D03303, doi:10.1029/2011JD016302.

Turner, D.B., T. Chico, and A. Catalano, 1986. TUPOS: A Multiple Source Gaussian Dispersion Algorithm Using OnSite Turbulence Data. U.S Environmental Protection Agency, Research Triangle Park, North Carolina (EPA600/886/010).

UNC, 2009. SMOKE v2.6 User's manual, http://www.smoke-model.org/index.cfm.

Van Loon, M., Vautard, R., Schaap, M., Bergstrom, R., Bessagnet, B., Brandt, J., Builtjes, P., Christensen, J.H., Cuvelier, K., Graf, A., Jonson, J., Krol, M., Langner, J., Roberts, P., Rouil, L., Stern, R., Tarrason, L., Thunis, P., Vignati, E., White, L., Wind, P, 2007. Evaluation of long-term ozone simulations from seven regional air quality models and their ensemble average. Atmos. Environ. 41, 2083–2097.

Vautard, R., Builties, P.H.J., Thunis, P., Cuvelier, C., Bedogni, M., Bessagnet, B., Honore, C., Moussiopoulos, N., Pirovano, G., Schaap, M., Stern, R., Tarrason, L.,Wind, P., 2007. Evaluation and intercomparison of ozone and PM10 simulations by several chemistry transport models over four European cities within the CityDelta project. Atmos Environ 41:173–188.

Vestreng V., 2003. Review and Revision Emission data reported to CLRTAP. EMEP-MSC Technical Report, ISSN 0804-2446.

Wesely M.L, 1989. Parameterization of surface resistance to gaseous dry deposition in regional-scale numerical models. Atmos. Environ., 23, 1293-1304. doi: 10.1016/0004-6981(89)90153-4.

Wexler, A. S., F. W. Lurmann, and J. H. Seinfeld, 1994. Modelling urban and regional aerosols. Part I: Model development. Atmos. Environ., 28, 531– 546.

Whyatt, J.D., Metcalfe, S.E., Nicholson, J., Derwent, R.G., Page, T., Stedman, J.R., 2007. Regional scale modelling of particulate matter in the UK, source attribution and an assessment of uncertainties. Atmospheric Environment 41, 3315–3327.

Yarwood, G., Rao, S., Yocke, M., Whitten, G., 2005. Updates to the Carbon Bond Chemical mechanism: CB05. report, Rpt. RT-0400675, US EPA, Res. Tri. Park.

Yttri, K. E., et al. ,2007. Elemental and organic carbon in PM10: A one year measurement campaign within the European Monitoring and Evaluation Program EMEP. Atmos. Chem. Phys., 7, 5711–5725, doi:10.5194/acp-7-5711-2007.

Zaveri R. Easter R.C., Fast J.D. and Peters L.K., 2008. Model for Simulating Aerosol Interactions and Chenistry (MOSAIC). Journal of Geophysical Research, 113, D13204, doi: 10.1029/2007JD008782.

Zaveri R.A. and Peters L.K., 1999. A new lumped structure photochemical mechanism for large-scale applications. J. Geophys. Research, 104(D23), 30,387-30,415.

Zhang, Y., 2008. Online-coupled meteorology and chemistry models: History, current status, and outlook. Atmos. Chem. Phys., 8, 2895–2932, doi:10.5194/acp-8-2895-2008.

5 INVESTIGATING AEROSOL - RADIATION – CLOUD FEEDBACKS UNDER EMISSION CONTROL STRATEGIES

A. Balzarini, G. Pirovano and G.M. Riva

Article in preparation

Air pollution results from a combination of different variables, i.e. emission, chemical processes, weather and climate.
Meteorology affects air quality through ventilation and transport processes (wind speed, convection, advection, mixing depth), and by altering natural emissions (biogenic compounds, dust, fires, lightning), precipitation scaveging, dry deposition and gas-phase reaction (Giorgi and Meleux, 2007; Jacob and Winner, 2009). Indeed variation in temperature, wind speed and surface wetness can affect the emissions of biogenic compounds from the trees and re-suspended particles; chemical transformations are closely related to temperature, humidity, incoming solar radiation and cloudiness; wet removal is tied to the precipitation processes and dry removal is essentially driven by turbulent transfer towards the Earth surface (Vautard et al., 2007).
At the same time, aerosols are known to affect both weather and climate. The fate of some pollutants in atmosphere determine the concentration of key radiatively active species, like ozone (the third

important greenhouse gas) and the hydroxyl radical (OH), which control the oxidative capacity of the atmosphere and it is one of the main sink of methane (Vautard et al., 2007). Ozone and PM also interact with solar and terrestrial radiation and they are recognized as important climate forcing agents (Foster et al., 2007), exerting a *direct radiative effect* on the climate system that influences solar radiation either through scattering or absorption.

Furthermore aerosols have an *indirect effect* on meteorology by altering microphysical and radiative properties of clouds ("*first indirect effect"*) and, thus, precipitations ("*second indirect effect"*). There is also an additional effect called "*semi-direct*" that is connected to the capability of absorbing aerosols (e.g. black carbon) to reduce cloud liquid water content by heating the surrounding environment (Hansen et al., 1997).

Chemistry and meteorology, thus, involve a large number of possible feedbacks that influence atmospheric processes and, then, human health and ecosystems.

As a consequence, interactions between aerosol and weather are becoming important aspects to be considered in air quality simulations that aim to investigate the pollution event over a specific region, as well as future scenario analysis that evaluate the effect of emission control policies and strategies on these polluted areas.

Although the existence of feedback mechanisms has been well documented in past years, only few studies considered the interactions between aerosols and meteorology in air quality simulations (e.g. Forkel et al., 2012; Zhang et al., 2010), especially when complex terrains are considered e.g. Italy.

Indeed, in Italy and, particularly, in the Po valley ground concentrations are strongly influenced by complex circulation conditions, often associated with low wind speeds and stable inversion, and particular local scale features, such as sea-land interface.

Accurately simulating these feedbacks requires the use of online-coupled meteorology and chemistry models; among which WRF-Chem represents an advance tool in coupled applications.

WRF-Chem model includes full coupled interactions between aerosols, radiation, clouds and precipitation for the direct, semi-direct, and first and second indirect effects as described in Chapman et al. (2009) and Fast et al. (2006).
The model has been extensively validated against observations as well as other chemistry and transport model (CAMx) previously in this work. As demonstrated in Chapter 4, WRF-Chem reveals good agreement with the benchmark simulation, confirming the skill of the model in reconstructing the main atmospheric pollutions and phenomena. The chemical and meteorological configuration adopted in the study were set up and evaluated in Chapter 2 and Chapter 4. Moreover, performance indicators presented in Chapter 3 are adopted here.
In order to understand the implication of feedback mechanisms on ground concentrations, in this study two numerical simulations of the WRF-Chem model have been performed over the Italian Peninsula for July 2010. The base case does not turn on any coupling, the second simulation accounts for both direct and indirect effect. The performance of the base approach with respect to the effect of feedback mechanisms between simulated aerosol concentrations and meteorological variables is analyzed here.
Moreover, a scenario analysis for the year 2030 has been carried out for both the presence or not of feedback effects. The proposed scenario takes into account emission variations induced by the application of the current legislation and the European Directives that will become law during the considered period (2010-2030). Results were compared to the previous simulations in order to understand the impact of feedbacks on emission control strategies and policies.

5.1 MODEL AND OBSERVATIONS

5.1.1 WRF-Chem model set up

In this application WRF-Chem was used in its 3.4.1 version released in September 2011. In this version of the code the Morrison double-

moment cloud microphysics scheme is completely coupled with the aerosol modules.

Physics options selected for meteorology were the Rapid Radiative Transfer Model for General circulation models (RRTMG) longwave and shortwave radiation scheme (Iacono et al., 2000), the Noah land surface model (Chen and Dudhia, 2001), the Morrison double moment microphysics scheme (Morrison et al., 2009), the Grell 3D ensemble cumulus parameterization (Grell and Devenyi, 2002), the Yonsei University Planetary Boundary Layer (Hong et al., 2006) and the MM5 surface model (Monin Obukhov, 1954).

The gas phase chemistry is based on Carbon Bond Mechanism version Z (Zaveri and Peters 1999). Aerosol chemistry is simulated with the MOSAIC 4-bins scheme (Zaveri et al., 2008).

Whether aerosol-radiation feedbacks are activated, the chosen chemistry module is coupled to aqueous phase chemistry. In particular, the bulk aqueous-phase chemistry of Fahey and Pandis (2001) is used, which includes 50 aqueous phase species and 147 aqueous-phase chemical reactions (21 dissolution equilibria, 17 dissociation equilibria, and 109 kinetic reactions).

To investigate the impact of aerosol-radiation feedback on meteorological variables as well as the aerosol effects on clouds and precipitation, two WRF-Chem simulations are performed. The first one does not account for any feedback effect (BASE); the second simulation includes both aerosol feedbacks (FBS).

When feedback mechanisms are disabled, the RRTMG radiation scheme and the Morrison double-moment microphysiscs do not interact with the aerosol modules. In this case, the radiation scheme uses climatologial aerosol vertical profiles to compute radiation fileds, and a default-prescribed droplet number concentration (250 cm^{-3}) is adopted in the Morrison double-moment microhpysics.

On the other hand, the fully coupling among aerosol mechanisms, microphysics and radiation schemes is completely activated whether feedbacks are turned on. The direct feedback is simulated based on Mie theory following Fast et.al (2006) and Ghan et al. (2001). Each chemical constituent of the aerosol is associated to a complex index of refraction. The overall refractive index for a given size bin is

determined by volume averaging and then used to calculate aerosol optical properties with the Mie theory. Information is then transferred to RRTMG shortwave ad longwave radiation schemes.
The model simulates also indirect feedbacks that accounts for the effects of aerosol activation on clouds and precipitation. Aerosols are activated following the parameterization of Abdul-Razzak and Ghan (2002), which determines the maximum supersaturation based on a Gaussian spectrum of updraft velocities. The number and mass fraction of activated aerosols particles to serve as CCN is then calculated following Chapman et al. (2009).
The Morrison double-moment predicts prognostic cloud droplet number and it treats the second indirect effect. The auto-conversion of cloud liquid water to rain droplets is simulated following Beheng (1994). The first indirect effect is modeled by accounting for the radiation changes due to alterations in droplet mean radius and cloud optical depth resulted from variations in cloud number concentration in the RRTMG shortwave and longwave radiation scheme.
More detailed information on feedback effects can be found in Fast et al. (2006), Gustafson et al. (2007), and Chapman et al. (2009).
The BASE simulation adopted a simple wet scavenging scheme, while the FBS used Easter et al. (2004) approach. Wesely (1989) dry deposition and Fast-J photolysis scheme (Barnard et al., 2004) are also considered. More details on the configurations are available in Table 18.
The modeling domain covers Italy (1290x1470 km^2) with 15 km horizontal resolution in a Lambert Conformal projection. The vertical resolution includes 30 layers from the surface to a fixed pressure of 50 hPa (Table 19), with the first model layer of 25 m from the ground.

Table 18 – Physical and chemical configurations for the BASE case and FBS simulation.

		BASE	FBS
Physics options	Cumulus parameterization	Grell 3D	Grell 3D
	Microphysics	Morrison 2-moment	Morrison 2-moment
	Planetary Boundary Layer	YSU	YSU
	Surface layer	MM5	MM5
	Land Surface Model	Noah LSM	Noah LSM
	Shortwave radiation	RRTMG	RRTMG
	Longwave radiation	RRTMG	RRTMG
Chemistry options	Gas phase chemistry	CBM-Z	CBM-Z
	Aerosol chemistry	MOSAIC	MOSAIC
	SOA formation	-	-
	Aqueous chemistry	-	Fahey and Pandis
	Aerosol dynamic	4 bin - sectional approach	4 bin - sectional approach
	Photolysis	Fast-J	Fast-J
	Dry deposition	Wesely	Wesely
	Wet deposition	Simple approach	Easter et al.
Feedbacks options	Radiation feedback	off	on
	Indirect feedback	off	on

Table 19 – Domain characteristics.

	u.m.	D01
SW X corner	[km]	-604.5
SW Y corner	[km]	-1023.5
NE X corner	[km]	685.5
NE Y corner	[km]	446.5
DX-DY	[km]	15
Pressure at top	[hPa]	50
NX	[n]	86
NY	[n]	98
NZ	[n]	30

Anthropogenic emissions have been arranged in WRF-Chem ready format by applying the SMOKE emission model as described in Chapter 4. The Italian emission inventory (http://www.sinanet.isprambiente.it/it/sia-ispra/inventaria) and the EMEP inventory (http://webdab.emep.int) have been used for Italy and neighboring countries, respectively. Biogenic emissions are calculated on-line using MEGAN model (version 2.04, Guenther et al., 2006) as well as sea salt and dust emissions (Gong et al., 2003; Shaw et al., 2008).

In order to assess the implications of direct and indirect effects on air quality, a month with high aerosol loading and cloudy conditions is needed. To this aim, the analysis will cover July 2010 characterized by a significant Saharan dust event over North of Italy and surrounding regions.

Since analysis nudging has been expected to suppress most feedback effects (Forkel et al., 2012), we chose a frequent re-initializations approach. The simulation is ran every 5 days with a spin up time of one day which is initialized by means of "a-priori" meteorological WRF simulation performed with analysis nudging and the same physical configuration. Differently, chemistry initialization is done using the chemistry outputs of the previous 5-days WRF-Chem run in order to preserve the continuity of the chemical simulation.

The first chemical initial and boundary condition for both gas and aerosol species is produced using the simulation results of the MACC-II project (www.gmes-atmosphere.eu/) over Europe (horizontal resolution of 1.125 degrees and 60 vertical levels up to 2 hPa) every 3 hours.

5.1.2 Observations

Surface concentrations of CO, NO, NO_2, SO_2, O_3, PM_{10} and $PM_{2.5}$ were available from the European network AirBase (http://air-climate.eionet.europa.eu/databases/airbase/) for the calendar year 2010.

Stations were selected accordingly to their annual availability higher or equal than 75%. Moreover, only rural background stations were considered in the analysis, because they are the most adequate for comparing model results over a 15km-grid resolution. A set of 134 stations was found to accomplish the selection criteria over Italy and other surrounding countries included in the computational domain.

Data of PM composition was selected from the EMEP network programme (European Monitoring and Evaluation Programme; http://ebas.nilu.no/). Suphate, nitrate and ammonium daily data were available only at Ispra site (IT0004R; 45.8 N and 8.63 E) for July 2010 together with elemental carbon and black carbon. Concentrations were analyzed as daily values.

In addition, Aerosol Optical Depth at the wavelength of 555nm (AOD555) were chosen at Lecce AERONET sites (Aerosol Robotic Network; http://aeronet.gsfc.nasa.gov/).

The WMO measurement network (World Meteorological Organization) provided meteorological observations. Surface data have 3-hours temporal coverage and they are available for temperature, dew point temperature, pressure, relative humidity, wind speed and direction. A total number of 72 meteorological stations were found over Italy. Finally global radiation data were collected at RSE S.p.A. site (Milan, 45.476 N and 9.261 E; http://www.rse-web.it/) by means of a pyranometer (CMP6 Kipp & Zonen, spectral range: 285-2800 nm; Marcacci et al, 2012).

Statistical indices for both chemical and meteorological evaluations are reported in Appendix A.

5.2 SCENARIO ANALYSIS

A scenario analysis of emission reductions has been defined over Italy for July 2030. Two WRF-Chem scenario simulations are performed: the first one does not account for any feedback effect (SCEN); the second simulation includes both radiation and cloud feedback (SCEN_FBS).
Computational domain, meteorological and chemical boundary conditions and chemical and meteorological configurations remain the same as the BASE and FBS run (see Table 19 and Table 18).
The emission reductions adopted in this work were defined by ENEA (Agenzia nazionale per le nuove tecnologie l'energia e lo sviluppo economico sostenibile) using the GAINS-Italy (Greenhouse Gas and Air Pollution Interactions and Synergies; http://gains-it.bologna.enea.it/) outcomes in time interval between 2005 and 2030. GAINS-Italy was applied in the framework of the Convention on Long-Range Transboundary Air Pollution (CLRTAP) and it is derived from GAINS-Europe model (GAINS, 2009; http://gains.iiasa.ac.at/). GAINS is an air pollution and greenhouse gas emission model that allows the analysis of controlling emission policies at national and international scale. The model can simultaneously analyze the effects of mitigation of greenhouse gases and air pollution emissions, thus taking into account interactions and synergies between these strategies (GAINS, 2009).
In order to define the emission scenario, the GAINS-Italy model needs to specify the anthropogenic activities involved in the emission process and a control strategy. The energy scenario was prepared by ISPRA applying the MARKAL-Italy model (MARKet ALlocation; http://www.iea-etsap.org/) in the framework of the Energy Technology System Analysis Programme (ETSAP) of the International Energy Agency (IEA). MARKAL uses linear optimization technique for each user-defined primary energy source, energy carrier, and transformation technology to identify the least-

cost way to satisfy the specified energy service demands. The methodology adopted here follows Gracceva and Contaldi (2004) and it accounts for more than 70 demands for energy services disaggregated by sectors (e.g. agriculture, industry, transportation and residential) and 1000 different energy technologies. The final emissions where calculated directly by MARKAL using the emission factors of the National emission inventory.

The other-sectors scenario was developed by ENEA using as base years 2005-2010 and considering different statistical parameters related to the Italian population as well as economic variables (e.g. Gross Domestic Product, GDP). In particular, different scenarios for industrial and solvent production processes were created based on field studies, industry association data, GDP and population growth. Moreover, a statistical model was applied to foresee the number of animals for the year 2030 together with a projection of the future consumption of nitrogenous fertilizers that takes into account the historical consumption of urea and other nitrogen fertilizers (EFMA, European Fertilizer Manufacturers Association).

For more details on the calculation of emissions see Klimont and Brink (2004), Cofala and Syri (1998a), Cofala and Syri (1998b), Klimont et al. (2002) and Klimont et al. (2000).

Finally a control strategy was applied. It includes all emission control technologies that will be penetrated in the given scenario during the 2005-2030 temporal period following the current National and European legislations (e.g. Industrial Emissions for Large Combustion Plants Directive, Dir. 2001/80/EC; Solvents Emissions Directive, Dir. 2004/42/EC; European Regulations on motor vehicles No. 692/2008 and No. 595/2009) as well as the European Directives that will become law in that time.

More information on this emission scenario is available in D'Elia and Peschi (2013) and on http://gains-it.bologna.enea.it/ (see *Baseline_2012_new* scenario).

The final Italian emission variations created with the GAINS-Italy model for the year 2030 with respect to the year 2010 are -39% for NOx, -18% for VOCs, +3% for NH_3, -5% for SO_2, -11% for PM_{10} and -15% for $PM_{2.5}$. All compound tend to reduce their emissions

over Italy, the only exception is NH_3 because of an increasing in the consumption of nitrogenous fertilizers and livestock. The main reductions of NOx, VOCs, PM_{10} and $PM_{2.5}$ are related to a decrease in road transport emissions, while the slightly decrease in SO_2 emissions is connected to an increase in international shipping.
The aforementioned reductions were processed with the SMOKE model starting from the Italian emission inventory (http://www.sinanet.isprambiente.it/it/sia-ispra/inventaria) and the EMEP database for the year 2010 (http://webdab.emep.int) in order to create the model-ready emission fields for the year 2030. The Italian emissions produced with the SMOKE model are reported for both years (2010 and 2030) in Table 20 at each SNAP sector, while the EMEP ones are listed in Table 21. Emission variations in Table 20 (Italy) are similar to those identified by ENEA, while a slightly difference is visible in Table 21 for EMEP regions. Discrepancies are related to sectors 1, 8 and 10. For SNAP 1 we assumed a reduction of -20% associated to its main contributors, namely power plants. Differently to the Italian inventory, in fact, EMEP data do not contain the separation among different activities (e.g. power plants, industries and refineries).
Differences in macro-sector 8 are related to international shipping emissions that are included only in the EMEP inventory, with the exception of the emissions from harbor activities. Finally, it was assumed that changes in consumption of nitrogenous fertilizers and livestock were negligible in EMEP regions, but they are mainly associated to the agricultural activities in the Po valley.
The WRF-Chem model ran for one month applying the 5-days re-initializations approach. Biogenic emissions are calculated on-line using MEGAN model (Guenther et al., 2006) as well as sea salt and dust emissions (Gong et al., 2003; Shaw et al., 2008).

Table 20 – Emission reductions for NOx, VOCs, NH_3, SO_2, PM_{10} and $PM_{2.5}$ in the 10 SNAP sectors over Italian regions. Emissions are expressed in ton/domain/year. Differences are calculated with respect to the year 2010.

SNAP CODE	NOX			VOC			NH3			SO2			PM10			PM2.5		
	2030	2010	DIFF(%)	2030	2010	DIFF(%)	2030	2010	DIFF(%)	2030	2010	DIFF(%)	2030	2010	DIFF(%)	2030	2010	DIFF(%)
1	6.7E+04	8.0E+04	-16%	3.5E+03	3.5E+03	0%	1.5E+02	1.5E+02	0%	7.1E+04	7.7E+04	-9%	2.9E+03	3.2E+03	-11%	2.7E+03	3.1E+03	-11%
2	8.9E+04	8.6E+04	3%	2.1E+05	1.7E+05	25%	8.0E+02	8.0E+02	0%	1.2E+04	1.1E+04	10%	9.5E+04	9.1E+04	5%	9.5E+04	9.0E+04	5%
3	9.7E+04	9.7E+04	0%	7.6E+03	7.6E+03	0%	1.2E+03	1.2E+03	0%	4.5E+04	4.5E+04	0%	1.1E+04	1.2E+04	-10%	1.1E+04	1.2E+04	-10%
4	1.0E+04	1.0E+04	0%	6.4E+04	6.4E+04	0%	4.0E+02	4.0E+02	0%	4.6E+04	4.6E+04	0%	1.6E+04	1.6E+04	0%	7.0E+03	7.0E+03	0%
5	0.0E+00	0.0E+00		4.8E+04	4.8E+04	0%	0.0E+00	0.0E+00		0.0E+00	0.0E+00		6.9E+02	6.9E+02	0%	6.9E+02	6.9E+02	0%
6	0.0E+00	0.0E+00		4.1E+05	4.1E+05	0%	0.0E+00	0.0E+00		0.0E+00	0.0E+00		1.0E+01	1.0E+01	0%	1.0E+01	1.0E+01	0%
7	2.0E+05	4.9E+05	-60%	1.1E+05	2.7E+05	-60%	7.1E+03	8.9E+03	-20%	4.4E+02	4.4E+02	0%	1.5E+04	3.4E+04	-55%	1.3E+04	3.0E+04	-55%
8	1.5E+05	1.4E+05	8%	7.9E+04	7.9E+04	0%	2.8E+01	2.8E+01	0%	5.1E+03	4.0E+03	27%	1.1E+04	1.0E+04	7%	1.1E+04	1.0E+04	7%
9	1.5E+04	1.5E+04	0%	1.4E+04	2.3E+04	-40%	5.5E+03	9.2E+03	-40%	7.0E+03	7.0E+03	0%	1.2E+04	1.2E+04	0%	1.0E+04	1.0E+04	0%
10	4.6E+02	4.6E+02	0%	1.2E+03	1.2E+03	0%	3.8E+05	3.6E+05	5%	0.0E+00	0.0E+00		1.8E+04	1.8E+04	0%	5.7E+03	5.7E+03	0%
TOTAL [ton/year]	**6.3E+05**	**9.2E+05**	**-32%**	**9.5E+05**	**1.1E+06**	**-12%**	**3.9E+05**	**3.8E+05**	**3%**	**1.9E+05**	**1.9E+05**	**-2%**	**1.8E+05**	**2.0E+05**	**-8%**	**1.6E+05**	**1.7E+05**	**-8%**

Table 21 - Emission reductions for NOx, VOCs, NH_3, SO_2, PM_{10} and $PM_{2.5}$ in the 10 SNAP sectors over EMEP regions. Emissions are expressed in ton/domain/year. Differences are calculated with respect to the year 2010.

SNAP CODE	NOX			VOC			NH3			SO2			PM10			PM2.5		
	2030	2010	DIFF(%)	2030	2010	DIFF(%)	2030	2010	DIFF(%)	2030	2010	DIFF(%)	2030	2010	DIFF(%)	2030	2010	DIFF(%)
1	1.8E+05	2.3E+05	-20%	9.0E+03	9.0E+03	0%	9.4E+02	9.4E+02	0%	5.6E+05	6.9E+05	-20%	4.8E+04	6.0E+04	-20%	2.0E+04	2.5E+04	-20%
2	9.7E+04	9.4E+04	3%	2.1E+05	1.7E+05	25%	1.6E+03	1.6E+03	0%	8.7E+04	7.9E+04	10%	1.1E+05	1.1E+05	5%	1.1E+05	1.0E+05	5%
3	1.2E+05	1.2E+05	0%	9.0E+03	9.0E+03	0%	1.1E+03	1.1E+03	0%	1.0E+05	1.0E+05	0%	1.3E+04	1.4E+04	-10%	9.8E+03	1.1E+04	-10%
4	2.5E+04	2.5E+04	0%	7.8E+04	7.8E+04	0%	9.7E+03	9.7E+03	0%	3.3E+04	3.3E+04	0%	3.1E+04	3.1E+04	0%	1.4E+04	1.4E+04	0%
5	7.7E+01	7.7E+01	0%	4.8E+04	4.8E+04	0%	8.2E+02	8.2E+02	0%	9.4E+02	9.4E+02	0%	1.9E+04	1.9E+04	0%	9.7E+03	9.7E+03	0%
6	7.8E+01	7.8E+01	0%	4.1E+05	4.1E+05	0%	3.5E+02	3.5E+02	0%	1.9E+02	1.9E+02	0%	7.7E+03	7.7E+03	0%	3.6E+03	3.6E+03	0%
7	2.3E+05	5.9E+05	-60%	6.4E+04	1.6E+05	-60%	8.3E+03	1.0E+04	-20%	7.1E+03	7.1E+03	0%	2.1E+04	4.6E+04	-55%	1.5E+04	3.4E+04	-55%
8	1.0E+06	8.5E+05	18%	6.6E+04	6.6E+04	0%	9.7E+01	9.7E+01	0%	6.7E+05	5.2E+05	30%	9.9E+04	8.0E+04	23%	9.0E+04	7.0E+04	28%
9	2.4E+03	2.4E+03	0%	5.2E+03	8.6E+03	-40%	5.5E+03	9.2E+03	-40%	3.7E+03	3.7E+03	0%	3.5E+03	3.5E+03	0%	2.8E+03	2.8E+03	0%
10	3.7E+04	3.7E+04	0%	1.1E+04	1.1E+04	0%	4.7E+05	4.7E+05	0%	1.2E+02	1.2E+02	0%	4.2E+04	4.2E+04	0%	7.8E+03	7.8E+03	0%
TOTAL [ton/year]	**1.7E+06**	**1.9E+06**	**-13%**	**9.1E+05**	**9.7E+05**	**-6%**	**5.0E+05**	**5.0E+05**	**-1%**	**1.5E+06**	**1.4E+06**	**2%**	**4.0E+05**	**4.1E+05**	**-4%**	**2.8E+05**	**2.8E+05**	**0%**

5.3 RESULTS AND DISCUSSION

5.3.1 Investigation of feedback effects on meteorology

Figure 65 shows the monthly mean pattern of the main meteorological variables as differences between the feedback (FBS) and the baseline (BASE) case.

The direct effect of aerosol scattering may cause a reduction of downward solar radiation as well as a decrease in planetary boundary layer height (Zhang et al., 2010).
The presence of feedback effects, in fact, is found to generally decrease the incoming solar radiation at the ground up to 20 W/m^2 (Figure 65a), particularly in the Po valley where variation of -5% are highlighted.
The direct effect of aerosol particles on incoming solar radiation shows up for clear sky conditions (Forkel et al., 2012). As a consequence, a detailed analysis of the hourly shortwave incoming solar radiation for clear sky conditions in polluted areas has been performed.
Results indicate that high average aerosol concentrations during daytime result in a reduction of solar radiation at noon by 20-40 W/m^2 (3-5%) over the city of Milan in FBS case. These values correspond to a decrease in the monthly mean global radiation of 17-20 W/m^2 (3-5%) over the Po valley caused only by the aerosol backscatter.
On the contrary, shortwave downward radiation was found to increase over the West Mediterranean, the Alps and Eastern domain. There the incoming solar radiation is 4-6% (12-20 W/m^2) higher for FBS case than for the BASE case because of a reduction of the vertically integrated cloud water content ($\sim$ 40%; 0.04-0.05 kg/m^2) and, then, cloud cover (Figure 65d). Conversely, the column rain water content increases of over those regions with respect to the baseline simulation (Figure 65e).

Discrepancies in cloud water content can be related to the different calculation of the droplet number concentration when indirect effects are included (Forkel et al., 2012). A default droplet number concentration of 250 cm^{-3} is specified in cloud microphysics scheme when indirect effect is not taken into account, whereas this number is prognosed from the simulated aerosol particle number in FBS run. A lower simulated total aerosol particle number results in droplet number that range between 60 and 80 cm^{-3} over the sea, the Alps and East of Europe.

As auto-conversion to rain droplet is higher for small cloud droplet concentrations (Forkel et al., 2012), the formation of rain droplets increases in FBS case.

In comparison with the strong effect of the indirect feedback over the sea and the Alps, only a small impact was found in cloud water content and rain water content over Italy, because of the higher amount of droplet number concentration from aerosol particles.

Modifications in cloud water content also affect the downward longwave radiation that is found to decrease of about 12 W/m^2 (3-4%) in those areas characterized by lower amount of droplet concentrations (Figure 65b).

Distribution of incoming solar radiation change is partly reflected in the distribution of the mean height of the planetary boundary layer that displays a general decrease over Italy. This reduction can reach up to 30 m (-5%) in the Po valley (Figure 65f).

a)

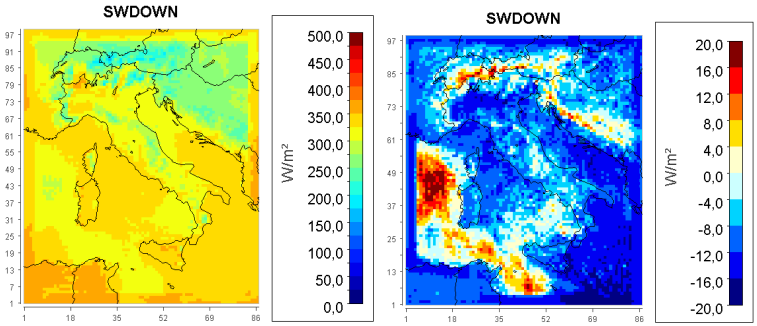

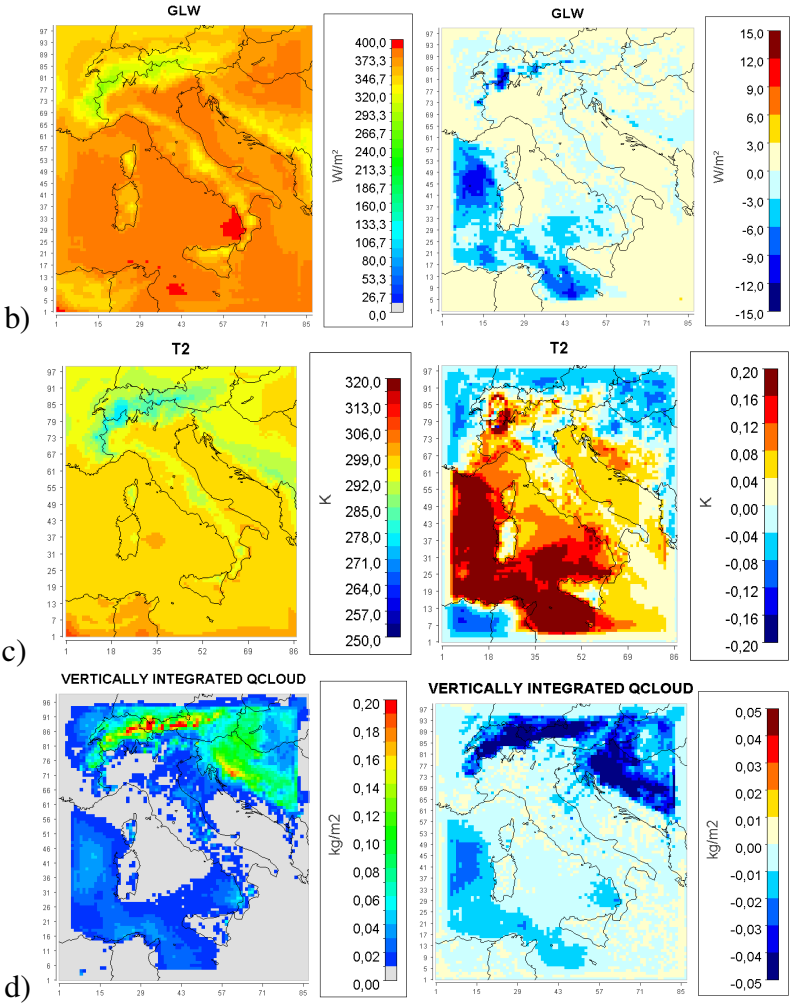
b)
GLW
400,0
373,3
346,7
320,0
293,3
266,7
240,0
213,3
186,7
160,0
133,3
106,7
80,0
53,3
26,7
0,0
W/m²
GLW
15,0
12,0
9,0
6,0
3,0
0,0
-3,0
-6,0
-9,0
-12,0
-15,0
W/m²
c)
T2
320,0
313,0
306,0
299,0
292,0
285,0
278,0
271,0
264,0
257,0
250,0
K
T2
0,20
0,16
0,12
0,08
0,04
0,00
-0,04
-0,08
-0,12
-0,16
-0,20
K
d)
VERTICALLY INTEGRATED QCLOUD
0,20
0,18
0,16
0,14
0,12
0,10
0,08
0,06
0,04
0,02
0,00
kg/m2
VERTICALLY INTEGRATED QCLOUD
0,05
0,04
0,03
0,02
0,01
0,00
-0,01
-0,02
-0,03
-0,04
-0,05
kg/m2

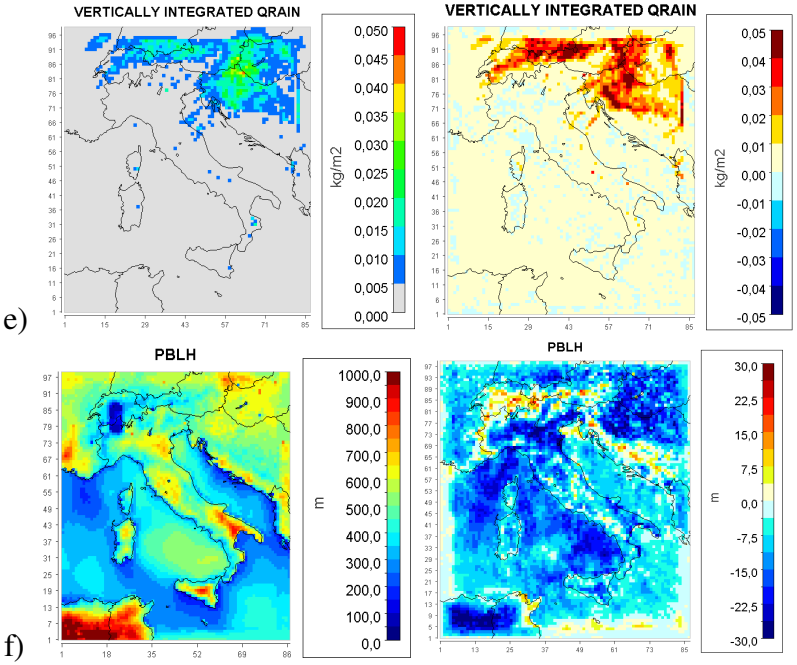

Figure 65- Monthly mean of (a) shortwave incoming solar radiation at the surface (SWDOWN), (b) downward longwave radiation (GLW), (c) 2-m temperature (T2), (d) vertically integrated cloud water content (e) vertically integrated rain water content and (f) Planetary Boundary Layer height (PBLH). On the left the BASE case, while on the right the difference between FBS and BASE simulation.

Moreover, incoming solar radiation affects 2-m temperature. In Figure 65d, 2-m temperature rises mainly over the Western Mediterranean sea, the Alps and the Eastern part of the domain. A weak warming effect is visible all over Italy when feedback mechanisms are turned on, while temperature decreases in the Eastern Po valley and outside the Italian boundaries. Conversely, 2m-temperature is warmer over the Western part of the Po valley.
Temperature is controlled by many factors such as soil moisture and soil temperature. A cooler skin surface temperature results from reduced solar radiation (not shown). The strongest reductions are

localized over those regions where 2-m temperature was found to decrease, namely the Eastern Po valley and foreign countries.
Temperature is also analyzed in terms of vertical profile, in order to investigate the changes in thermal stratification. As an example, vertical profile of monthly mean potential temperature and wind speed is reported in Figure 66 for the city of Milan, in the Midwest of the Po plain, as differences with respect to the baseline case.
Monthly mean potential temperature increases by up to 0.13 °K in the first 100 m of troposphere, and even more at higher altitudes, reaching a maxima increase of 0.18°K around 1700 m. Furthermore, wind speed shows a decrease along vertical profile by up to 0.15 m/s near surface. Such changes further stabilize the lower atmosphere, already characterized by lower PBL height, and, thus, enhance air pollution (Zhang et al., 2010).

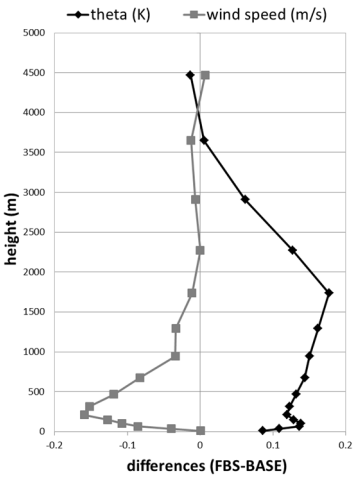

Figure 66 – Vertical variation of potential temperature and wind speed in the city of Milan (45.46 N; 9.19 E).

Results on meteorological variables agree with other studies over Europe. Forkel et al. (2012) found only a small impact of direct and indirect effect over Southern European regions. Moreover, Zhang et

al. (2010) and Yang et al. (2011) showed a less pronounced impact of indirect effect in the most polluted regions of the US.
However, in order to investigate the development of the indirect effect in more detail, cloud resolving simulations may be necessary (Forkel et al, 2012). Moreover, it is worth nothing that the frequent re-initialization approach may have modulated variation in meteorological variables induced by feedback effects.
Meteorological results of 2m-temperature, 2-m mixing ratio and 10m-wind speed were compared against measurement stations in Table 22 at all 72 WMO stations.

Table 22 - Performance statistics of 2m-temperature, 2m-mixing ratio and 10m-wind speed in BASE and FBS case at 72 WMO stations. Best performances are highlighted in grey.

Statistics	BASE			FBS		
	Temperature (K)	Mixing ratio (g/kg)	Wind speed (m/s)	Temperature (K)	Mixing ratio (g/kg)	Wind speed (m/s)
Mean Obs	298.68	14.38	3.45	298.68	14.38	3.45
Mean Mod	296.80	13.32	3.54	296.86	13.36	3.52
NMB (%)	-0.63	-7.36	2.76	-0.61	-7.13	2.24
NME (%)	0.97	17.21	46.93	0.96	17.21	46.71
RMSE	3.63	3.19	2.15	3.58	3.18	2.15
AC	0.75	0.62	0.46	0.76	0.63	0.46

Temperature and mixing ratio are under predicted by the simulations for July 2010. Model simulates 2-m temperature with a NMB of -0.63% and -0.61% for the baseline and FBS case, respectively. Mixing ratio shows a NMB of -7.36% for BASE case and -7.13% for FBS case. Conversely, wind speed is overestimated by the model (BASE NMB = 2.76%; FBS NMB = 2.24%). Feedback effects are found to improve the overall meteorological performances, increasing 2m-temperature and, thus, mixing ratio, as well as decreasing wind speed. The simulation shows a slightly smaller NME for temperature (BASE = 0.97%; FBS = 0.96%) and wind

speed (BASE = 46.93%; FBS = 46.71%) when FBS case is considered. Moreover, feedbacks seem to improve the reconstruction of the hourly variation for both temperature and mixing ratio. Anomaly Correlation (AC) slightly enhances in FBS simulation (BASE = 0.75 and FBS = 0.76 for temperature; BASE = 0.62 and FBS = 0.63 for mixing ratio).

Comparable results were found by other application of WRF-Chem. Yang et al. (2011) concluded that agreement between observation and model data improve when indirect feedbacks are included in the analysis.

Finally, in order to better analyze the effect of model coupling on global radiation, downward shortwave radiation has also been compared to measurement observations collected in Milan (RSE S.p.A., http://www.rse-web.it/; 45.476 N and 9.261 E). Figure 67 displays observed and modeled hourly time series from 7th to 16th of July 2010. Simulations show comparable results in good agreement with observations. However, both runs fail to capture cloud cover on 8th of July that reduces the measured radiation at the ground, while they reproduce cloud cover on 7th of July when clear sky is observed. Feedback effects improve the skill of model in reconstructing the radiation hourly trend at the surface, as they moderate solar radiation around noon because of aerosol scattering and absorption. Variations at noontime are in line with values identified previously in the analysis of clear sky shortwave radiation (20-40 W/m^2).

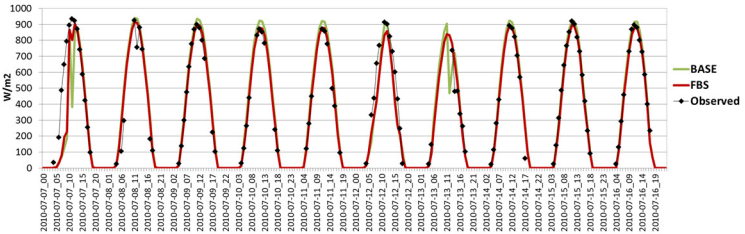

Figure 67- Comparison between hourly observations (dark) and model results at Milan (RSE S.p.A.; 45.476N and 9.261E) for baseline (green) and feedback (red) case from 7th to 16th of July 2010.

5.3.2 Investigation of feedback effects on air quality

In this section, results are reported as differences between the feedback (FBS) and the baseline (BASE) case.

Figure 68 depicts the monthly mean variation of NH_3, NO_2, O_3 and SO_2 over the region. Inclusion of both direct and indirect effects is found to have only minor influence on gas-species.

NH_3 is not affected by feedback mechanisms. Only a negligible variation is observed in Lombardy region (1 ppb; about 5%), where the main emissive sources are localized (e.g. agriculture and livestock).

NO_2 concentrations tend to increase when feedback effects are turned on, especially in high-emissive areas, namely Milan, Turin and Naples, and along the major transit routes with variations that range between 0.04 and 0.2 ppb ($\underset{\sim}{}$ 2%). NO_2 from international shipping rise beyond Sicily region as well as in correspondence of the main harbors (e.g. Marseille) and naval routes. On the contrary, O_3 concentrations decrease in many regions of the domain of about 1% (from -0.2 to -0.4 ppb). Differences in near surface ozone are associated with the decreasing in solar radiation over the domain that will result in a reduced photochemical activity. Differently, ozone increases of about 0.4 ppb ($\underset{\sim}{}$ 1%) over the Western Mediterranean Sea where incoming solar radiation rises because of a reduction in cloud cover.

SO_2 generally declines its concentrations in FBS run from -0.02 to -0.1 ppb (from 2% to 4%), particularly in those geographical areas dominated by power plant emissions (e.g. Slovenia, Croatia), while it increases over the sea up to 0.1 ppb where strong SO_2 surface emissions are derived from the international shipping. This pattern suggests a possible change in turbulent vertical diffusion when feedback effects are included. The analysis of meteorological variables, in fact, highlighted an enhanced stabilization of the lower atmosphere in FBS run, accompanied by a decrease of Planetary Boundary Layer height and wind speed. As demonstrated previously (Chapter 4), a reduced vertical diffusion can explain the increased

concentrations of primary emitted compounds, such as NO_2 and NH_3, and the decreasing of aloft-emitted species in high emissive areas. Moreover, variations observed in gaseous compounds have the same order of magnitude as changes in meteorological variables, confirming that gas concentrations are mainly influenced by variation in dispersion processes (e.g. wind speed and Planetary Boundary Layer height) as well as incoming solar radiation.

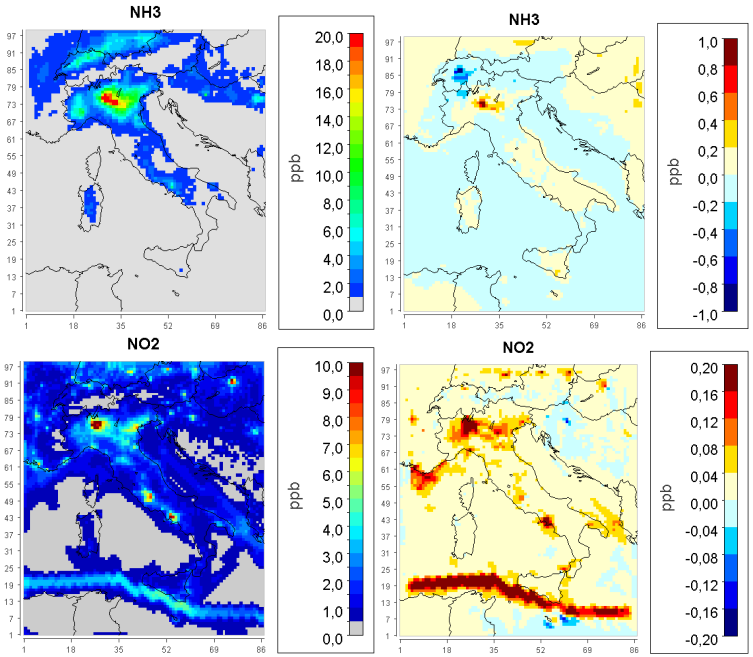

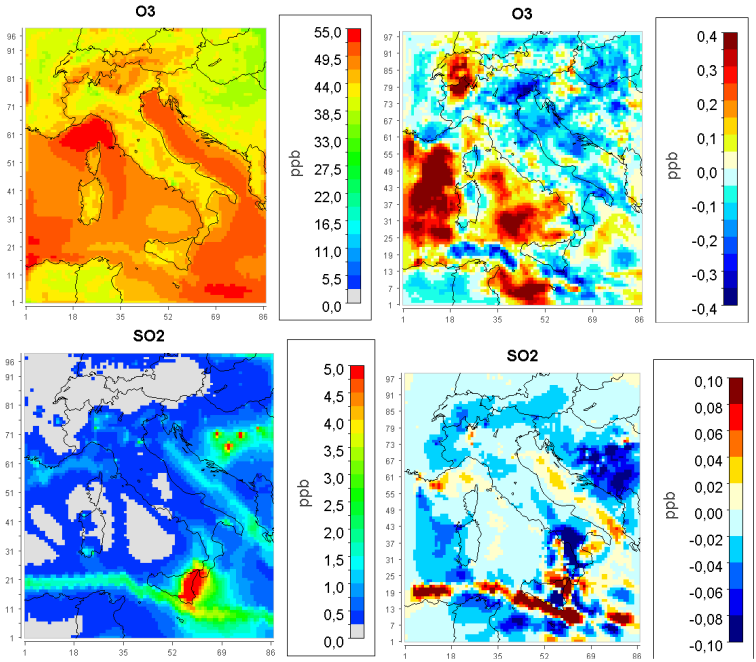

Figure 68- Monthly mean concentrations of gaseous species in the BASE case (left); differences between FBS and BASE simulation (right).

Results are analyzed against observations. Only NO_2, O_3 and SO_2 data were available for July 2010.

Comparisons with measurement stations are in agreement with the variations observed before. Feedback effect proved to increase monthly mean concentrations of ground-emitted compounds, such as NO_2, and decreasing aloft-emitted compound concentrations as SO_2. Both simulations underestimate concentrations of gas species, even though performances may vary from compound to compound. NO_2 performances improve when aerosols-meteorology interactions are considered. The NMB and NME move from -51.57% (NMB) and 55.71% (NME) in baseline case to -50.25% (NMB) and 54.66% (NME) in FBS run. Conversely, SO_2 is better reproduced by the baseline simulation. NMB is -54.36% and -56.25% in BASE and

FBS simulation, respectively. However, Index of Agreement shows an increase if feedbacks are turned on (BASE = 0.59; FBS = 0.63).
O_3 concentrations decrease when feedback effects are included, because of the reduction in shortwave incoming solar radiation. This leads to a worsening in model performances, even though statistical indices are quite good in both simulations. NMB ranges from -3.56% (BASE) to -3.64% (FBS), while NME shows variations from 18.92% (BASE) to 18.97% (FBS).
Reasons of underestimation for gaseous species where discussed previously in this work (Chapter 4) and are mainly related to lacks in some emission sources in emission inventories as well as the limited model resolution.

Table 23 – Performance statistics of gas species in BASE and FBS case at all rural background stations inside the computational domain. Best performances are highlighted in grey.

Statistics	BASE			FBS		
	NO_2 (ppb)	SO_2 (ppb)	O_3 (ppb)	NO_2 (ppb)	SO_2 (ppb)	O_3 (ppb)
Mean Obs	4.59	0.78	44.13	4.59	0.78	44.13
Mean Mod	2.40	0.35	42.55	2.46	0.34	42.52
NMB (%)	-51.57	-54.36	-3.56	-50.25	-56.25	3.64
NME (%)	55.71	70.49	18.92	54.66	71.82	18.97
RMSE	4.00	0.76	10.66	3.95	0.77	10.69
IA	0.51	0.59	0.48	0.52	0.63	0.47

Figure 69 depicts variations in PM_{10}, $PM_{2.5}$. Aerosols concentrations show a stronger influence by feedback effects.
PM_{10} and $PM_{2.5}$ have a similar spatial variation over the domain. They increase over Italy, Adriatic Sea and the Eastern domain. On the contrary they show a decrease in the Northern domain (e.g. Austria and Switzerland) as well as over the Western Mediterranean Sea (from 1 to 2 $\mu g/m^3$, $\simeq$ -10%). The highest variations are localized at Taranto, Naples, and Budapest, as well as all over the Po valley.

There PM_{10} and $PM_{2.5}$ concentrations rise of 25% and 30% (5 $\mu g/m^3$), respectively. Differently from gaseous species, variation in meteorological variables (e.g. Planetary Boundary Layer height and wind speed reduction) are not directly correlated to variation in aerosols concentrations.

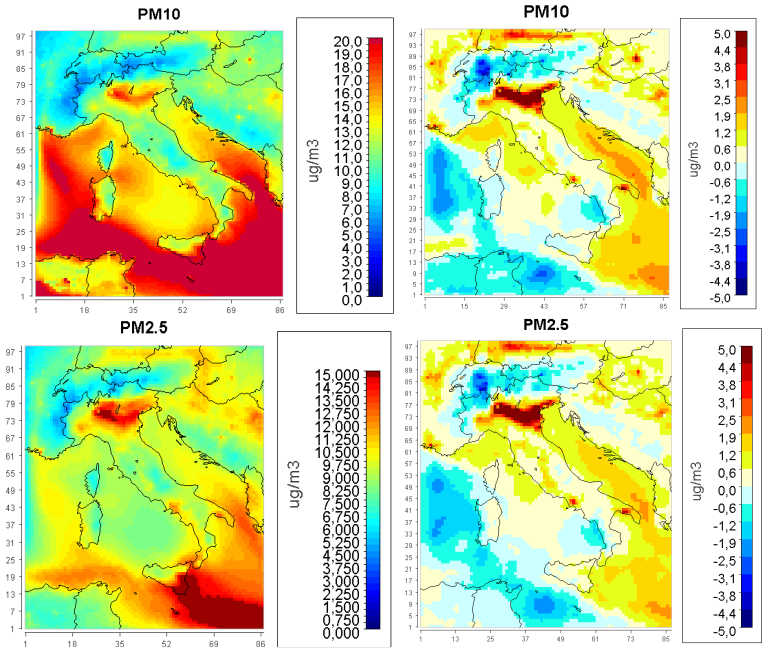

Figure 69- Monthly mean concentrations of PM_{10} and $PM_{2.5}$ in BASE case (left) and differences between FBS and BASE simulation (right).

In order to understand discrepancies between the two simulations, aerosols components as well as particle vertical profiles are analyzed in Figure 70 and Figure 71.

NH_4 and NO_3 concentrations show similar behavior with higher increase of about 50% in the Po valley (Figure 70). There NO_3 concentrations rise of 4 $\mu g/m^3$, while NH_4 grows of about 1 $\mu g/m^3$. Higher concentrations of gaseous precursors (NO_2 and NH_3) can clarify only a small part of these variations.

SO_4 changes are less pronounced (8-10%) and partially reflect SO_2 variation. Moreover, it is worth noting that feedback run includes the aqueous phase reactions. However, liquid phase sulfate formation can only explain a minor fraction of this effect.
Also black carbon and organic carbon show an increase in the Po valley and along international shipping routes. In particular, BC variations are up to 0.5 μg/m^3 (60%), while OC show a smaller increase of about 30% (0.2-0.8 μg/m^3). The warming effect caused by the absorbing BC and some absorbing OC in the PBL and the cooling at soil resulted from reduced solar radiation can further stabilize PBL and thus exacerbate air pollution in high emissive areas (Zhang et al., 2010). PBL reductions can be also partially explained by the increased black carbon concentrations. Indeed, it showed the highest variations over the Po valley. However, in order to better explore this effect a finer grid resolution simulation is necessary.

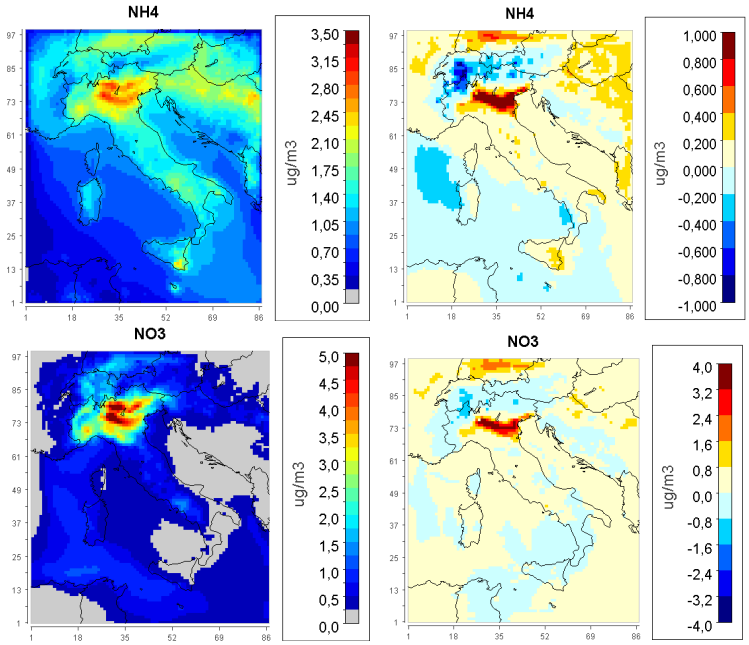

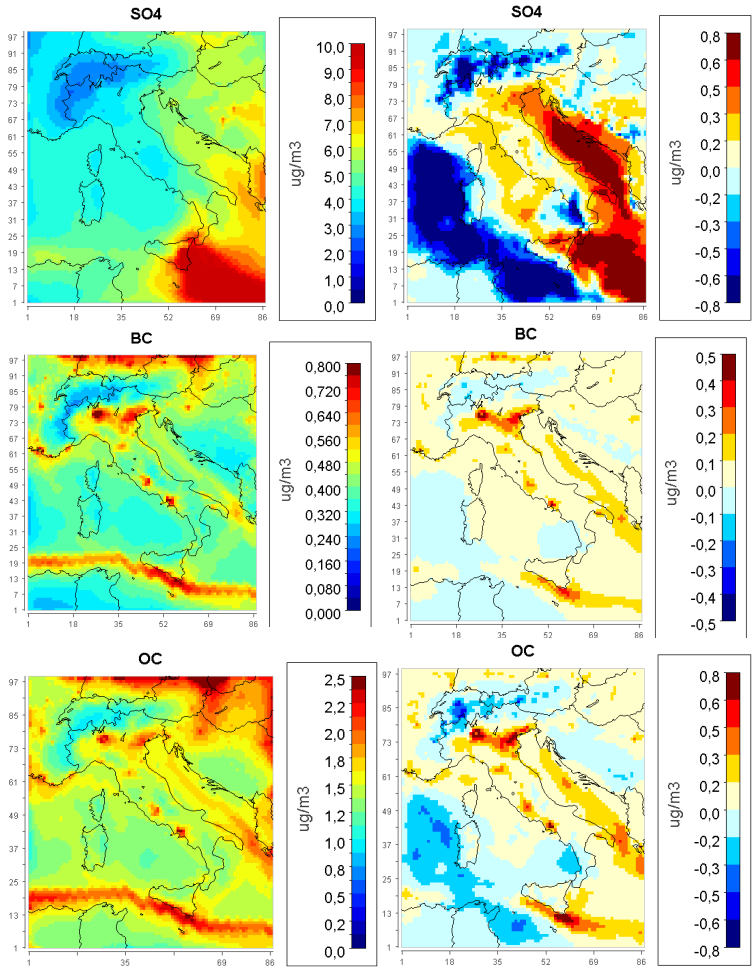

Figure 70- Monthly mean concentrations of $PM_{2.5}$ components in the BASE case (left); differences between FBS and BASE simulation (right).

The main variations of aerosols mass and components are associated to changes in turbulent vertical mixing. As an example, Figure 71 depicts vertical profiles of NO_2 and $PM_{2.5}$ concentrations in Milan city, where the main variations are found.

The first hour run (06/25/2010 at 01UTC) is chosen because it is not influenced by the residual concentrations of the previous days, thus, enabling to understand the differences related only to changes in model behavior.

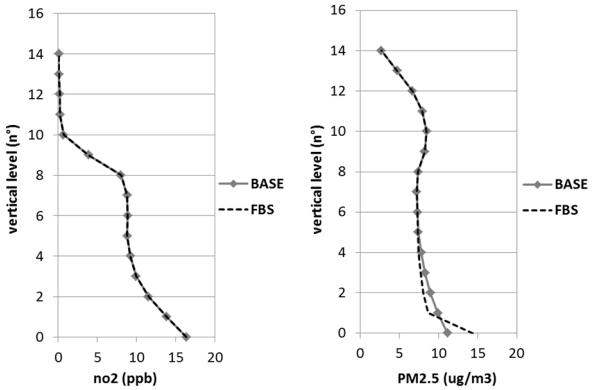

Figure 71 – Vertical profiles of NO_2 (left) and $PM_{2.5}$ (right) concentrations in Milan (45.46 N; 9.19 E) on 06/25/2010 at 01 UTC. Height is expressed as number of vertical levels up to 4000 m.

Vertical distribution of the gaseous compound does not significantly change moving from baseline to feedback simulations. On the contrary, for $PM_{2.5}$ a completely different vertical structure is visible in the first 150m (4^{th} vertical level). When feedbacks effects are turned on, a reduced vertical mixing is present and aerosols tend to be concentrated in the first level of atmosphere. This is caused by the different treatment of turbulent vertical diffusion for gas and aerosols in the presence of indirect feedback. Whether indirect feedback is included in the simulation, vertical diffusivity of aerosols is calculated taking into account for the number of particles that are activated and vertically diffused as cloud droplet, whereas in baseline simulation the treatment of vertical diffusion for both gas and aerosol is based only on the vertical dispersion coefficient (Kz) delivered from the PBL module. Moreover, vertical diffusion of gaseous species is the same between the simulations with and without indirect

feedback. This can explain why remarkable discrepancies between the two simulations were found only for aerosol compounds.
Comparisons with measurement stations are shown in Table 24.

Table 24 – Performance statistics in BASE and FBS case for all rural background stations inside the computational domain. Best performances are highlighted in grey.

Statistics	BASE		FBS	
	PM_{10} (μg/m3)	$PM_{2.5}$ (μg/m3)	PM_{10} (μg/m3)	$PM_{2.5}$ (μg/m3)
Mean Obs	20.62	14.06	20.62	14.06
Mean Mod	11.84	10.72	12.99	12.64
NMB (%)	- 42.57	-23.74	-37.01	-10.09
NME (%)	45.48	35.30	42.12	33.28
RMSE	12.19	6.58	11.15	6.23
IA	0.72	0.41	0.79	0.41

Variations between the two simulations are higher for aerosol particles. Increasing in PM_{10} and $PM_{2.5}$ concentrations leads to an improvement in model performances when feedbacks are included. However, model still underestimates the magnitude of observed values.
PM_{10} Normalized Mean Bias decreases from -43.57% (BASE) to -37.01% (FBS) as well as NME. It shows a variation from 45.48% (BASE) to 42.12% (FBS). Including feedbacks also improves the Index of Agreement. Reconstruction of daily trend is better in FBS (IA = 0.79) than in BASE (IA = 0.72).
A general improvement of model performances can be shown when only fine fraction is considered, suggesting that both simulations difficulty reconstruct the coarse fraction. As extensively discussed in Chapter 4, it is related to missing sources (e.g. resuspension and local mineral dust sources) that contribute mainly to the coarse fraction (Hendriks, 2009; Hodzic et al., 2007; Vautard et al., 2007) as well as lacking in aerosol processes. Moreover, discrepancies in PM_{10} NFB and NFE are similar to NO_2 ones, confirming that there is

inaccuracy in the reconstruction of some emission sources inside emission inventories.

$PM_{2.5}$ monthly mean concentrations vary from 10.72 μg/m^3 (BASE) to 12.64 μg/m^3 (FBS). NMB improves from -42.57% (baseline simulation) to -37.01% (feedback case).

It wasn't possible to perform a statistical analysis of $PM_{2.5}$ components, since not enough stations were available for July 2010.

As can be shown from the NMB spatial distribution of PM_{10} and $PM_{2.5}$ concentrations (Figure 72 and Figure 73), improvements in model performances are mainly associated to the Northern regions, namely Southern Germany and Northern Italy (Po valley) that are characterized by rather complex circulation conditions. Particularly, the Po valley often suffers of stagnant thermal inversions that lead to high aerosols concentrations that frequently exceed threshold limits, making it an interesting case study especially for the analysis of the feedback effects that are strongly influenced by high aerosol loads. For this reason, particular attention will be dedicated to the Po valley area in the following.

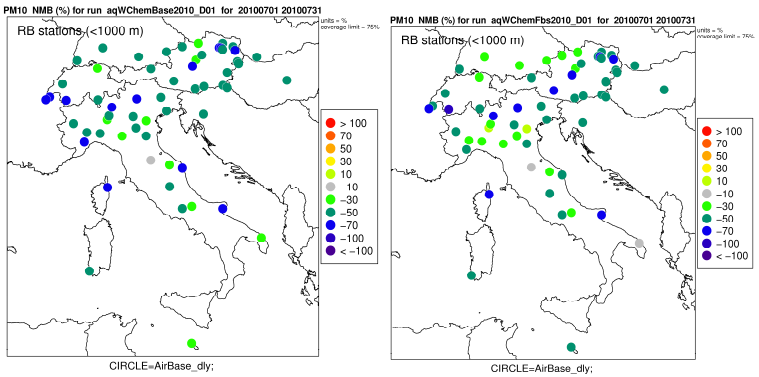

Figure 72 – PM_{10} spatial distribution of Normalized Mean Bias over Italy in Rural Background stations. *aqWchemBase2010_D01* indicates BASE simulation (left), while *aqWchemFbs2010_D01* is used for FBS case (right).

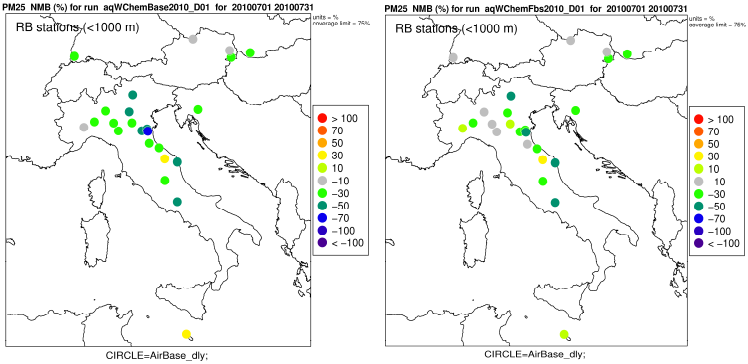

Figure 73 – $PM_{2.5}$ spatial distribution of Normalized Mean Bias over Italy in Rural Background stations. *aqWchemBase2010_D01* indicates BASE simulation (left), while *aqWchemFbs2010_D01* is used for FBS case (right).

Figure 74 reports the monthly time series of daily values in all background stations of the Po valley for both PM_{10} and $PM_{2.5}$.

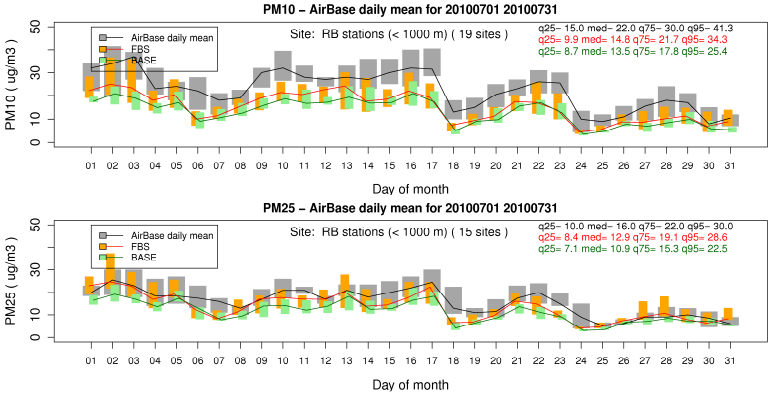

Figure 74 – Time series of daily values for PM_{10} and $PM_{2.5}$ in Rural Background stations of the Po valley.

The time evolution is well represented by the two simulations. Single events correspond in time with the observations.

Feedback improves the skill of model in reconstructing the magnitude of observed $PM_{2.5}$ values. Particularly, it is able to capture the highest values of the observed time series. The 95° percentile moves from 22.5 $\mu g/m^3$ (BASE) to 28.6 $\mu g/m^3$ (FBS), reaching the observed value of 30 $\mu g/m^3$.
An improvement is also visible in PM_{10} concentrations, even though model still underestimates measurement data, confirming an incorrect reconstruction of the coarse fraction.
$PM_{2.5}$ components were available only at one station of the Po valley, namely Ispra (IT004R; Figure 75). However, this site is not representative of the general pattern observed in the mean concentrations over the Po valley. Indeed, simulations reveal similar behavior and not any remarkable difference is noticeable when feedbacks are included.
$PM_{2.5}$ total mass is well reproduced by the simulations, but it is higher in BASE simulation than in FBS as well as NH_4 and SO_4 concentrations. However, time series analysis allows understanding the causes of $PM_{2.5}$ underestimations. As identified previously (Chapter 4), they are mainly associated to under predictions of unidentified PM, namely organic carbon. It is worth noting that simulations do not include secondary organic aerosol (SOA) processes that can contribute to the total organic carbon mass.

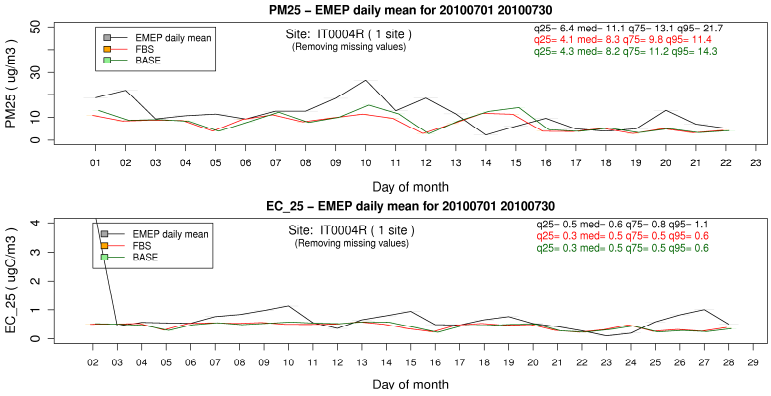

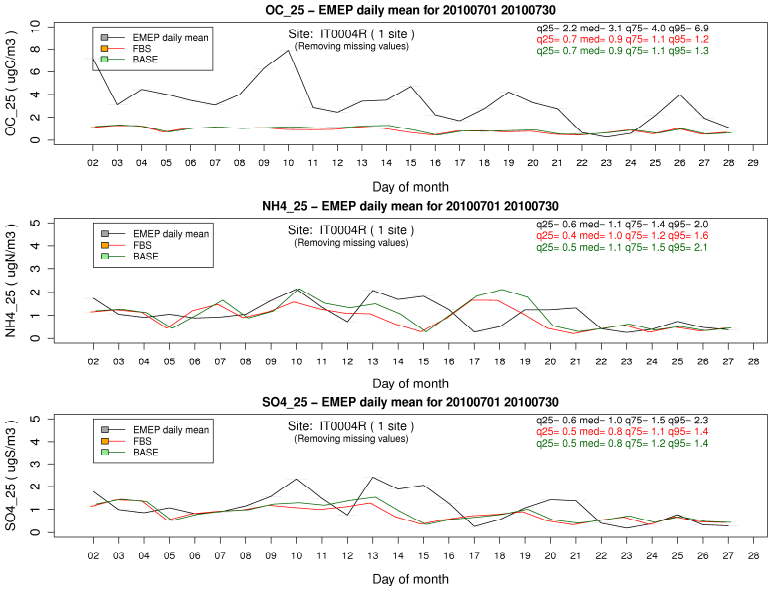

Figure 75 – Time series of daily data at EMEP station of Ispra (IT0004R).

Finally, a preliminary evaluation of Aerosol Optical Depth has been done at Lecce. Time series are reported in Figure 76. The optical depth expresses the quantity of light removed from a beam by scattering or absorption during its path through atmosphere. Therefore, there is not a simple linear relationship between column aerosol optical depth and the near surface atmospheric aerosols (Che et al, 2009). The aerosol optical depth may be affected by many factors, such as the chemical composition, the particle size and the shape of aerosol as well as the water vapor in the atmosphere (Che et al., 2009). However, feedbacks seems to increase the AOD values in Lecce, in agreement with the highest amount of aerosols loads

Both simulations follow the time evolution of the observed time series, and in some episodes they are able to capture its magnitude (e.g. 12/12/2010, 12/15/2010, from 22 to 23 of July 2010).

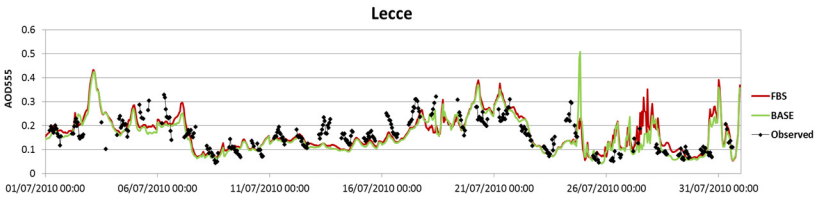

Figure 76 – Time series of Aerosol Optical Depth at 555nm (AOD555) in Lecce AERONET site.

5.3.3 Scenario analysis at 2030

The scenario evaluation has been conducted for July 2030 and compared to the 2010 simulations.

In order to understand the effect of emission control policies on aerosol interactions, results were analyzed as differences between the scenario and baseline simulations without feedback effects (SCEN - BASE) and the scenario with feedback effects and feedback simulation (SCEN_FBS - FBS).

Figure 77 shows monthly mean variations between future cases and reference simulations for gaseous species, namely NH_3, NO_2, O_3 and SO_2.

Variations in gaseous compound are proportional to emission changes.

Both simulations show an increase of ammonia concentrations up to 2 ppb (5-10%) only over the Po valley because of the assumption of enhanced emissions from the consumption of nitrogenous fertilizers and livestock in this area.

On the contrary, NO_2 concentrations were found to decrease all over the land of about 40% (3-4 ppb) either when feedback effects are considered or not. The main reductions are localized in the main cities of Italy (e.g. Milan, Rome and Naples) and neighboring countries (e.g. Vienna, Budapest, Zurich and Marseille), as well as along the major highways and transit routes. These variations are related to changes in NOx emissions from road transport and domestic heating. However, NO_2 concentrations increase beyond Sicily region due to the enhanced international shipping emissions.

For the same reason, SO_2 concentrations rise over the Mediterranean Sea. Variations range between 0.2 and 1 ppb ($\simeq$ 10%) in both simulations. Conversely, SO_2 decreases in foreign countries because of the different reduction between Italian and EMEP emissions of SNAP sector 1 related to power plants.
As a secondary pollutant, ozone variations are influenced by emissions of its main precursors, namely NO_2 and VOCs. Indeed, this species reduces its concentrations of about 2-3 ppb (8-10%) all over the domain due to lower emissions of NOx and anthropogenic VOCs. However, an increase in O_3 concentrations is observed in the most polluted cities (e.g. Milan, Rome and Budapest). Indeed, in urban areas O_3 concentrations rise as NOx emissions decrease (Sillman, 1999).
Looking at Milan city, the ozone increase is higher when feedback effects are turned on. If interactions between aerosols and meteorology are activated, in fact, the radiation scheme calculates the global radiation field using aerosol profiles provided by the aerosol module. Consequently, a lower amount of aerosol particles in the atmosphere, due to reduced emissions, leads to an enhanced incoming solar radiation at the ground. Increased solar radiation will generally result in higher photochemical activity. In regions with sufficiently high levels of NOx and VOC, an enhanced formation of near surface ozone can be expected. This further increase of ozone concentrations is not visible in simulations without feedback at Milan site, as in this case the treatment of particle loads does not change inside the RRTMG scheme when aerosol emissions are decreased.
For gaseous species, discrepancies between the future cases and their reference simulations are similar. As previously discussed, it is related to the fact that feedback effects have only a minor influence on NH_3, NO_2, O_3 and SO_2 concentrations.
As the variations with respect to the baseline simulations do not change with and without feedbacks, it is possible to state that emission reductions of gaseous compounds do not affect directly feedback mechanisms.

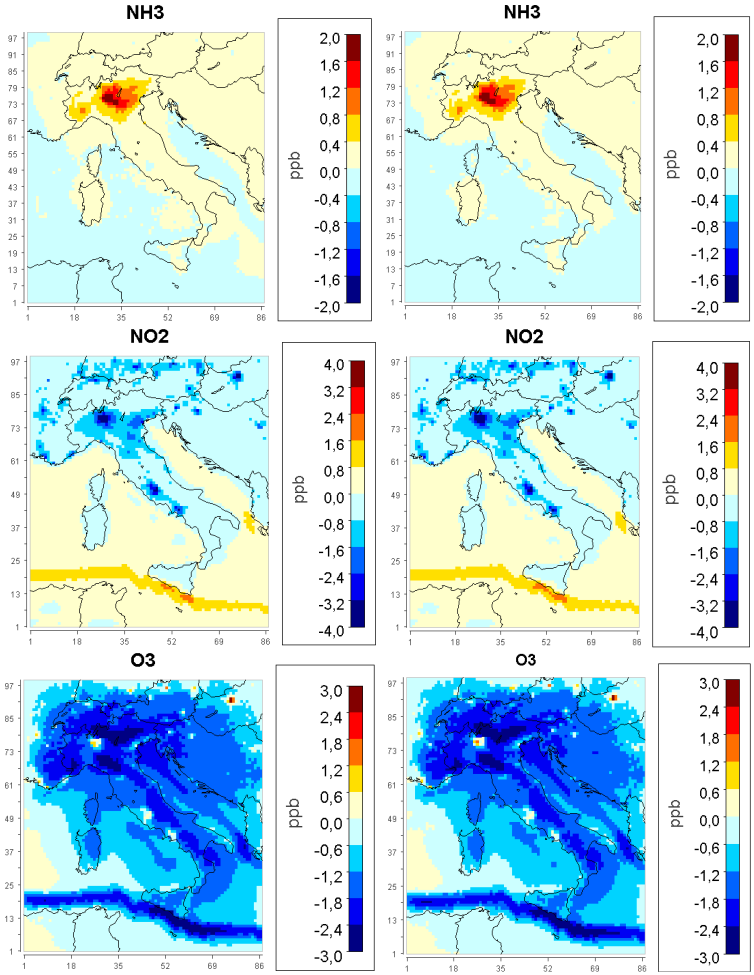
NH3
ppb
2,0
1,6
1,2
0,8
0,4
0,0
-0,4
-0,8
-1,2
-1,6
-2,0
NH3
ppb
2,0
1,6
1,2
0,8
0,4
0,0
-0,4
-0,8
-1,2
-1,6
-2,0
NO2
ppb
4,0
3,2
2,4
1,6
0,8
0,0
-0,8
-1,6
-2,4
-3,2
-4,0
NO2
ppb
4,0
3,2
2,4
1,6
0,8
0,0
-0,8
-1,6
-2,4
-3,2
-4,0
O3
ppb
3,0
2,4
1,8
1,2
0,6
0,0
-0,6
-1,2
-1,8
-2,4
-3,0
O3
ppb
3,0
2,4
1,8
1,2
0,6
0,0
-0,6
-1,2
-1,8
-2,4
-3,0

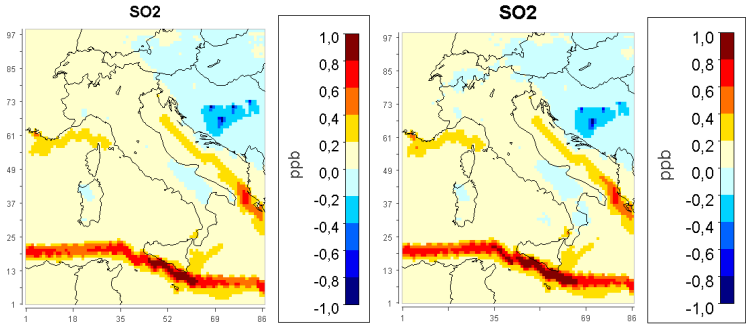

Figure 77 - Monthly mean differences between scenario (SCEN) and baseline (BASE) simulation without feedback effects (left), and between scenario with feedbacks (SCEN_FBS) and feedback simulation (FBS) (right).

PM_{10} and $PM_{2.5}$ differences between future case and reference simulation are represented in Figure 78 either when feedbacks effects are included (right) or not (left). Results are also analyzed for PM2.5 components.

PM_{10} and $PM_{2.5}$ show a decrease over land with respect to the reference cases due to lower emissions of aerosols and their main gaseous precursors. Considering the simulations without feedback, variations range between -1 and -3 $\mu g/m^3$ (5-15%). Discepancies in aerosols concentrations can reach up to -4 $\mu g/m^3$ ($\sim$ 16%) whether feedbacks simulations are compared together.

On the contrary, PM_{10} and $PM_{2.5}$ concentrations increase over the sea where international shipping enhances emissions.

Changes in aerosols concentrations are connected to a variation of $PM_{2.5}$ main components, namely sulphate, nitrate, ammonium and black carbon. These compounds show a general decrease over the domain, especially in the highest emissive areas of the Po valley. In SCEN simulation, nitrate reduces of about 1 $\mu g/m^3$ ($\sim$ 20%) with respect to BASE case, whereas ammonium decreases between 0.4 and 0.8 $\mu g/m^3$ (10-20%).

As for total aerosol mass, variations in aerosol components are more remarkable when simulations with feedbacks are considered.

Whether feedbacks are taken into account, in fact, nitrate and ammonium reduce of about 3 $\mu g/m^3$ (30%) and 1 $\mu g/m^3$ ($\simeq$ 20%), respectively. The presence of lower aerosols load in the atmosphere, indeed, leads to a reduced response of feedback mechanisms with respect to the reference simulation (FBS), that generates lower increase of aerosol concentrations in the atmosphere, and, thus, higher variation in comparison to the simulations without feedbacks.
Finally, sulphate and black carbon are analyzed. They increase over the sea in both simulations. Particularly, sulphate reveals a reduction that ranges between 0.1 and 0.5 $\mu g/m^3$ (2-10%) in the Eastern domain while it follows SO_2 increase over the sea (0.1-0.6 $\mu g/m^3$; 2-10%).
In conclusion, it is possible to state that emission reductions of aerosol compounds seem to affect feedback mechanisms.

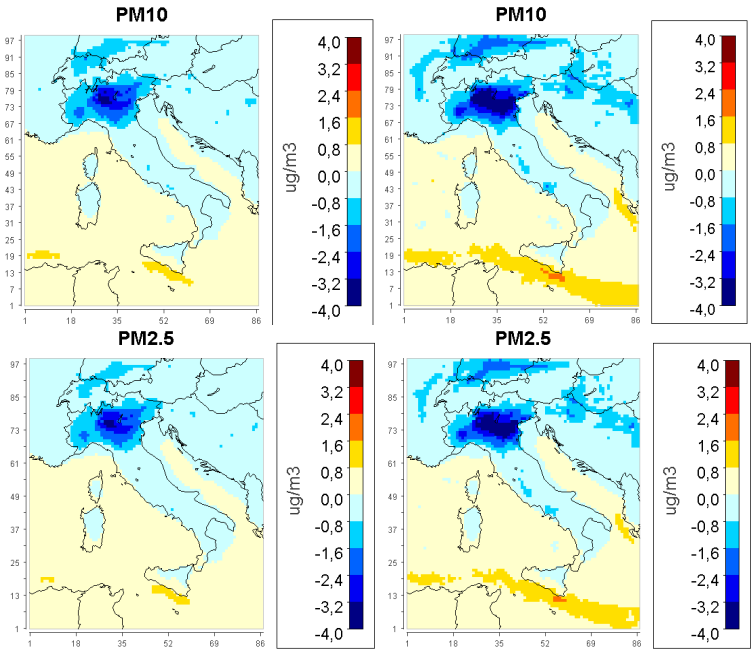

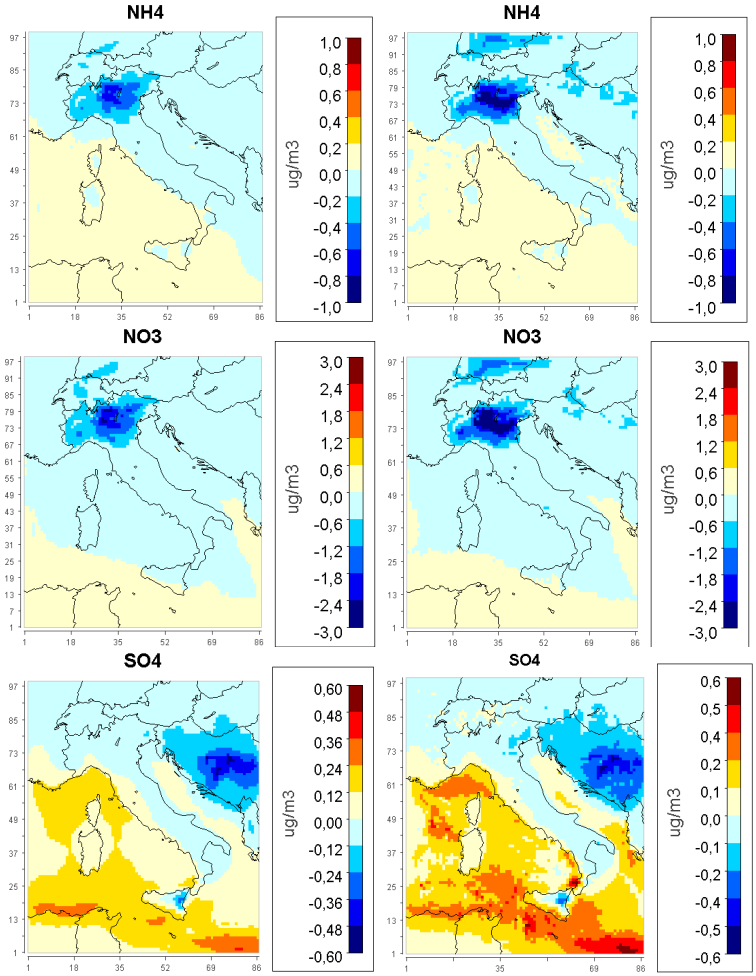
NH4
ug/m3
1,0
0,8
0,6
0,4
0,2
0,0
-0,2
-0,4
-0,6
-0,8
-1,0
NH4
ug/m3
1,0
0,8
0,6
0,4
0,2
0,0
-0,2
-0,4
-0,6
-0,8
-1,0
NO3
ug/m3
3,0
2,4
1,8
1,2
0,6
0,0
-0,6
-1,2
-1,8
-2,4
-3,0
NO3
ug/m3
3,0
2,4
1,8
1,2
0,6
0,0
-0,6
-1,2
-1,8
-2,4
-3,0
SO4
ug/m3
0,60
0,48
0,36
0,24
0,12
0,00
-0,12
-0,24
-0,36
-0,48
-0,60
SO4
ug/m3
0,6
0,5
0,4
0,2
0,1
0,0
-0,1
-0,2
-0,4
-0,5
-0,6

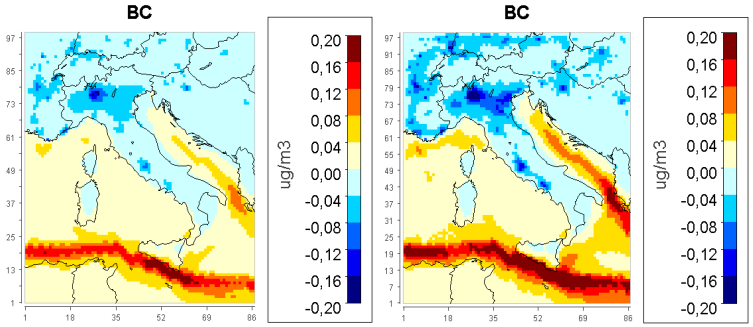

Figure 78 – Monthly mean differences between scenario (SCEN) and baseline (BASE) simulation without feedback effects (left), and between scenario with feedbacks (SCEN_FBS) and feedback simulation (FBS) (right).

5.4 CONCLUSIONS

In order to investigate the impact of direct and indirect feedback on meteorological variables and pollutants, WRF-Chem simulations have been performed over Italy accounting or not for the presence of feedback mechanisms. WRF-Chem has been applied with 15 km grid resolution for July 2010.

The presence of feedback effects is found to decrease the incoming solar radiation at the ground up to 20 W/m^2 (-5%), particularly in the Po valley, due to aerosol backscatter. On the contrary, shortwave downward radiation was found to increase over the Western Mediterranean, the Alps and Eastern domain of about 4-6% (12-20 W/m^2) because of a reduction of the vertically integrated cloud water content and, then, cloud cover. Inclusion of indirect effect has a strong influence on cloud water content that shows a local decrease of about 40% (0.04-0.05 kg/m^2). As auto-conversion to rain droplet is higher for small cloud droplet concentrations, the formation of rain droplets increases.

Distribution of incoming solar radiation change is partly reflected in the distribution of the mean height of the planetary boundary layer that displays a general decrease over Italy. This reduction can reach

up to 30 m (-5%) in the Po valley. The response of aerosol-radiation-cloud interaction was found to be stronger here than in other region of Italy due to high aerosol loads that are commonly present in the region.

Meteorological variations were in line with other European application of the same model (Forkel et al., 2012). However, a detailed analysis at cloud resolving resolution will be necessary to further analyze indirect feedback.

Concerning the gaseous compounds, the inclusion of both direct and indirect effects is found to have only minor influence on them, with variations that range between 2-5%. Moreover, variations observed in gaseous compounds have the same order of magnitude as changes in meteorological variables. This suggests that gas concentrations are mainly influenced by variation in dispersion processes (e.g. wind speed and Planetary Boundary Layer height) as well as incoming solar radiation.

Aerosols concentrations show a stronger influence by feedback effects, because of changes in their main components. The highest increases are in the Po valley. There PM_{10} and $PM_{2.5}$ concentrations rise of 25% and 30% (5 $\mu g/m^3$), respectively. Differently from gaseous species, variations in meteorological variables cannot always be connected with variation in aerosols concentrations. On the contrary, variations can be related to a reduced turbulent vertical mixing whether feedback effects are turned on.

Increasing in PM_{10} and $PM_{2.5}$ concentrations leads to an improvement in model performances when feedbacks are included. Particularly, feedback improves the skill of model in reconstructing the magnitude of highest values of the observed time series. However, model still underestimates PM_{10} and $PM_{2.5}$ measured values.

A preliminary evaluation of Aerosol Optical Depth has also been done at Lecce station. Feedbacks seem to increase the AOD values in Lecce, in agreement with the highest amount of aerosols loads.

In order to understand the effect of emission control policies on aerosol-meteorology interactions, a scenario evaluation has been conducted for July 2030 using the emission scenario developed by

ENEA. WRF-Chem has been applied over Italy with and without feedback effects and compared to both 2010 cases.
Variations in gaseous compound between 2030 and 2010 cases are proportional to emission changes. Moreover discrepancies between future cases and their reference simulations are similar with and without feedbacks. This is related to the fact that feedback effects have only a minor influence on gaseous concentrations. As the variations with respect to the reference simulations do not change with and without feedbacks, it is possible to state that emission reductions of gaseous compounds do not directly affect feedback mechanisms.
A different behavior is identified for aerosol compounds. PM_{10} and $PM_{2.5}$ concentrations decrease over land of about 5-15% (1-3 $\mu g/m^3$) with respect to the 2010 simulation, due to lower emissions of aerosols and their main gaseous precursors. Aerosol variations can reach up to -16% ($\simeq$ -4 $\mu g/m^3$) whether feedbacks are turned on. Indeed, as feedback effects are not linear, the presence of lower aerosol loads in the atmosphere leads to a reduced response of these mechanisms compared to the reference simulation, and, thus, a higher reduction of ground-based aerosol concentrations with respect to the simulation without feedbacks. In conclusion, it is possible to state that emission reductions of aerosol species seem to affect feedback mechanisms.

5.5 REFERENCES

Abdul-Razzak, H., Ghan, S.J., 2002. A parameterization of aerosol activation. 3. Sectional representation. Journal of Geophysical Research 107 (D3). doi:10.1029/2001JD000483.

Beheng K.D., 1994, A parameterization of warm cloud microphysical conversion processes, Atmospheric Research Volume 33 (1–4), 193–206.

Barnard J., Chapman E.G., Fast J., Schmelzer J.R., Slusser J.R., Shetter R.E., 2004. An evaluation of the FAST-Jphotolysis algorithm for

predicting nitrogen dioxide photolysis rates under clear and cloudy sky conditions. Atmospheric Environment 38, 3393–3403. doi:10.1016/j.atmosenv.2004.03.034.

Chapman, E.G., Gustafson Jr., W.I., Easter, R.C., Barnard, J.C., Ghan, S.J.,Pekour, S.M. and Fast, J.D., 2009. Coupling aerosol-cloud-radiative processes in the WRF-Chem model: Investigating the radiative impact of elevated point sources. Atmospheric Chemistry and Physics, 9, 945-964.

Che H., Yang Z., Zhang X., Zhu C., Ma Q., Zhou H., Wang P., 2009. Study on the aerosol optical properties and their relationship with aerosol chemical compositions over three regional background stations in China. Atmospheric Environment 43, 1093-1099. doi: 10.1016/j.atmosenv.2008.11.010.

Chen, F., Dudhia, J., 2001. Coupling an Advanced Land Surface–Hydrology Model with the Penn State–NCAR MM5 Modeling System. Part I: Model Implementation and Sensitivity. Monthly Weather Review 129, 569–585.

Cofala J., Syri S., 1998a. Sulfur emissions, abatement technologies and related costs for Europe in the RAINS model database. International Institute for Applied Systems Analysis. Internal Report.

Cofala J., Syri S., 1998b. Nitrogen oxides emissions, abatement technologies and related costs for Europe in the RAINS model database. International Institute for Applied Systems Analysis. Internal Report.

D'Elia I. and Peschi E., 2013. Lo scenario emissive nazionale nella negoziazione internazionale, ENEA report.

Easter, R. C., Ghan, S. J., Zhang, Y., Saylor, R. D., Chapman, E. G., Laulainen, N. S., Abdul-Razzak, H., Leung, L. R., Bian, X., and Zaveri, R. A., 2004. MIRAGE: Model description and evaluation of aerosols and trace gases. J. Geophys. Res., 109(D2), 0210. doi:10.1029/2004JD004571.

EU, 2009. Commission Regulation No. 595/2009 of the European Parliament and of the Council of 18 June 2009 on type-approval of motor vehicles and engines with respect to emissions from heavy duty vehicles (Euro VI) and on access to vehicle repair and maintenance information and amending Regulation (EC) No 715/2007 and Directive 2007/46/EC and repealing Directives 80/1269/EEC, 2005/55/EC and

2005/78/EC. Official Journal L 188/1, 18.7.2009, p. 1-13. http://eur-lex.europa.eu/LexUriServ/LexUriServ.do?uri=OJ:L:2009:188:0001:0013:EN:PDF.

EU, 2008. Directive 2008/50/EC of the European Parliament and of the Council of 21 May 2008 on ambient air quality and cleaner air for Europe. Official Journal L 152, 11.6.2008, p. 1–44 http://eur-lex.europa.eu/LexUriServ/LexUriServ.do?uri=OJ:L:2008:152:0001:0044:EN:PDF.

EU, 2008. Commission Regulation No. 692/2008 of the European Parliament and of the Council of 18 July 2008 on implementing and amending Regulation (EC) No 715/2007 of the European Parliament and of the Council on type-approval of motor vehicles with respect to emissions from light passenger and commercial vehicles (Euro 5 and Euro 6) and on access to vehicle repair and maintenance information. Official Journal L 199/1, 28.7.2008, p. 1-136. http://eur-lex.europa.eu/LexUriServ/LexUriServ.do?uri=OJ:L:2008:199:0001:0136:EN:PDF

EU, 2004. Directive 2004/42/EC of the European Parliament and of the Council of 21 April 2004 on the limitation of emissions of volatile organic compounds due to the use of organic solvents in certain paints and varnishes and vehicle refinishing products and amending Directive 1999/13/EC. Official Journal L 143/87, 30.4.2004, p. 1-10. http://eur-lex.europa.eu/LexUriServ/LexUriServ.do?uri=OJ:L:2004:143:0087:0096:EN:PDF

EU, 2001. Directive 2001/80/EC of the European Parliament and of the Council of 23 October 2001 on the limitation of emissions of certain pollutants into the air from large combustion plants. Official Journal L 309, 27.11.2001, p. 1-27. http://eur-lex.europa.eu/LexUriServ/site/en/consleg/2001/L/02001L0080-20011127-en.pdf

Fast, J. D., W. I. Gustafson Jr., R. C. Easter, R. A. Zaveri, J. C. Barnard, E. G. Chapman, G. A. Grell, and S. E. Peckham, 2006. Evolution of ozone, particulates, and aerosol direct radiative forcing in the vicinity of Houston using a fully coupled meteorology-chemistry-aerosol model. J. Geophys. Res., 111, D21305, doi:10.1029/2005JD006721.

Fahey K.M. and Pandis, S.N., 2001. Optimizing model performance: variable size resolution in cloud chemistry modeling. Atmospheric Environment, 35, 4471-4478.

Forkel R., Werhahn J., Hansen A.B., McKeen S., Peckham S., Grell G., Suppan P., 2012. Effect of aerosol-radiation feedback on regional air quality - A case study with WRF/Chem. Atmospheric Environment, 53, 202-211.

Forster, P., et al., 2007. Changes in atmospheric constituents and in radiative forcing. In: Solomon, S. (Ed.), Climate Change 2007: The Physical Science Basis. Contribution of Working Group I to the Fourth Assessment Report of the Intergovernmental Panel on Climate Change. Cambridge University Press, Cambridge, United Kingdom and New York, NY, USA.

GAINS Development Team, 2009. GAINS Online: Tutorial for advanced users, version 1.0, International Institute for applied systems analysis, Austria. http://gains.iiasa.ac.at/index.php/home-page

Ghan, S. J., Easter, R. C., Chapman, E. G., Abdul-Razzak, H., Zhang, Y., Leung, L. R., Laulainen, N. S., Saylor, R. D., and Zaveri, R. A., 2001. A physically-based estimate of radiative forcing by anthropogenic sulfate aerosol. J. Geophys. Res., 106, 5279–5293.

Giorgi and Meleux, 2007. Modelling the regional effects of climate change on air quality. C. R. Geoscience, 339, 721-733.

Gong, S. L., 2003. A parameterization of sea-salt aerosol source function for sub- and super-micron particles. Global Biogeochemical Cycles 17: 1097-1104.

Gracceva F. and Contaldi M., 2004. Scenari energetici italiani. Valutazione di misure di politica energetica. ENEA, ISBN 88-8286-108-2.

Grell, G. A., Devenyi, D., 2002. A generalized approach to parameterizing convection combining ensemble and data assimilation techniques. Geophys. Res. Lett. 29(14), 1693.

Grell, Peckham, Schmitz, McKeen, Frost, Skamarock and Eder, 2005. Fully coupled “online” chemistry within the WRF model. Atmospheric Environment, 39(37), 6957-6975.

Guenther, A., Karl, T., Harley, P., Wiedinmyer, C., Palmer, P., Geron, C., 2006. Estimates of global terrestrial isoprene emissions using MEGAN

(Model of Emissions of Gases and Aerosols from Nature). Atmos. Chem Phys., 6, 3181-3210.

Gustafson, W. I., Chapman, E. G., Ghan, S. J., Easter, R. C., and Fast, J. D., 2007. Impact on modeled cloud characteristics due to simplified treatment of uniform cloud condensation nuclei during NEAQS 2004. Geophys. Res. Lett., 34, L19809, doi:10.1029/2007GL0300321.

Hansen, J. E., Sato, M., and Ruedy, R., 1997. Radiative forcing and climate response. J. Geophys. Res, 102, 6831–6864.

Hendriks E.C.J., H.A.C. Denier van der Gon, M. Schaap, 2009. Constraining the potential source strength of various soil dust sources contributing to atmospheric PM10 concentrations in Europe. Proceedings of the 30th NATO/CCMS ITM conference, San Francisco, U.S.A.

Hodzic, A., Madronich, S., Bohn, B., Massie, S., Menut, L., Wiedinmyer, C., 2007. Wildfire particulate matter in Europe during summer 2003: meso-scale modeling of smoke emissions, transport and radiative effects. Atmospheric Chemistry and Physics 7, 4043–4064.

Hong, S.-Y., Noh, Y., Dudhia, J., 2006. A New Vertical Diffusion Package with an Explicit Treatment of Entrainment Processes. Monthly Weather Review 134, 2318-2341.

Iacono M.J., Mlawer E.J, Clough S.A., Morcrette J-J., 2000. Impact of an improved longwave radiation model, RRTM, on the energy budget and thermodynamic properties of the NCAR community climate model, CCM3. Journal of Geophysical Research 105(D11), 14873–14890. doi: 10.1029/2000JD900091.

Jacob D.J. and Winner D.A., 2009. Effect of climate change on air quality. Atmospheric Environment, 43, 51-63, doi:10.1016/j.atmosenv.2008.09.051.

Klimont Z. and Brink C., 2004. Modelling of Emissions of Air Pollutants and Greenhouse Gases from Agricultural Sources in Europe. International Institute for Applied Systems Analysis, Internal Report.

Klimont Z., Cofala J., Bertok I., Amann M., Heyes C., Gyarfas F., 2002. Modelling Particulate Emissions in Europe - A Framework to Estimate Reduction Potential and Control Costs International Institute for Applied Systems Analysis, Internal Report.

Klimont Z., Amann M., and Cofala J., 2000. Estimating Costs for Controlling Emissions of Volatile Organic Compounds (VOC) from Stationary Sources in Europe. International Institute for Applied Systems Analysis, Internal Report.

Marcacci P., Toppetti A.M., Collino E., 2012. Classificazione delle proprietà ottiche delle nubi da satellite Meteosat e completamento della stazione solare di Milano. Rapporto RSE n° 12001018.

Mlawer, E.J., Taubman, S.J., Brown, P.D., Iacono, M.J., Clough, S.A., 1997. Radiative transfer for inhomogeneous atmospheres: RRTM, a validated correlated-k model for the longwave. Journal of Geophysical Research 102, 16663–16682.

Monin, A. S., Obukhov, A. M., 1954. Basic Laws of Turbulent Mixing in the Ground Layer of the Atmosphere. Trans. Geophys. Inst. Akad. Nauk. USSR 151, 163–187.

Morrison, H., Thompson, G., Tatarskii, V, 2009. Impact of cloud micrpohysics on the development of trailing stratiform precipitation in a simulated squall line: Comparison of one- and two-moment schemes. Monthly Weather Review 137, 991-1007, doi: 10.1175/2008MWR2556.1.

Shaw W.J., Allwine K, Fritz B.G., Rutz F.C., Rishel J.P., Chapman E.G., 2008. An evaluation of the wind erosion module in DUSTRAN. Atmospheric Environment 42, 1907–1921. doi:10.1016/j.atmosenv.2007.11.022.

Sillman S., 1999. The relation between ozone, NOx and hydrocarbons in urban and polluted rural environments. Atmospheric Environment 33 (12), 1821–1845.

UNC, 2009. SMOKE v2.6 User's manual, http://www.smoke-model.org/index.cfm.

Vautard, R., Builties, P.H.J., Thunis, P., Cuvelier, C., Bedogni, M., Bessagnet, B., Honore, C., Moussiopoulos, N., Pirovano, G., Schaap, M., Stern, R., Tarrason, L.,Wind, P., 2007. Evaluation and intercomparison of ozone and PM10 simulations by several chemistry transport models over four European cities within the CityDelta project. Atmos Environ 41:173–188.

Wesely M.L, 1989. Parameterization of surface resistance to gaseous dry deposition in regional-scale numerical models. Atmos. Environ., 23, 1293-1304. doi: 10.1016/0004-6981(89)90153-4.

Yang, Q., Gustafson Jr., W.I., Fast, J.D., Wang, H., Easter, R.C., Morrison, H., 2011. Assessing regional scale predictions of aerosols, marine stratocumulus, and their interactions during VOCALS-REx using WRF-Chem. Atmospheric Chemistry and Physics Discussions 11, 22663e22718, doi:10.5194/acpd-11-22663-2011.

Zaveri R. Easter R.C., Fast J.D. and Peters L.K., 2008. Model for Simulating Aerosol Interactions and Chenistry (MOSAIC). Journal of Geophysical Research, 113, D13204, doi: 10.1029/2007JD008782.

Zaveri R.A. and Peters L.K., 1999. A new lumped structure photochemical mechanism for large-scale applications. J. Geophys. Research, 104(D23), 30,387-30,415.

Zhang Y., Wen X.-Y., Jang C.J., 2010. Simulating chemistry – aerosol – cloud –radiation – climate feedbacks over the continental U.S. using the online-coupled Weather Research Forecasting Model with Chemistry (WRF/Chem). Atmospheric Environment, 44, 3568-3582, doi: 10.1016/j.atmosenv.2010.05.056.

6 GENERAL CONCLUSIONS

In recent years the atmospheric modeling community is moving toward a new modeling approach that integrates meteorological and chemical processes in the same model (on-line), consenting a more complete and realistic representation of the lower atmosphere and its driving phenomena and also allowing feedback effects to be included (coupled) and quantified. However these models are still poorly investigated and many of these feedback mechanisms are scarcely understood, especially over complex terrains characterized by land-sea interfaces and complex circulation conditions, such as the Italian one.

In this contest, the state-of-the-art WRF-Chem (Grell et al., 2005) on-line coupled model has been applied over Italy in order to investigate the impacts of aerosols-radiation-cloud interactions on air quality simulations.

The analyses carried out on WRF-Chem model outcomes demonstrated that it can be a valid and efficient tool to simulate both direct and indirect feedback processes. Indeed, these mechanisms tend to improve the skill of model in reconstructing both meteorological fields and aerosol concentrations especially in complex circulation systems like the Po valley.

Performance variations were demonstrated to be in line with results reported in literature for other applications of the same model (Forkel et al., 2012; Yang et al., 2011; Zhang et al., 2010). In particular, the presence of feedback effects decreased the incoming solar radiation at the ground up to 20 W/m^2, due to aerosol backscatter, and the Planetary Boundary Layer height of about 5% in the Po valley area.

Inclusion of indirect effect had a strong influence on cloud water content that showed a local decrease of about 40%.
The coupled approach was found to have minor influence on gas species, while a strong impact was shown for aerosols (PM_{10} and $PM_{2.5}$) and their main components. In the Po valley PM_{10} and $PM_{2.5}$ concentrations increased of about 25% and 30% when aerosol-radiation-cloud interactions were considered due to the induced reductions of turbulent vertical mixing that concentrated particles in the first atmospheric layers.
Moreover it was demonstrated the effectiveness of using these tools to analyze future scenarios that explores the impact of emission control strategies on air pollution either when feedbacks are turned on. Feedback effects tended to be influenced by policies of aerosol emission reductions. The presence of lower aerosols load in the atmosphere, in fact, leads to a reduced response of feedback mechanisms.
Analyzing only the effect of on-line approaches without aerosols coupling no significant differences were found between on-line and off-line chemistry and transport models. This result suggested that WRF-Chem model performances were in line with other extensively-evaluated and well-known instruments, but the main improvements were related to the inclusion of the coupled approach. In particular, WRF-Chem confirmed to have similar performances as the off-line CAMx model (ENVIRON, 2011), that was widely validated in the framework of the AQMEII initiative (Rao et al., 2011; Pirovano et al., 2012), with the additional advantage to simulate meteorology simultaneously with chemistry thus allowing a significant reduction of inconsistency between meteorological and chemical processes.
Finally the project aimed at investigating the reconstructions of meteorological processes that influenced aerosol concentrations at the ground in order to reduce uncertainties related to the representation of dispersion process, namely the Planetary Boundary Layer (PBL) height. A sensitivity test on five PBL schemes (ACM2, MRF, MYJ, YSU and UW) demonstrated that model scarcely reproduced the Boundary Layer evolution because of an overestimation of vertical mixing during the PBL development.

Indeed, the daytime evolution of PBL appeared too rapid in all simulations. However, the comparison with a quite unique set of experimental data (ground level measurements, particle vertical profiles by balloon soundings, meteorological balloons and Lidar measurements) allowed identifying a parameterization that improved the overall model performances in the peculiar area of the Po valley. The selected scheme was the Yonsei University PBL (YSU; Hong et al., 2006) that proved to give reasonable results in terms of concentrations in air quality simulations.

In conclusion, the results of this project allowed a better understanding of the complex interactions between meteorology and air quality. It represents an important contribution to evaluate the potential added value of a more realistic reconstruction of the atmosphere through incorporating feedback mechanism in chemistry and transport models (coupled approach). All the collected information in the present study opens the way for a more comprehensive assessment of future air quality studies and scenario analysis that aim at investigating emission control policies and strategies either in a climate change perspective.

As showed here aerosols can affect the evolution of the atmospheric boundary layer and local scale dynamics through their impact on the radiative balance. Furthermore it was demonstrated that aerosols-radiation-cloud interactions can be locally predominant due to heterogeneity in emissions and processes. This work was, therefore, able to prove the importance of including aerosol-radiation-cloud interactions in emission regional policy, decision support, and risk management at local scale. It can be also a useful starting point for scenario analysis related studies, especially over complex terrain systems.

Moreover, as temperature change is expected to significantly impact atmospheric composition, all the regional strategies to reduce air pollution below a specified threshold need to be reconciled with strategies to limit climate warming. Recently, there has been an increased focus in the global climate modeling community on studying the impacts and mitigation of short-lived climate forcers, such as aerosols and ozone, on climate change (Alapaty et al., 2012;

Forster and Ramaswamy, 2007; Penner et al., 2010). However, many studies directed at aerosol forcing ignored aerosol-cloud interactions and used crude representations of aerosol properties with various degrees of simplifying assumptions thereby injecting uncertainty in the projected climate impacts (Alapaty et al., 2012; Koch et al. 2011). As pointed out by Raes and Seinfeld (2009), there is a growing need for climate models dealing with short-lived climate forcers to assess process representation of aerosols and two-way feedbacks. This study, furnishing a comprehensive validation of aerosols mechanisms as well as evaluating aerosol impacts on radiation and clouds, can increase confidence in modeling studies of regional climate impacts of short-lived climate forcers.

6.1 REFERENCES

Alapaty, K., et al., 2012. New Directions: Understanding interactions of air quality and climate change at regional scales. Atmospheric Environment. doi:10.1016/j.atmosenv.2011.12.016

ENVIRON, 2011. User's Guide to the Comprehensive Air Quality Model with Extensions (CAMx). Version 5.4. Report prepared by ENVIRON International Corporation Novato, CA.

Forkel R., Werhahn J., Hansen A.B., McKeen S., Peckham S., Grell G., Suppan P., 2012. Effect of aerosol-radiation feedback on regional air quality - A case study with WRF/Chem. Atmospheric Environment, 53, 202-211.

Forster, P., and V. Ramaswamy, 2007. Changes in Atmospheric Constituents and in Radiative Forcing. In: Climate Change 2007: The Physical Science Basis. Contribution of Working Group I to the Fourth ssessment Report of the Intergovernmental Panel on Climate Change [Solomon, S., D. Qin, M. Manning, Z. Chen, M. Marquis, K.B. Averyt, M.Tignor and H.L. Miller (eds.)]. Cambridge University Press, Cambridge, United Kingdom and New York, NY, USA.

Grell, Peckham, Schmitz, McKeen, Frost, Skamarock and Eder, 2005. Fully coupled "online" chemistry within the WRF model. Atmospheric Environment, 39(37), 6957-6975.

Hong, S.-Y., Noh, Y., Dudhia, J., 2006. A New Vertical Diffusion Package with an Explicit Treatment of Entrainment Processes. Monthly Weather Review 134, 2318-2341.

Koch, D., Bauer,S.E., Del Genio, A., Faluvegi, G., McConnell, J.R., Menon, S., Miller, R.L., Rind, D., Ruedy, R., Schmidt, G.A., Shindell, D., 2011. Coupled Aerosol-Chemistry-Climate Twentieth Century Transient Model Investigation: Trends in Short-Lived Species and Climate Responses. J. Clim., 24, 2693-2714.

Penner, J.E., Prather, M.J., Isaksen, S.A., Fgulestvedt, J.S., Klimont, Z., Stvenson, D., 2011. Short-Lived Uncertainty?. Nature Geoscience, 3, 587-588.

Pirovano G., Balzarini A., Bessagnet B., Emery C., Kallos G., Meleux F., Mitsakou C.,Nopmongcol U., Riva G.M., Yarwood G., 2012. Investigating impacts of chemistry and transport model formulation on model performance at European scale. Atmospheric Environment 53, 93-109. doi:10.1016/j.atmosenv.2011.12.052.

Rao, S. T., Galmarini, S., Puckett, K., 2011. Air Quality Model Evaluation International Initiative (AQMEII): Advancing the State of the Science in Regional Photochemical Modeling and Its Applications. BAMS, Volume 92, Issue 1, 23-30.

Raes, F., Seinfeld, J.H., 2009. New Directions: Climate Change and Air Pollution Abatement: A Bumpy Road. Atmospheric Environment 43, 5132-5133.

Yang, Q., Gustafson Jr., W.I., Fast, J.D., Wang, H., Easter, R.C., Morrison, H., 2011. Assessing regional scale predictions of aerosols, marine stratocumulus, and their interactions during VOCALS-REx using WRF-Chem. Atmospheric Chemistry and Physics Discussions 11, 22663e22718. doi:10.5194/acpd-11-22663-2011.

Zhang Y., Wen X.-Y., Jang C.J., 2010. Simulating chemistry – aerosol – cloud –radiation – climate feedbacks over the continental U.S. using the online-coupled Weather Research Forecasting Model with Chemistry (WRF/Chem). Atmospheric Environment, 44, 3568-3582, doi: 10.1016/j.atmosenv.2010.05.056.

APPENDIX A: PERFORMANCE INDICATORS

A1) Chemistry

The statistical indicators selected to evaluate the model performances for chemistry have been defined as follows:

Normalized Mean Bias (NMB):

$$NMB = \frac{\frac{1}{N}\sum_{t=1}^{N}\left(C_{\mathrm{mod}}(x,t) - C_{obs}(x,t)\right)}{\frac{1}{N}\sum_{t=1}^{N} C_{obs}(x,t)}$$

Normalized Mean Error (NME):

$$NME = \frac{\frac{1}{N}\sum_{t=1}^{N}\left|C_{\mathrm{mod}}(x,t) - C_{obs}(x,t)\right|}{\frac{1}{N}\sum_{t=1}^{N} C_{obs}(x,t)}$$

Mean Fractional Bias (FB):

$$FB = \frac{1}{N}\sum_{t=1}^{N}\frac{C_{\mathrm{mod}}(x,t) - C_{obs}(x,t)}{(C_{obs}(x,t) + C_{\mathrm{mod}}(x,t))/2}$$

Mean Fractional Error (FE):

$$FE = \frac{1}{N}\sum_{t=1}^{N}\frac{\left|C_{\mathrm{mod}}(x,t) - C_{obs}(x,t)\right|}{(C_{obs}(x,t) + C_{\mathrm{mod}}(x,t))/2}$$

Correlation Index (r):

$$r = \frac{\sum_{t=1}^{N}\left(C_{\mathrm{mod}}(x,t) - \overline{C}_{\mathrm{mod}}(x)\right)\cdot\left(C_{obs}(x,t) - \overline{C}_{obs}(x)\right)}{\sqrt{\sum_{t=1}^{N}\left(C_{\mathrm{mod}}(x,t) - \overline{C}_{\mathrm{mod}}(x)\right)^2}\cdot\sqrt{\sum_{t=1}^{N}\left(C_{obs}(x,t) - \overline{C}_{obs}(x)\right)^2}}$$

Index of Agreement (IA):

$$IA = 1 - \frac{\sum_{t=1}^{N}\left(C_{\mathrm{mod}}(x,t) - C_{obs}(x,t)\right)^2}{\sum_{t=1}^{N}\left(\left|C_{\mathrm{mod}}(x,t) - \overline{C}_{obs}(x)\right| + \left|C_{obs}(x,t) - \overline{C}_{obs}(x)\right|\right)^2}$$

Root Mean Square Error (RMSE):

$$RMSE = \sqrt{\frac{1}{N}\sum_{t=1}^{N}\left(C_{\mathrm{mod}}(x,t) - C_{obs}(x,t)\right)^2}$$

$C_{mod}(x,t)$ – *Computed concentration*

$C_{obs}(x,t)$ – *Observed concentration*

N – *Number of pairs*

A cut-off threshold has been applied to the observed concentrations to avoid numerical problems due to unrealistic observations. Thresholds have been defined as follow:

NO_2= 0.5 ppb; O_3= 5 ppb; PM_{10}=1 μg/m^3; SO_2=0.2 μg/m^3; SO_4=0.01 μg/m^3; NO_3= 0.01 μg/m^3; NH_4=0.01 μg/m^3

A2) Meteorology

The statistical indicators selected to evaluate the model performances for meteorology have been defined as follows:

Mean Bias (MB):

$$MB = \frac{1}{N}\sum_{t=1}^{N} M(x,t) - O(x,t)$$

Mean Absolute Error (MAE):

$$MAE = \frac{1}{N}\sum_{t=1}^{N} \left| M(x,t) - O(x,t) \right|$$

Root Mean Square Error (RMSE):

$$RMSE = \sqrt{\frac{1}{N}\sum_{t=1}^{N} \left(M(x,t) - O(x,t)\right)^2}$$

Pearson correlation index (r):

$$r = \frac{\sum_{t=1}^{N} \left(M(x,t) - \overline{M}(x)\right) \cdot \left(O(x,t) - \overline{O}(x)\right)}{\sqrt{\sum_{t=1}^{N} \left(M(x,t) - \overline{M}(x)\right)^2} \cdot \sqrt{\sum_{t=1}^{N} \left(O(x,t) - \overline{O}(x)\right)^2}}$$

M(x,t) – Computed field

O(x,t) – Observed field

N – Number of pairs

A cut-off threshold has been applied to observed and modeled fields to correct data from the presence of outliers. Data are rejected when difference between model and observation are:
Temperature $\geq$ 20 °K; Mixing ratio $\geq$ 10 g/kg; Wind speed $\leq$ 0.5 m/s and Wind speed $\geq$ 100 m/s